EVALUATION OF THE BEHAVIOR OF CERAMIC POWDERS UNDER MECHANICAL VIBRATION AND ITS EFFECT ON THE MECHANICS OF AUTO-GRANULATION

By

NICHOLAS KU

A dissertation submitted to the

Graduate School-New Brunswick

Rutgers, The State University of New Jersey

In partial fulfillment of the requirements

For the degree of

Doctor of Philosophy

Graduate Program in Material Science and Engineering

Written under the direction of

Professor Richard A. Haber

And approved by

_____

_____

_____

_____

New Brunswick, New Jersey

MAY, 2015

ABSTRACT OF THE DISSERTATION

Evaluation of the Behavior of Ceramic Powders under Mechanical Vibration and its Effect on the Mechanics of Auto-Granulation

By NICHOLAS KU

Dissertation Director:

Professor Richard A. Haber

In ceramic powder processing, the correlations between the constituent particles and the product structure-property outcomes are well established. However, the influence of static powder properties on the dynamic bulk powder behavior in such advance powder processes remains elusive. A multi-scale evaluation is necessary to understand the full effects of the particle ensemble on the bulk powder behavior, ranging from the particle micro-scale to the bulk powder macro-scale. Fine powders, with particle size of 10 μm or less, often exhibit cohesive behavior. Cohesion in powders can cause poor flowability, affect agglomerate formation, as well as induce powder caking, all of which can be detrimental to the processing of the powders and/or final product structure-property outcomes. For this reason, it is critical to correlate the causal properties of the powders to this detrimental behavior.

In this study, the bulk behavior of ceramic powders is observed under a simple powder process: harmonic, mechanical vibration. Four powder samples, two titania and two alumina powders, were studied. The main difference between the two powder variants of each material is particle size. The two alumina (Al_2O_3) powder samples had a

primary particle size at 50% less than, or d_{50} of, 0.5 and 2.3 μm and the titania (TiO_2) powder samples had a d_{50} particle size of 0.1 and 1 μm. Due to mechanical vibration, the titania powder variant with a primary particle size of 0.1 μm exhibited a clustering behavior known as auto-granulation. Auto-granulation is the growth of particle clusters within a dry, fine powder bed without the addition of any binder or liquid to the system. The amplitude and frequency of the mechanical vibration was varied to view the effect on the equilibrium granule size and density. Furthermore, imaging of cross-sections of the granules was conducted to provide insight into to the internal microstructure and measure the packing fraction of the constituent particles. As this auto-granulation behavior was unique to only one of the powder variants, an investigation was made into the differences in the powder fundamentals of the variants to identify the causal properties influencing the bulk dynamic behavior of all the powders in this study.

The work performed in this thesis involved conducting extensive characterization of the properties of the powder samples. These properties ranged from micro-scale, discrete particle characteristics to viewing the bulk powder as a continuum material. The multi-scale linkages attained in this work provided an improved insight of cohesive behavior in powders to help guide improved structure-property outcomes in ceramic engineering.

ACKNOWLEDGEMENTS

The graduate school process is often referred to as running a marathon; you must pace yourself to get through the entire 26.2 mile journey as well as have the perseverance to push on when you "hit the wall" and your body says it has had enough. As with a marathon, significant coaching and support is necessary to get to the finish line. Even though it is an individual event, you cannot get through it alone. In the culmination of this thesis, all those who have helped and motivated me deserve to be recognized.

This thesis would not have been possible without the guidance, support, and mentorship of my advisor, Professor Richard A. Haber. Nearly eight years ago, as an undergraduate, he offered me a position as a lab tech conducting research in his group, and much of the knowledge I have gained since then is owed to his tutelage. His help through the years has had a profound effect on the person I am today, not only academically but personally as well. Thank you, Rich.

A key member of my research committee, Dr. Martin J. Murtagh, has been invaluable through my graduate school experience. He always had advice when needed and helped me to keep perspective of the objective through the entire process. On multiple occasions, Marty has gone out of his way to aid me and is critical to the completion of this work. He is deserving of many thanks.

My thanks need to be extended to Professor Richard L. Lehman and Dr. Vladislav Domnich for being on my committee. Professor Lehman's personality was a constant reminder that materials engineering can and should be fun, which I first learned as an undergraduate student in his lectures. Vlad's vast knowledge was most helpful and he was always willing to lend an ear.

I gratefully acknowledge Corning, Inc. for funding this research. The steering committee at Corning, Inc. has been involved with driving this project from the very beginning, and thanks must be given for their expertise, patience, and guidance. The many time-consuming phone conferences were ever helpful to this thesis. The members include, but are not limited to, Drs. Amy Rovelstad, Dell St. Julien, and Pascale Oram.

My year abroad at the University of Leeds was a defining experience in my graduate school process. Many thanks have to be given to Professor Mojtaba Ghadiri, the advisor I worked with during my time there, as well as Dr. Colin Hare, a post-doc who was greatly involved with my research. This dissertation would not have been possible without their assistance. I also must recognize the members of the Ghadiri Research Group, all of whom I have come to consider good friends: Massih, Umair, Mehrdad, Tina, Selasi (YNWA), Pom, Vincenzino, Ali, and Sandra.

At Rutgers, I have had the opportunity to work with some great post-doctoral researchers in the Haber Research Group. I need to give thanks to Drs. Mihaela Jitianu, Sara Reynaud, Fabio Nicodemi, Steve Miller, and Sukanya Murali, who were all involved in my research at one time or another.

Additionally, I would like to thank all the members of the Rutgers MSE staff, who keep the department running smoothly. This includes Claudia Kuchinow, Laura Chirichillo, and, especially, Michelle Sole, who has taught me to drink Guinness if I am ever low in iron.

My appreciation goes out to all the members of the Haber Research Group over the years. I would like to thank past members Steve M., Dan, Steve B., Doug, Fatih, Minh, and Joe. You all have taught me a lot during the time we were colleagues and

were a deciding factor when I made my decision to pursue a PhD in the research group. I also want to thank present members Tyler, Kanak, Metin, Anthony, Azmi, and Zeynep. I wish you all luck in completing the graduate school process and have the utmost confidence that you will all do well.

I have purposefully omitted one Haber graduate student from the previous list as he deserves praise in his own paragraph. Vince DeLucca joined the research group nearly the same time as me when we were both undergraduates, and we later both stayed on together as graduate students (which makes me the senior grad student). Through the years we have experienced the same highs and lows associated with school, and shared many drinks in celebration and commiseration. Vince has always helped me when I had a random question or was seeking advice, although most often in providing distraction. Thank you Vince, and I want you to know that, without a doubt, I can beat you in a fight.

My final, but most important, acknowledgements belong to my family. Thank you to my sisters, Tiffany, Stephanie, and Brittany. You are the best sisters a brother can have. Thank you for always supporting me and listening to my complaints when I needed to vent. Lastly, thank you to my parents. Everything I have I owe to you, and this would not have been possible without your encouragement to let me know I could do this, even when I was not so sure myself. The fact I have made it this far is a reflection of how amazing you both are, and I hope I have made you proud. This dissertation is dedicated to you, mom and dad.

TABLE OF CONTENTS

LIST OF TABLES

LIST OF FIGURES

1. Introduction

A wide range of products are produced by ceramic powder processing, including electronics, structural materials, chemical processing components, and refractories [1]. Characterization of the behavior of powders is necessary for the efficient processing of such products, but there is an added complexity when dealing with powders over standard bulk materials. Materials can all be classified from a chemical point of view into three distinct classes: solids, liquids, and gases. The mechanical properties of such materials can be attributed to the molecular scale of these materials, as the systems are fundamentally controlled by the intermolecular forces as well as the molecular size and shape [2].

A powder system differs as there are multiple material states within the bulk of the powder. Generally, powders consist of solid particles, with the pores existing between the particles being filled with a gas or a mixture of a gas and liquid. For this reason, the fundamental molecular properties of the material making up the powder can have little effect on the bulk mechanical properties of the powder. Instead, the physical properties of the particles within the powder, such as size distribution and shape, have a significant impact on the bulk powder behavior. Thus, the ability to characterize the properties of particles within a powder is important in characterizing the powder as a bulk [2].

Whenever dealing with a dry powder process, the individual particles within the powder will have an affinity to clump or cluster together due to interparticle, attractive forces. The scale of this clustering is dependent on the particle properties and can range from the creation of agglomerates up to granules [3]. If during the process, the dispersion

of the powder into individual particles is necessary, enough force must be applied to deform and break the particle clusters. This deformation is again dependent on particle properties as the attractive force between particles must be overcome for separation to occur [4].

The interparticle attraction between particles is measured as a particle adhesion, or the force holding two particles together and preventing separation. This is a function of the surface energy of the particles and includes both the van der Waals forces and electrostatic attraction between particles [5]. When dealing with the adhesion between two particles, the factors attributing to the quantity of the interactions are particle size, particle shape, and the degree of compression. The quality of the interactions is dependent on the surface chemistry and the surface free energy of the particles. Particle size has an effect due to the significance of gravity. With the larger particle sizes, gravitational forces dominate, but with the smaller particles, adhesion and friction have a much larger role [2]. This is the reason fine particles tend to agglomerate with one another, especially when the size of individual particles becomes smaller than several microns. At this scale, the attractive forces between particles become comparable to the gravitational forces pulling them apart [6]. The term agglomerate refers to a weakly bonded cluster of particles. This is in contrast to an aggregate, which are cluster where the particles are strongly held together, usually involving chemical bonding [7].

While adhesion is important in understanding particle-to-particle interactions, there are other factors affecting the bulk powder as a continuum material. Capillary forces due to moisture present on the surface of particles can increase particle attraction. Frictional forces affect the flow of particles adjacent to each other and are dependent on

the coefficient of friction of the particle surface and the normal force at the point of contact. The normal force at the contact is controlled by the axial load on the bulk powder assemblage and the configuration of the constituent particles. Each point of contact between two particles is a point for adhesive, capillary, and frictional forces to be present, thus the coordination number of the particle as well as the load at each contact point has a huge impact on the bulk behavior of the powder [8].

Interparticle adhesion, packing fraction, particle friction, and capillary forces all contribute to the aforementioned complexity of characterizing bulk powder behavior. A common metric for measuring this bulk behavior is cohesion. It is important to emphasize the difference between the terms adhesion and cohesion. The former refers to the attraction between two different material surfaces, and generally measured as a pull-off force to separate two individual particles, while the latter refers to the attraction between two surfaces of the same material, and measured as the shear stress necessary to induce flow in a bulk powder bed [9]. The term cohesion will be used throughout this work as a powder descriptor, but is far from a singular, unifying index for determining if a powder is suitable for a particular process. This is due to the wide range of powder processes that impart very different stresses on and deal with very different states of the powder bed. For example, powder flowing from a silo through a hopper is in a very different state and under very different stresses than a powder being compacted in a die for tableting [10]. A model piece of work that comprehensively describes the behavior of a powder for a specific process was conducted by Geldart [11]. Geldart [11] created a regime map showing the effect of the powder properties on the bulk behavior of a powder aerated within a fluidized bed column.

Vibration is very common in particulate process, with it used for applications such as powder conveyers, flow promotion. sieving and screening, comminution, compaction, mixing, and granulation [10]. Furthermore, unintentional vibrations commonly can be a byproduct of noise from other industrial processes [12]. For these reasons, the dynamic behavior of powders under mechanical vibration is of great importance to powder processing. Nevertheless, there is currently not an adequate understanding of the behavior of a bed of particles undergoing vibration, and a scheme for classifying the behavior as a function of the powder properties is necessary [13].

The objective of this dissertation was to evaluate the bulk behaviors of powders under mechanical vibration. Differences in the behaviors between different powders were identified and characterized. Insight into the mechanics of the dynamic behavior was made as an effort for better understanding of the mechanisms responsible for the powder performance. By investigating these mechanics, the reason for the differing behaviors among powder variants was determined. This was conducted by establishing the influence of various powder properties, specifically the cohesion and compressibility, on the bulk dynamic behavior of the powder samples, creating a link between dynamic powder behavior and static powder property.

Additionally, the process of auto-granulation under mechanical vibration of a powder was extensively characterized as part of this dissertation. There has yet to be any mention in the literature on the study of this behavior. Therefore, this novel work evaluated the mechanics of the process to understand the size enlargement as well as the granule deformation involved in this process. The properties of the formed granules were measured, including the size, density, impact strength, and microstructure. The effect of

the mechanical vibration applied to the powder on these measured properties was also determined.

By investigating static powder properties, such as cohesion and compressibility, as well as creating links to the bulk, dynamic powder behavior, insight into the mechanisms which control powder performance was gained. The performance related issue of agglomeration is addressed in the analysis of the auto-granulation behavior by gaining an understanding of the process of how particle interactions create particulate structures. This is a multi-scale study, encompassing individual particles and aggregates up to the bulk powder scale.

In this dissertation, the work will be presented according to the size scale within the bulk powder. First, the micro-scale level will be discussed. This will cover particle properties such as size and density. The next scale to be discussed is the bulk, macro-scale, where the flow behavior of the bulk powder will be the subject. This will be presented from the particle perspective to connect the understanding from the micro- to macro-scale. Building on this understanding, the final scale is the meso-scale, where multiple particles interact, such as in granule formation and also deformation. The mechanism behind particles coming together to form a structure, and the subsequent failure of that structure, will be investigated. Discussion creating links between the properties measured at different scales is then presented followed by concluding remarks.

2. Micro-scale – Particle characterization

2.1. Background

2.1.1 Nomenclature of particulate matter

The study of particulate systems is multidisciplinary since many industries have interest in powder science and technology, due to the wide range of processes dealing with particulate matter. As with most multidisciplinary areas of study, the terminology used can be inconsistent between different disciplines, causing misinterpretation in the technical literature. Therefore, it is important to begin by establishing a uniform nomenclature when discussing powders and particulate systems [7].

Powders are comprised of particles, which is any discontinuous subdivision within the bulk particulate matter. The smallest identifiable subdivision is referred to as the primary particle. Aggregation is a general term given to the process by which particles collect to form a larger cluster. The resulting structure of particulate subunits is referred to as an aggregate [7].

The manners in which the particles within an aggregate are held together denote more specific terminology. A hard-aggregate is a specific kind of aggregate where the subunits have been chemically bonded or fused together. Therefore, hard-aggregates cannot be easily dispersed into their subunits. Conversely, an agglomerate refers to an aggregate held together only by physical or electrostatic forces, resulting in a weaker bonding of the subunits [7].

For different size scales, the terms particle and aggregate refer to a system where the size of the subunit is less than 40 microns. The term powder is generally used to describe such a system. For greater than 40 microns, the system is a granular material and the subunits are referred to as granules [2]. In using this terminology, fine particles may clump together to form a cluster smaller than 40 microns, which will be called an aggregate. If this cluster continues to grow, reaching a size larger than 40 microns, the particles will have clumped together to form a granule.

The effective particle size of a powder is the smallest discrete unit of the powder in relation to the powder process. For example, in an aggregated powder under flow, the smallest unit moving in relation to one another, may be aggregates of one another, not the actual primary particles. In this case, the effective particle size is the size of those aggregates, not the primary particles, as the aggregates are the defining units affecting the bulk flow of the powder.

2.1.2. Measurement of particle size

The measurement of the particle size distribution of a powder is most often required as a quality control technique, a method for investigating changes in processes, or a requirement in product specification applications. Therefore, any industrial process dealing with particulate materials has a need for a method of measuring particle size. There are many sizing methods which are well-developed, each with its own disadvantages [10].

There are two main classes of sizing methods: particle counting and ensemble methods. In particle counting methods, the size of each individual particle is assessed,

resulting in the population being based on a number percent. Specific techniques include microscopy and light obscuration. Ensemble methods assess the nature of the entire, or at least a large portion, of the measured population. Techniques which are ensemble methods include sieving, sedimentation, and light scattering [2].

Dynamic light scattering is a popular method for measuring the particle size distribution of a powder. There are many commercially available instrument models, offering many different capabilities. The method is versatile, with the capability of using either liquid or gas as a dispersant. The possible size range capability is relatively large and analysis time is often in the range of a few minutes. The technique has grown in popularity due to its precision, speed of analysis, ease of operation, versatility, and low maintenance [1].

In a laser diffraction instrument for particle sizing, a sample of dispersed particles is passed through a measuring zone, where the particles interact with an incident light beam. The interaction between the light beam and the ensemble of dispersed particles results in a scattering pattern. This pattern will have different light intensities scattered at various angles dependent on the size of the particles. The intensity distribution of the scattering pattern is then focused onto a multi-element detector [14].

The measured light intensity scattering pattern is converted into a particle size distribution using mathematical model algorithms developed for this purpose. The two most commonly used models are the Fraunhofer approximation and the Mie model. The Fraunhofer approximation assumes the particle absorbs light completely and diffraction only occurs at the contour of the particle. Only the optical properties of the dispersing media are needed, and the size of the particles must be much larger than the wavelength

of the incident light beam. For the Mie scattering model, where the particle size is roughly the same size as the wavelength of the incident light beam, the optical properties of the particles most be known, specifically the refractive index and the absorption of the particle material. Absorption is the reduction of intensity of a light beam not due to scattering [14].

The absorption of a particle is dependent on its molecular make-up, the presence of chromophores, and the roughness of its surface structure. Therefore, the absorption of a powder is sample related, and two powder variants of the same material may have different absorption values. Generally, the absorption for laser diffraction measurements only has to be specified to an accuracy of an order of magnitude [15].

2.1.3. Particle density

Density is defined as a ratio of mass to volume of a material. For particulate matter, where porosity will be present, the inclusion or exclusion of these pores will change the density value of the sample. There are often open and closed pores present on particles, as shown in Figure 1. Therefore, it is important to define the terminology for different measurements of density [16].

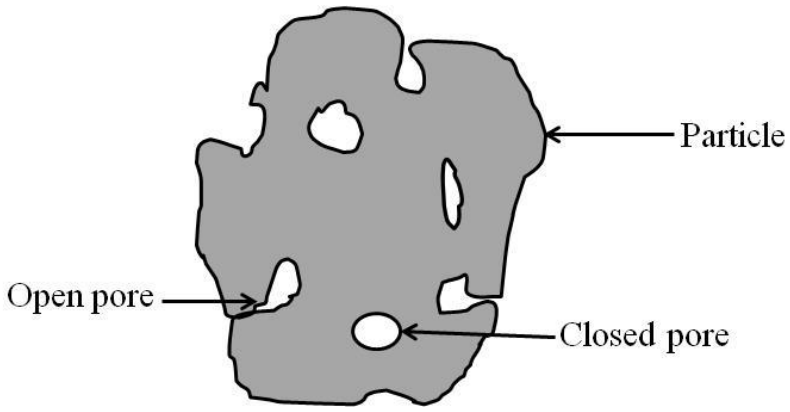

Figure 1. Illustration of a cross section of a particle showing open and closed pores.

Material or theoretical density is the term given to the density of 100% pure and 100% dense samples of the material. It is theoretically calculated from the atomic unit cell of the material.

The true density is defined as the ratio of the mass of the particle to its actual volume, excluding all pores. This can be measured by grinding the particle so fine in size that the closed pores are opened to the surface [16]. The true density differs from the theoretical density as it includes impurities that are present in the powder sample.

The particle density is the mass of the particle divided by the particle volume, including the inside closed pores but excluding the surface open pores [16]. This is also known as skeletal density.

Other terminology used to describe the density of particles includes the envelope density, which is the measurement of the particle density including all pores, both open and closed. Bulk density is defined for bulk powder beds. This measurement includes the voids between particles and will be discussed further in Chapter 3.

The measurement of particle density involves two steps: the measurement of the sample mass and the measurement of the sample volume. The mass can be easily measured using a precise balance. The volume, often measured using pycnometry, is less trivial and defines which type of density is being measured. The medium used within the pycnometer is often a gas or a liquid. Gas pycnometers are used to measure the skeletal density of particles, as the volume measured will exclude any open pores in which the gas can infiltrate into. When using a liquid as the pyncnometer medium, the density measurement will be an envelope measurement, as the liquid will be prevented from

infiltrating into open pores due to capillary forces. Differing liquids, such as water versus mercury, will have different wetting abilities, limiting the minimum pores size the liquid can infiltrate [16].

2.1.4. Moisture in particulate systems

Moisture appears in particulate systems in two forms: bound water and free water. Bound water is attached by hydrogen bonding, and therefore, relatively difficult to remove, such as adsorption water. Bound water also includes combined water, which exists inside crystals and is bound directly to the lattice. In contrast, free water is captured by materials by relatively weak bonds and occurs in funicular, capillary, and moving states. Free water has a significant effect on the bulk mechanical behavior of powders, and dry powders are generally considered to be free of free water [17].

Dried powders can adsorb moisture onto its surface in the form of bound water from the humidity of the air in which it is stored. The amount of adsorbed moisture and rate of adsorption can be measured as a function of relative humidity of the ambient environment using dynamic vapor sorption. The nature of the moisture sorption can be attained by measuring both the adsorption and desorption isotherms of the powder. A hysteretic behavior of the isotherms suggests moisture being internally absorbed into the crystal lattice, which can be irreversible and prevent the water from being released by physical means [18].

2.2. Experimental method

2.2.1. Primary particle imaging

Imaging of the primary particles of the powder samples were conducted using a scanning electron microscope (SEM) to provide the necessary magnification and resolution. The SEM used in this study was a Zeiss Sigma Field Emission SEM (Carl Zeiss Microscopy GmbH, Jena, Germany). The secondary detector provided topographical contrast and a relatively low gun voltage was used to minimize charging of the sample during imaging. Samples were prepped by creating a low concentration dispersion of the particles in ethanol. A pipette was used to place a drop of the dispersion on an aluminum, SEM sample stud, which was allowed to dry before imaging.

2.2.2. Particle sizing by dynamic light scattering

Measuring the primary particle size of powders was conducted by dynamic light scattering using a Malvern MasterSizer 2000 with the Hydro 2000S cell (Malvern Instruments, Malvern, UK). The instrument was set to obtain five consecutive measurements with no time delay between each, and the average of the five measurements was taken as the particle size distribution of the powder. The internal stirrer/pump of the Hydro 2000S cell was set to the maximum 3500 rpm to aid in the dispersion of the powder. The sample concentration for the measurement was set to obtain a laser obscuration level of 10% to 15% of the instrument.

A major issue with particle sizing by DLS is to ensure the sample measured is representative of the bulk powder. A common method for sample preparation is to

create a large volume of dispersed powder and use a pipette to collect particles to feed into the instrument to obtain the correct laser obscuration level. This method of sampling can create issues, as the dispersed powder will naturally segregate due to the different settling rates of different sized particles. Therefore, the pipette may only collect a portion of the particle size distribution of the bulk powder. To prevent this, before an actual sample was measured, the MasterSizer 2000 was set up and the amount of powder needed was measured to obtain the correct obscuration level. This was obtained by adding dry powder directly into the instrument until an obscuration level of 10% was obtained. The mass of the powder added was measured. The machine was then flushed and cleaned before the actual test was run, using a dispersed sample of that exact mass of powder. This allows the entire dispersion to be added to the instrument, preventing any effect of particle segregation on the sampling. The mass needed to obtain an obscuration of only 10% was used because the obscuration value will rise as agglomerates within the dry powder are dispersed.

Powder dispersion was conducted by adding the required mass of powder to 30 mL of deionized water in a beaker. The beaker was then placed in a Heat Systems – Ultrasonics, Inc. Sonicator W-380 to disperse any agglomerates in the sample. The sample was sonicated for 30 seconds using a continuous pulse and added into the MasterSizer immediately afterwards for measurement.

To use Mie theory to measure particle size, two parameters must be inputted into the calculations: the material refractive index and the particle absorption. The refractive indices of the samples being measured were collected using material property databases, but as the particle absorption is dependent on surface structure of the particle, post-

measurement analysis was conducted to determine the correct absorption value for the sample. Absorption values had a significant effect on the measured particle size distribution, and an absorption value within the correct order of magnitude had to be selected. After a measurement was made, the size distribution was recalculated for absorption values of 1, 0.1, 0.01, and 0.001.

It is possible to determine the absorption of a powder by using the Mie model "backwards." Using this method, the scattering data of a distribution is measured, and the Mie model with a given absorption value is used to predict a particle size distribution. The Mie model is then used again with the predicted distribution to calculate a scattering pattern. The measured scattering pattern and calculated scattering pattern can be compared to determine the correctness of the fit. Comparing the fit using different absorption values allow for the correct value to be determined [15].

The MasterSizer 2000 software reports a both the measured scattering data and the calculated scattering data derived from the Mie model, which allows the user to compare the data to the model and determine the level of fit. The absorption value that yields the best fit was then selected and the corresponding particle size distribution was used. The detectors number 51 and 52 have a response related to light extinction of the sample and have the greatest dependence on absorption misfits [15].

2.2.3. Particle density measurement

Particle density measurement was conducted using a Micromeritics Accu Pyc II 1340 (Micromeritics Instrument Corporation, Georgia, USA). The instrument uses helium gas to measure the density of a powder sample. The density provided is a skeletal

density, with all pores open to the helium gas being excluded from the particle volume. Closed pores are included in the volume and affect the density.

2.2.4. Moisture sorption of particles

To prevent environmental storage conditions from affecting powder samples, all powders were preconditioned before testing. For a minimum of 12 hours, powder samples were stored in a 120°C drying oven before any testing. This creates a baseline moisture level on the surface of the powders before testing.

Powders were tested in a Dynamic Vapor Sorption (DVS) apparatus (DVS-ADVANTAGE, UK), which controls the relative humidity within a chamber and measures the change in mass of a powder sample over time. The relative humidity can be ranged from 0% to 90%. Ramps were conducted at steps of 10% relative humidity. Both increasing and decreasing ramps were run to observe the absorption and desorption behavior of the powders.

2.3. Results and discussion

2.3.1. Powder variants

For this thesis, two different particle systems will be studied: alumina (Al_2O_3) and titania (TiO_2). Both materials are commonly used in industrial ceramic processes and offer difference in physical particle properties. For each material, two different powder variants were chosen to provide a difference in particle size and surface area. For the alumina powders, two powders from Almatis (Almatis GmbH, Frankfurt, Germany), the

A16SG and A3500SG, were chosen. Both of these powders are Bayer processed aluminas with similar surface chemistries. This allows for the physical differences between the two powders to be isolated, as the powder are very similar chemically. For the titania powders, two powder variants from Cristal Global (Cristal Global, Jeddah, Saudi Arabia), the AT1 and DT51, were chosen. These powders are both sulfate processed with a main difference in their surface area. Again, by choosing powder processed in a similar manner, the chemical differences are minimal.

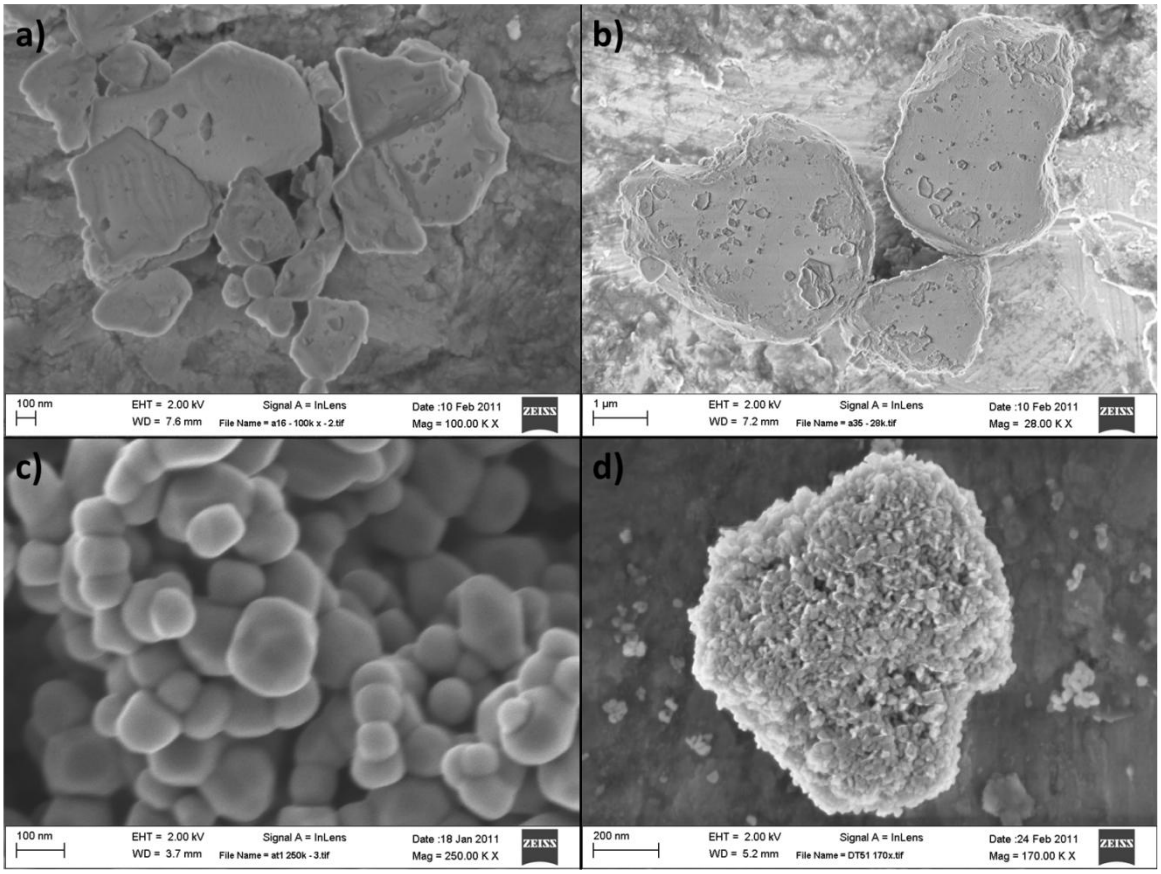

Figure 2. SEM images of powder variant showing a) Almatis A16SG alumina, b) Almatis A3500SG alumina, c) Cristal Global AT1 titania, and d) Cristal Global DT51 titania.

Shown in Figure 2 are the SEM images of the four powders chosen to be studied in this thesis. The two alumina variants from Almatis, the A16SG and A3500SG powders, both have a very similar prismatic shape. The main difference between the two powders is the size of the primary particles. The manufacturer lists the d_{50} particle size to be 0.5 μm and 2.3 μm for A16SG and A3500SG, respectively. In comparison, the AT1 titania from Cristal Global has a relative spherical particle shape. Finally, the DT51 titania is shown as a hard aggregate. The powder cannot easily be dispersed to the primary particle scale, and instead is shown as a hard, shear-stable aggregate, giving the effect particle a high surface area. For the titania powders, the manufacturer lists the d_{50} particle size to be 0.1 μm for AT1 and 2.3 μm for DT51. These values correlate well with the SEM images taken of the primary particles in Figure 2.

The BET surface areas of the four powders were also measured, with the results of a single measurement shown in Table 1. As expected, the surface area of the powders increases with decreasing particle size. The DT51 titania powder has a significantly higher surface area than the other three tested powders. This is explained by the nature of the DT51 particles being hard aggregates, with the primary particle size being around 20 nm. With such a fine primary particle size, it is expected for a powder to have such a large surface area.

Table 1. BET surface area of powder samples.

Powder	Surface Area (m^2/g)
A16SG	8.80
A3500SG	3.49
AT1	10.53
DT51	80.88

The powder variants chosen for this study allow for the isolation of different physical particle variables, while holding the chemical variables between the variants constant. The two alumina powders, A16SG and A3500SG, have very similar chemical properties due to their similar processing, as well as a similar particle shape. The main difference is the particle size, and the effect of which on the bulk behaviors of the powders can therefore me investigated. Likewise, the AT1 and DT51 both are processed in the same manner and, chemically, are quite similar. The aggregated structure of the DT51 particles give rise to the nearly eight times greater surface area value than the AT1 powder, shown in Table 1. Such a difference allows for the investigation of aggregation on the bulk behaviors of the powder.

2.3.2. Particle size distributions

The particle size distributions of the four powders are shown in Figures 3, 4, 5, and 6. Varying levels of agglomeration is visible in all the powders at above 10 μm, with the alumina powders in Figures 3 and 4 exhibiting shoulders off the main peak and the titania powders in Figures 5 and 6 showing separate peaks. The two alumina powders also have a bimodal distribution, but the appearance of the secondary peak is dependent on the absorption value in both cases. These larger peaks are indicative of fine, cohesive powders that are prone to agglomeration. The method of using water as a dispersant and ultrasound as the only means of mechanical dispersion is not aggressive, and it would be expected that evidence of agglomeration to remain in the dispersed samples.

Each particle size distribution was calculated using four different absorption values: 1, 0.1, 0.01, and 0.001. Shown in Figure 3, the size distribution of the A16SG

alumina powder varies greatly with particle absorption. At absorption values of 1 and 0.1, the distribution is distinctly bimodal. As the absorption value is reduced to 0.01, the two distinct peaks become convoluted, and at an absorption value of 0.001, the distribution is monomodal.

Figure 4 shows the particle size distribution for the A3500SG alumina powder. For every absorption value, the position of the main peak does not shift greatly. Like the A16SG alumina powder, a finer-sized, secondary peak is present at high absorption values, but diminishes as the absorption value is decreased. The two distributions with absorption values at 0.01 and 0.001 are very similar.

In Figure 5, the AT1 titania powder exhibits a different behavior to that of the two alumina powders. While the position of the major peak does greatly shift with changing absorption value, the width of the distribution does change significantly. As the absorption value is decreased, the peak widens. Likewise the A3500SG, the distributions at absorption values of 0.01 and 0.001 are very similar.

In comparison to the other powders, the particle size distribution of DT51, shown in Figure 6, does not vary greatly when the absorption value of the powder is changed. For all four particle absorption values, the size distributions are similar.

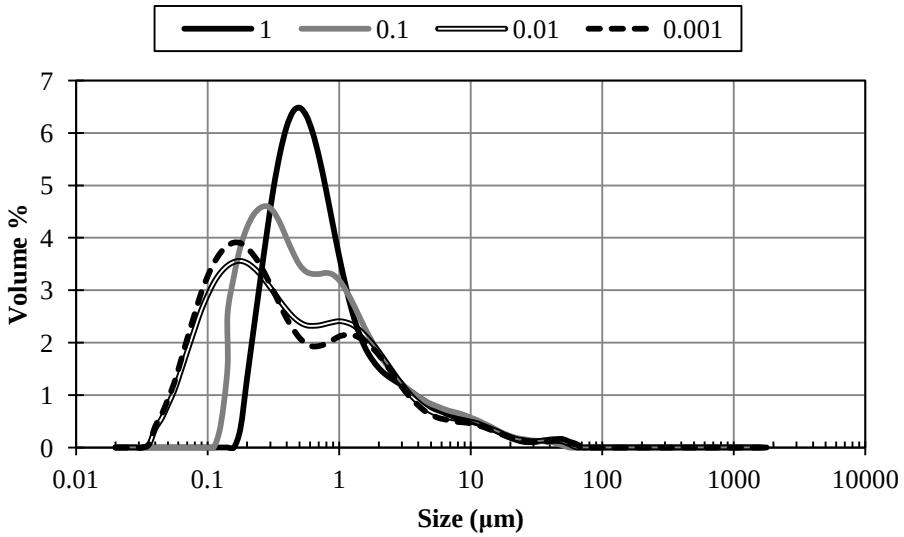

Figure 3. Particle size distribution of A16SG alumina powder calculated using 4 different particle absorption values.

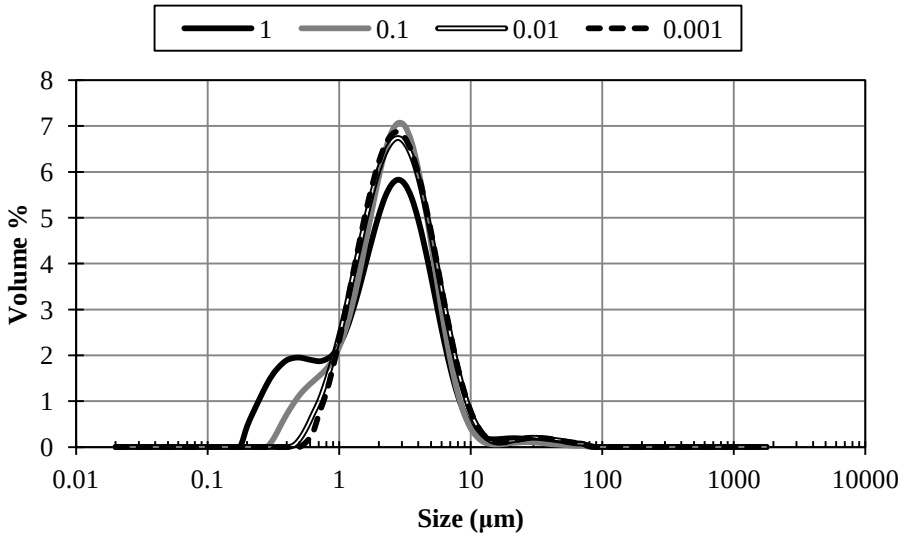

Figure 4. Particle size distribution of A3500SG alumina powder calculated using 4 different particle absorption values.

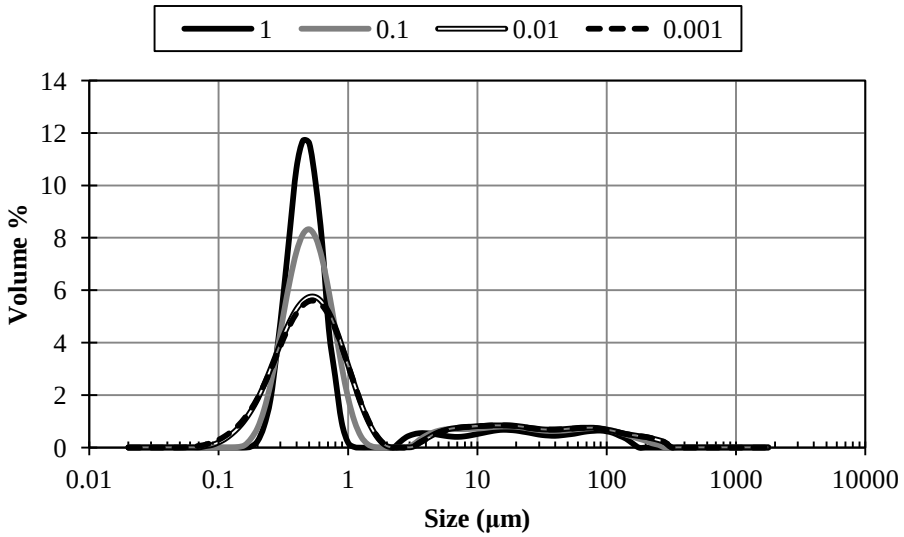

Figure 5. Particle size distribution of AT1 titania powder calculated using 4 different particle absorption values.

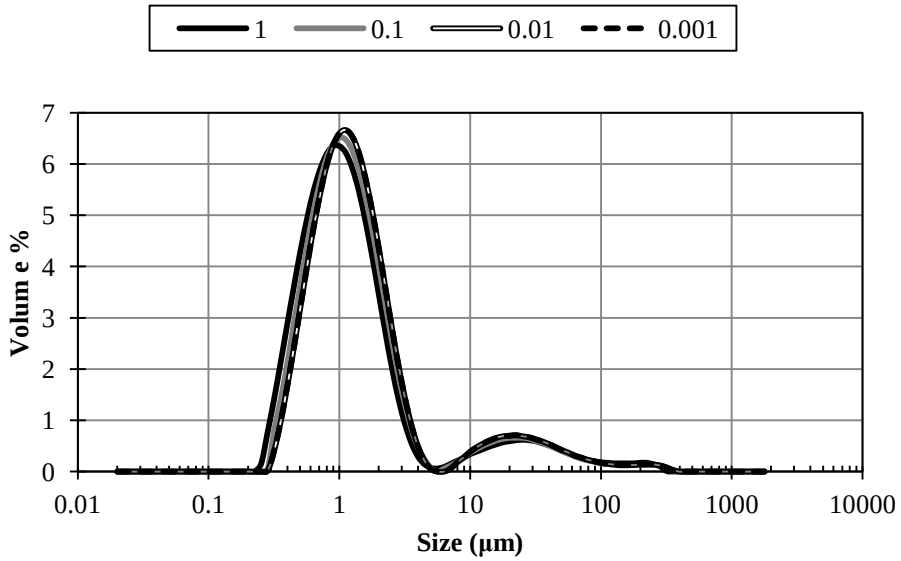

Figure 6. Particle size distribution of DT51 titania powder calculated using four different particle absorption values.

Shown in Figure 7, the Malvern software can create a fit graph to compare the actual light energy measured by each detector and the expected light energy calculated from the size distribution. As discussed in the literature, the greatest discrepancy between the two is seen in detectors 51 and 52 and comparing the difference between measured and expected light intensities at these detectors can be used to determine the correct absorption value [15].

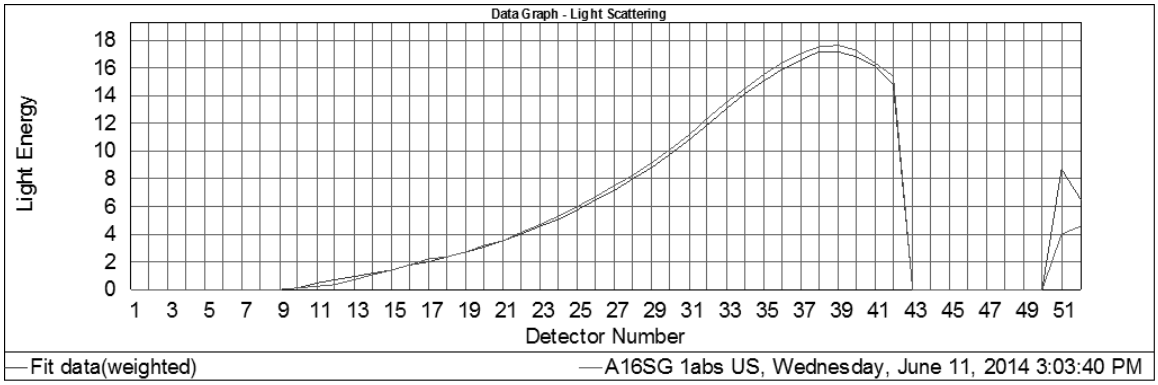

Figure 7. Fit data graph from Malvern MasterSizer 2000 of A16SG alumina powder with absorption value of 1, showing difference in measured and expected scattering data.

In Table 2, the absolute difference between the actual light energy measured and the expected light energy calculated from the size distribution for detectors 51 and 52 are shown for each of the four powders using each of the four absorption values. The total absolute difference is also shown. For every powder, the lowest light energy difference was given by an absorption value of 0.001. This suggests the absorption value of 0.001 provides the best fit for each powder, yields the correct particle size distribution, and is the correct absorption value for each powder.

The effect of changing the absorption values varied between the different powder variants, although all the distributions were altered. Using an incorrect value of

absorption can greatly affect the result given by the measurement. Also, the fit difference between the actual light energy measured by each detector and the expected light energy calculated from the size distribution changed due to the absorption value, especially in detectors 51 and 52. Comparing the differences allows for a method to determine the correct absorption value of a powder. For each of the four powders tested, the correct absorption value was found to be 0.001, with the particle size distribution using other parameter values being incorrect.

Table 2. Fit difference in measured and expected light intensity values for powders at different absorption values.

A16SG

	Fit difference		
Absorption	Detector 51	Detector 52	Total
1	4.70	1.82	6.52
0.1	5.06	2.60	7.66
0.01	0.79	0.78	1.57
0.001	0.31	0.66	0.97

A3500SG

	Fit difference		
Absorption	Detector 51	Detector 52	Total
1	3.34	2.67	6.01
0.1	3.06	3.00	6.06
0.01	1.14	1.09	2.23
0.001	0.52	0.58	1.10

AT1

	Fit difference		
Absorption	Detector 51	Detector 52	Total
1	0.61	0.06	0.67
0.1	0.41	0.23	0.64
0.01	0.32	0.14	0.46
0.001	0.3	0.13	0.43

DT51

	Fit difference		
Absorption	Detector 51	Detector 52	Total
1	1.90	1.30	3.20
0.1	1.49	0.95	2.44
0.01	1.18	0.75	1.93
0.001	1.10	0.70	1.80

From the correct absorption value, the measured d_{50} particle size for each powder was found to be 0.33 μm for A16SG, 2.93 μm for A3500SG, 1.30 μm for DT51, and 0.68 μm for AT1. Values for the first three listed powders correlate well with the

manufacturer listed d_{50} particle size and SEM imaging shown in Figure 2. All three measured values are slightly higher, but that can be due to the agglomeration present in the measured samples skewing the size distribution of the population. The measured d_{50} particle size of the AT1 powder was significantly higher than the value given by the manufacturer and the SEM image of the particles. This powder is therefore extremely difficult to disperse. The particles are prone to agglomeration and may be in a strongly-bonded, aggregate state.

The results of this study show the importance of correct particle absorption value for the measurement of particle size by dynamic light scattering. A significant change to the particle size distribution can be made by inputting the incorrect particle absorption value. Most prominent is the A16SG powder, shown in Figure 3. The correct absorption value of 0.001 results in a bimodal distribution, but using an incorrect value of 1.0 produces an erroneous distribution that is monomodal and discounts the fines in the powder. Such a vast different can have profound affects in batching and manufacturing if the wrong absorption value is used. Conversely, the particle size distribution of the DT51 powder was unaffected by changing the absorption value. It can be speculated that this is due to the aggregated nature of the DT51 particles, which is not present in the other three powders.

2.3.3. Particle density

The densities of the particles were measured using He pyncnometry and results are shown in Table 3. The values represent skeletal densities, which include closed pores, but exclude pores open to the He gas. All samples have particle densities that are

similar to their theoretical material densities, resulting in particles that are relatively dense with minimal internal porosity. The results are an average of five measurements and the standard deviations are shown.

Table 3. Particle density of powder samples.

Powder	Particle density (g/cm^3)
A16SG	3.942 ± 0.001
A3500SG	3.939 ± 0.002
AT1	3.760 ± 0.002
DT51	3.668 ± 0.002

Note that these values are all lower than the theoretical densities of the materials. The theoretical density of alumina is 3.98 g/cm^3 [19], and the theoretical density of titania is 3.895 g/cm^3 [20]. The particle density of the powder samples is expected to be lower than the theoretical density of the material. Internal, closed pores and impurities or additives to the powders would all lower the measured particle density. The low standard deviation shows the accuracy of this measurement.

2.3.4. Dynamic vapor sorption

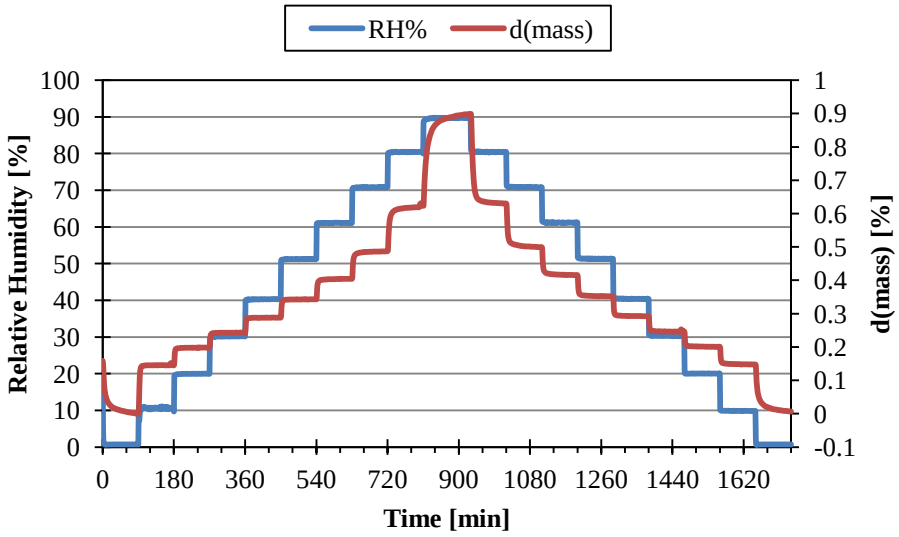

Figure 8. Change in mass of AT1 titania in environments of different relative humidity.

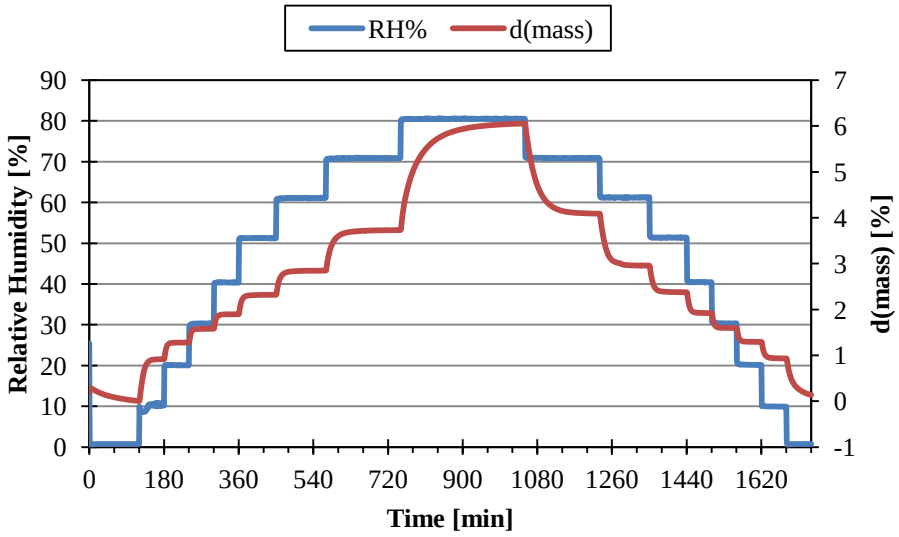

Figure 9. Change in mass of DT51 titania in environments of different relative humidity.

The effect of moisture on the powder behavior was studied by testing the powders at different levels of relative humidity. Powders were tested in a Dynamic Vapor

Sorption (DVS) apparatus, which is shown in Figures 8 and 9 for the two titania powders. The relative humidity of the system is shown in the blue line, with the red line showing the percent change in mass of the sample, assumed to be moisture being absorbed onto the sample. For each given relative humidity, the powder gained mass over time, absorbing moisture. An equilibrium mass was reached at each relative humidity, with the equilibration time within four hours for any condition. When the relative humidity was decreased, the mass of the powder also decreased for both samples, as moisture was lost.

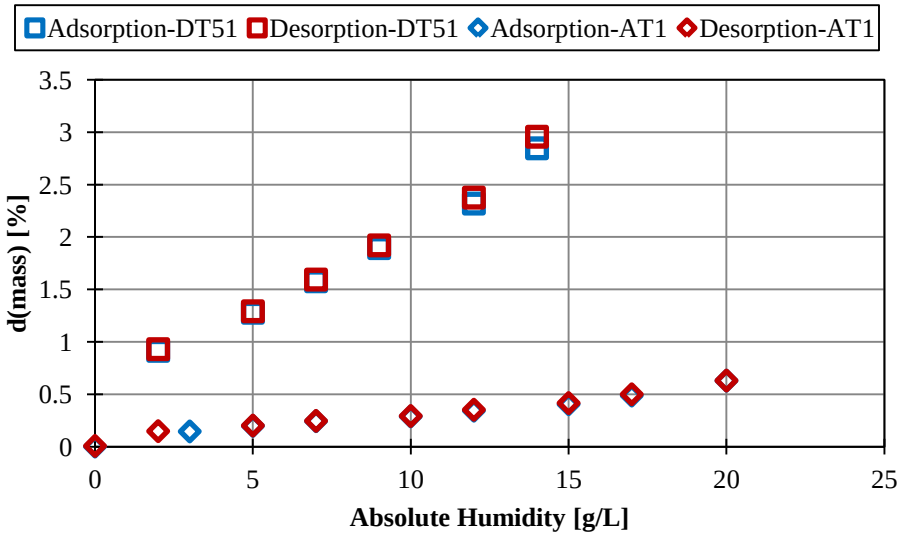

Figure 10. Absorption and desorption curves the two titania powders.

Using the equilibrium values from the DVS measurement, absorption and desorption curves of the two titania powders were constructed, shown in Figure 10. Using the ambient temperature and barometric pressure, the relative humidity was converted to an absolute humidity [21]. The DT51 titania absorbed nearly an order of magnitude more mass of moisture than the AT1 powder at the same absolute humidity. At 12 g/L humidity, DT51 had adsorbed 2.32% of its mass in moisture. Conversely, AT1

had only adsorbed 0.35% of its mass at the same absolute humidity. This is understandable due to DT51 being a high surface area titania powder. For both powders, the adsorption and desorption curves overlap, with no hysteresis in the behavior. The conclusion be made that the absorbed moisture in entirely physical on the surface of the powder, and the entire process is reversible.

The results from this section show that dry ceramic powders can adsorb a significant amount of moisture from the ambient environment. This adsorption can potentially be problematic for processes requiring a precision measure of the amount of water in the system, such as with ceramic paste formulation. In such processes, it would be important to include the amount of moisture adsorbed onto the surface of powders and include that water in the formulation.

Furthermore, the amount of moisture absorbed is dependent on the humidity of the environment. Therefore, the amount on the powder can vary day-to-day as the absolute humidity of the ambient environment changes. When dealing with powder processes where moisture levels are critical, controlling the ambient environment to keep the absolute humidity stable from day to day is important. Additionally, the amount of moisture adsorbed increases with increased surface area, as illustrated in Figure 10 showing the comparison between the high surface area DT51 powder and low surface area AT1 powder. The implications of this result mean that finer or aggregated powders with higher surface areas will adsorb a greater amount of moisture than coarser powder variants.

3. Macro-scale – Bulk powder characterization

3.1. Background

3.1.1. Bulk powder density

Bulk density is simply the mass of a powder divided by the bulk volume that powder occupies. It is given by the mass of a powder bed divided by the volume the bed occupies, including all voids between the particles within the bed. The packing fraction is the fraction of the powder bed occupied by particles and is given by the ratio of the bulk powder density, ρ_b, to the particle density, ρ_p. The porosity of the powder bed is the fraction of the bed not occupied by particles, or one minus the packing fraction, shown in Equation 1 [16].

$$\varepsilon = 1 - \frac{\rho_b}{\rho_p} \qquad \text{Equation 1}$$

The state, or configuration, of the powder system greatly affects the bulk density measurement. Shown in Figure 11, two powder beds made of the same particles can occupy different volumes given the packing configuration of those particles. The method of loading will affect this configuration. Therefore, the preparation of the powder sample and the resultant state is of extreme importance in the scope of the measurement [22].

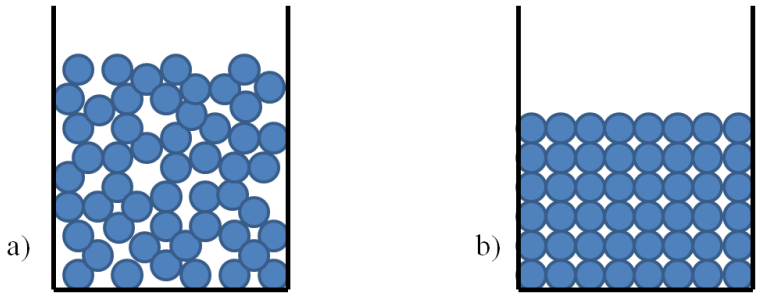

Figure 11. Illustration of two powder beds of spherical particles with different packing fractions.

Standardized states for the powder system can be split into two bulk density measurements: an aerated bulk density and tapped bulk density. An aerated bulk density refers a powder bed in its loosest packing density. This state has the lowest bulk density of the powder, which is generally prepared by being dispersed and allowed to settle only by the aid of gravity. In contrast, tapped bulk density is measured by assisting the settling of an aerated powder bed by the means of mechanical tapping. The tapping induces particle rearrangement, leading to the particles taking a more tightly-packed configuration and having a higher bulk density [23].

Svarovsky [22] addresses the confusion and difficulties often associated with the measurement of an aerated bulk density [22]. When testing a cohesive powder, it becomes difficult to uniformly load the powder and prevent uncharacteristic voids from forming. Harnby [24] noted extreme variability in the aerated bulk powder measurement results effect of cohesive powders due to this artifact [24]. A standard method for the measurement involves pouring powder into a container of a known volume and measuring the mass of the powder needed to fill the container. The procedure of pouring

can involve a funnel-type feeder, a sieve, and/or some form of mechanical tapping or vibration [14].

A common instrument used to make such measurements to provide more reliable results is the Hosokawa Powder Tester. The conditioning and loading of the powder using the outlined method with the instrument provided reproducible measurements of powder characteristics. The instrument involves pouring powder thru a vibrating sieve. The resultant particles fall thru a chute leading into a 100 mL cup, as shown in Figure 12 [25].

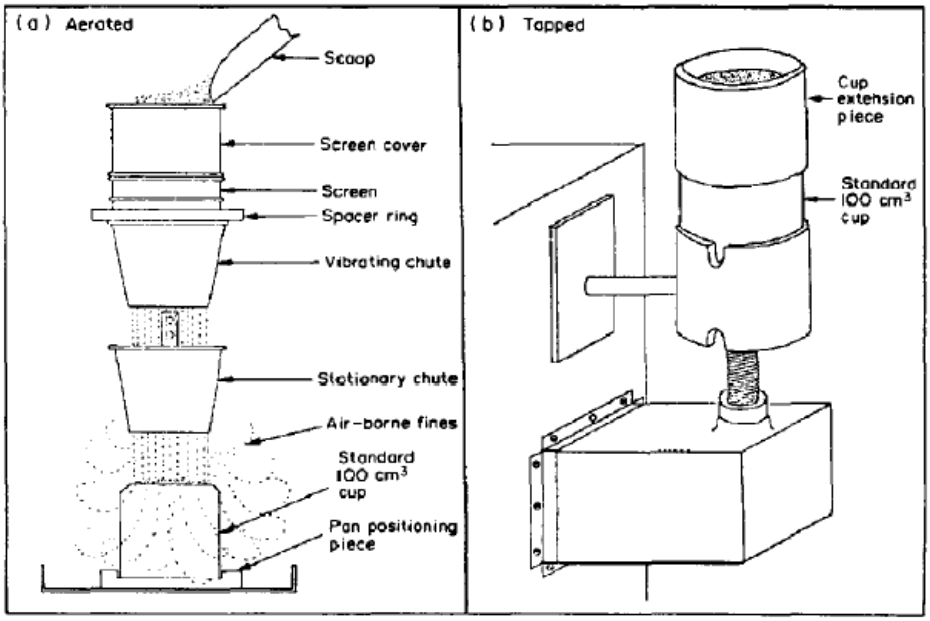

Figure 12. Schematic of Hosokawa Powder Tester showing configuration for measuring (a) aerated bulk density and (b) tapped bulk density [25].

As the cohesion of powders increase, the difficulty in measuring the aerated density of a bulk powder also increases. The cohesion allows for the particle configuration to resist collapsing even under a loose state [24]. This causes the preconditioning of the powder to be extremely sensitive to the measurement, and is

further compounded by presence on agglomerates within the powder [26]. Other methods to measure the loose-packed powder bulk density include the Gravitational Displacement Rheometer (GDR) [27] and the Freeman FT4 powder rheometer [28]. Vasilenko *et al.* [29] compared the three measurements and found each provided a loose-packed bulk density that was statistically equivalent. While the results of the tests correlated well, the methods were vastly different, with the GDR require a ten times greater mass of powder sample for testing than the Hosokawa Powder Tester or Freeman FT4. The conclusion of the study was that a critical loose-packed density value occurs for a powder that is independent of the measurement method and can be considered a material property [29].

As previously stated, the difficulty in measuring the bulk density arises from removing the stress history from the powder sample [25]. The Freeman FT4 rheometer accomplishes this by pre-conditioning the powder. The impeller blades of the instrument are rotated through the powder bed before measuring. This gently disturbs the powder, removing any stress history and creating a uniform, loosely packed sample for measurement [28].

Tapped bulk density is measured by assisting the settling of an aerated powder bed by the means of mechanical tapping. The method for measuring tapping powder is standardized [30], but Svarovsky again states that as the cohesiveness of the powder increases, issues arise using the standard method [22]. Abdullah and Geldart [23] performed a comparison of tapping techniques to see their effect on bulk density measurements. In the study, the standard method using a Copley Tap Density Volumeter and Hosokawa Powder Tester were both used to measure the same powder samples. It

was found that the Hosokawa instrument, due to its improved loading procedure and tapping method, produced more reliable results [23].

Comparisons between the aerated bulk density and tapped bulk density offer insight into the compressibility of a powder, and thus its flowability. The simple ratio of the tapped density to the aerated density was found to measure the relative magnitude of the friction between particles in the powder [31]. This ratio, shown in Equation 2, was termed the Hausner Ratio [32]. Another method developed using the same principle was the Carr's Compressibility Index, shown in Equation 3 [33].

$$\mathrm{HR} = \frac{\rho_{\mathrm{tapped}}}{\rho_{\mathrm{aerated}}} \qquad \text{Equation 2}$$

$$I_{\mathrm{C}} = \frac{\rho_{\mathrm{tapped}} - \rho_{\mathrm{aerated}}}{\rho_{\mathrm{aerated}}} \times 100 \qquad \text{Equation 3}$$

There have been many studies on the measurement of bulk densities of various powder systems. Results of these studies have shown the bulk density of powders are dependent on many different properties of the particles, including the material [34], the particle size distribution [24], and the particle shape [35]. It is therefore difficult to deconvolute the effect of particle cohesion on the bulk flowabilty from the previous studies. Furthermore, the stress placed on the powder by tapping cannot be measured.

3.1.2. Bulk powder compaction

The increase in bulk density of a powder by the application of a load is known as compaction. The simplest way to measure the compaction behavior of a powder is by uniaxial compression. A sample of powder is compressed axially in a cylindrical die which confines the powder and prevents lateral strains and the die displacement is

measured as a function of the pressure applied on the punch [22]. Critical to the test is the method of loading powder into to die. Zafar [36] found that the mechanical behavior and microstructure of the compacted bed differed with loading method. The most reproducible measurements and homogeneous compacts were made by using a loading method where powder was sieved to break up large clusters into a funnel, which then fed powder into the cylindrical die for testing [36].

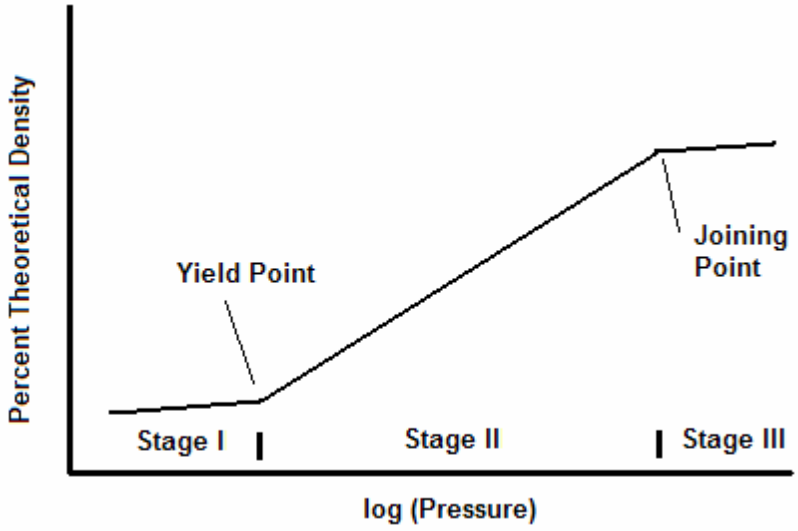

Figure 13. Schematic of a powder compaction curve showing various stages of densification [37].

A typical behavior of a powder being compressed using the die pressing procedure is shown in Figure 13. The graph shows the theoretical density of the compacted powder assemblage as a function of the log of the applied pressure. It is important to note the three distinct stages of compaction, which is due to different mechanisms controlling the rate of compression of the powder. The different mechanisms are explained as:

Stage I – Granule flow and rearrangement

Stage II – Granule deformation predominates

Stage III – Granule densification predominates

In Stage I, the particles in the powder assemblage begin to rearrange themselves due to the applied pressure to achieve the maximum packing configuration. The compressibility of the powder in this stage is dependent on the flowability of the powder. In Stage II, the particles deform into the interstices as densification occurs. The transition from particles to grains occurs in Stage III, as the granules individually begin densification [1].

The yield point is the transition pressure between the Stage I and Stage II compaction and can provide information on the characteristic structure within a powder. Niesz *et al.* [38] used the yield point to determine the strength of aggregates of alumina. Their work was concerned with powders of primary particle size in the submicron range with surface areas ranging from 3 m^2/g to 13 m^2/g exhibiting different degrees of porous aggregation based on varying levels of calcinations. The technique ceded by this investigation was the extrapolation of the apparent Stage I and Stage II regimes on a semi-log plot to an intersection point. The pressure corresponding to this intersection point was argued to be the extrapolated yield point [38].

This yield point is dependent on the characteristics of the aggregates within the powder. Golomb [39] investigated differences in compaction behavior of alumina powder. The powder was processed using different spray drying techniques to produce granulated powder of different quality. The study found that the different spray dried powders created powder compacts with very different microstructures, especially when

compacted at lower pressures. At higher pressures, in the advanced stages of Stage II compaction, the microstructure of the compacts had less variability between samples [39]. This is attributed by the different spray dried samples being processed from the same starting powder. At higher pressures, the spray dried granules have all broken, leaving the compaction behavior and microstructure dependent only on the constituent particles that are the same for all samples.

A similar conclusion was made by Smith [40]. Powder was granulated by spray drying lead-zirconate-titanate powder. By changing the properties of the slurry before spray drying, the density of the granules produced was varied. The study found the Stage I to Stage II yield point increased with increasing granulated sample density [40].

The measurement of a yield point is dependent on there being a clear transition point between the two stages of compaction. In most cases when dealing with a fine dry powder, the result is not the same as when dealing with a very uniform, granulated powder as in the studies by Golomb [39] and Smith [40], and the transition point is not apparent, with the two stages overlapping, creating a curved graph [41]. The convolution of the transition can be attributed to aggregation in the powder. Fine powders commonly are aggregated in the dry state, and when compressed, the aggregates become rearranged. As pressure increases, the aggregates begin to deform and break into their smaller, constituent particles. Those particles are then rearranged with increasing pressure before undergoing deformation themselves. This behavior continues with compression until the powder is broken down to the scale of its primary particles [42].

Compaction equations have therefore been developed to interpret compaction curves by modeling mechanisms of compaction. It is important to note that most are

empirical equations fitted to experimental data, but have still been found to be useful descriptors of bulk powder compaction behavior. One such equation is the Heckel equation, which considers the compaction of a powder bed to be analogous to a first-order chemical reaction [43]. The Heckel equation is

$$ln\left(\frac{1}{1-D}\right) = KP_a + B \qquad \text{Equation 4}$$

where D if the relative density of the powder, P_a is the applied pressure, K is a constant relating to yield strength of the powder, and B is a constant that represents the maximum degree of packing of the powder achieved at low pressures solely due to rearrangement of particles [43].

Another commonly used compaction equation is the Kawakita equation, which is given by

$$\frac{P_a}{C} = \frac{1}{ab} + \frac{P_a}{a} \qquad \text{Equation 5}$$

where C is the relative volume decrease of V_0, the initial volume, and V, the compacted volume,

$$C = \frac{V_0 - V}{V_0} \qquad \text{Equation 6}$$

and a and b are constants, related to the degree of compression and structural strength of the powder, respectively. [44].

The definition of each parameter was found by Nordstrom *et al.* [45]. Microcrystalline cellulose powders were compressed by uniaxial compression. Single particle compression tests were also conducted to measure the mechanical properties of the single particles of the tested powders. The results were compared to the Kawakita parameters calculated using the compaction curves. It was found that the parameter a

represents a maximum engineering strain or degree of compression experienced by the bulk powder. Free flowing powders tend to have low *a* value as their default packing is high and cannot be compressed further. The parameter 1/*b* has a unit of stress and represents the applied pressure needed to achieve and engineering strain of *a*/2. Used as a measure of the strength of powder structure, cohesive powders tend to have high 1/*b* as the particle network must be broken before compaction can occur [45].

The effect of particle size on the Kawakita parameters was studied by Nordstrom *et al.* [41]. A sodium chloride powder was dry sieved to create samples of different sizes. The results showed that with decreasing size, generally, the *a* parameter increased and the 1/*b* parameter decreased. It was concluded that since finer particles deform less than larger particles, the significance of particle deformation on the compaction behavior decreased. This left particle rearrangement to become the significant compaction mechanism for the overall powder, reflected by the trends of the Kawakita parameters [41].

The Heckel and Kawakita equations are the two most commonly used compaction equations used for powders. Many others have been proposed over the years, although most are derivatives either the Heckel or Kawakita equations or versions specified to better fit specific compaction mechanisms [46]. Denny [42] showed mathematically that at low pressures relative to the yield strength of the particles within a powder, the Kawakita equation is simply a special case of a more general Heckel equation. The modification allows for the Kawakita equation to take into account unexplainable curvatures that are a common problem in Heckel plots [42]. These curves are often attributed to agglomeration in powders and empirical work has also been conducted

confirming the Kawakita equation is better suited for dealing with agglomerated powders at low pressures [47, 48].

3.1.3. Powder flowability

The measurement of powder flowability index is not a trivial matter and there are many methods in the literature developed to measure powder flow behavior. These include the angle of repose [49], the Hall Flowmeter [50], the Gravitational Displacement Rheometer [27], and the Freeman FT4 powder rheometer dynamic tester [51]. There also exists measurements based on the bulk density of the powder, such as the Hausner Ratio [32] and Carr's Compressibility Index [33].

The issue with such methods is that there is no way to measure the stress history or the stress being exerted on the sample. This means the tests are entirely qualitative and cannot be related to the first principles [52]. In a comparison test using seven different fine powder samples, six commonly used methods for measuring bulk powder behavior were examined by Leturia *et al.* [53]. The study showed only one technique measured intrinsic parameters of packed powder beds: shear testing [53].

The uniaxial shear test is a method capable of measuring the flowability of a powder bed using first principles, which is shown in the schematic in Figure 14. The pre-stress of the powder is controlled and the direct yield stress of the powder assemblage is measured. In this measurement, a powder is confined by σ_2 and a consolidation load, or the major principal stress is applied to form a powder assemblage. The pressure and confinement is then removed, and the axial load is then reapplied until the powder

assemblage fails. That critical load for failure is the unconfined yield stress of the powder for the applied major principal stress [54].

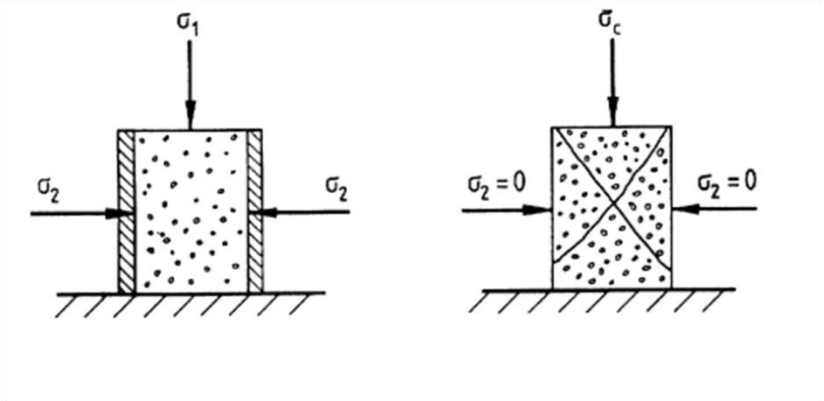

Figure 14. Schematic of uniaxial shear test [54].

The flow function of a powder is a commonly used and well-established metric to measure the cohesiveness of a powder. The flow function is measured by taking the ratio of the major principal stress, σ_1, to the unconfined yield stress, σ_c, of the powder, shown below in Equation 7.

$$ff_c = \frac{\sigma_1}{\sigma_c} \qquad \text{Equation 7}$$

Tomas found the flow function of several common powders and constructed a qualitative table showing the values of the flow function for varying degrees of cohesiveness, shown in Table 4 [55].

Table 4. Flowability assessment.

Flow function, ff_c	**Evaluation**
>10	Free flowing
4-10	Easy flowing
2-4	Cohesive
1-2	Very cohesive
<1	Not flowing

The issues of the uniaxial shear testing arise from the powder sample. The powder must be able to form an assemblage strong enough to stand on its own without confinement. This limits the test to relatively cohesive powders, as free-flowing powders cannot form strong enough assemblages. This issue also limits the test to relatively high consolidation pressures [54].

An alternative method to the uniaxial shear testing of powders is the use of a powder shear tester. Much of the work was pioneered by Jenike [56], but others have built on his work, and many other shear testers now exist [54]. Schulze clearly outlines the theory of how a powder shear tester is able to measure the major principal and unconfined yield stresses of a powder [9].

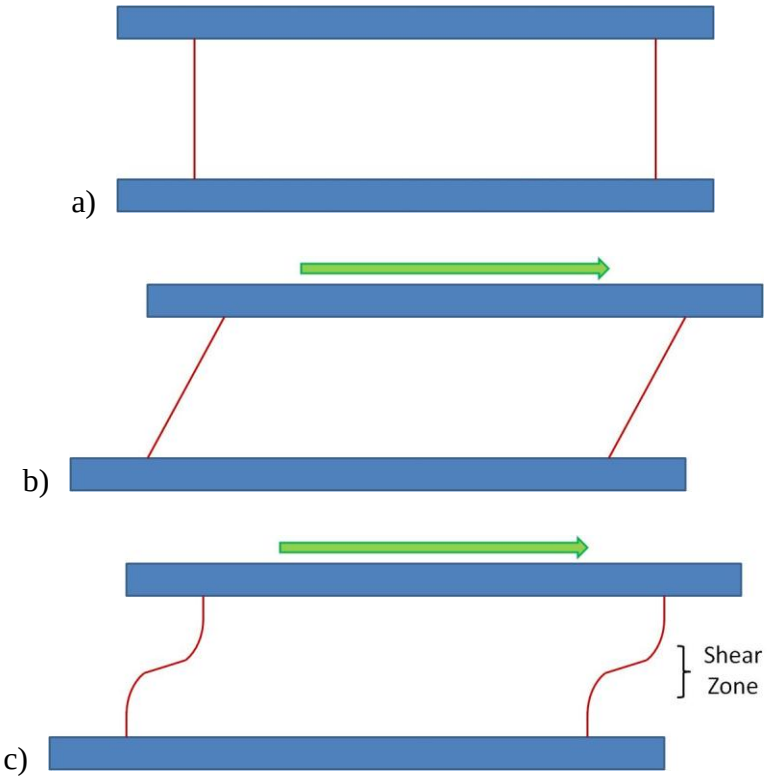

Figure 15. Deformation patterns of a material under shear, showing a) the initial shape, b) viscous liquid, and c) particulate solid.

The flow of a powder bed under shear differs from a traditional continuum material. Rather than exhibiting a linear shear profile, where shear deformation occurs through the entire volume of the material, flowing powders exhibit a narrow shear zone, as shown in Figure 15. Within this shear zone, the powder bed fails across a planar band of particles parallel to the direction of the shear, where the strain is high. Above and below the shear zone are two blocks of material in which there is little internal displacement [57]. The thickness of this band is dependent on the amount of consolidation on the powder, as shown in Figure 16 [58].

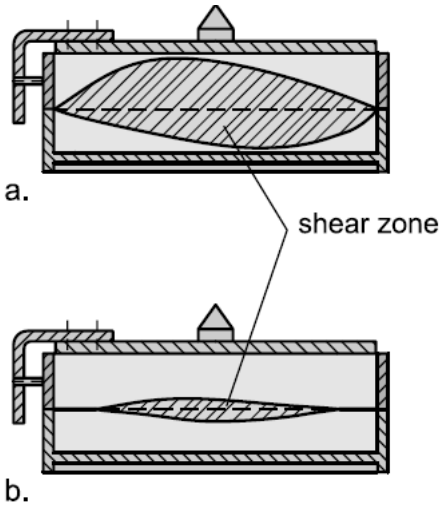

Figure 16. Shear zones of powder samples in a Jenike shear tester of an (a) underconsolidated sample and (b) overconsolidated sample [58].

As shown in Figure 16, the height of the shear zone of a powder under shear is dependent on the amount of consolidation of the sample. This is due to the configuration of the particles within the powder bed and amount of dilation needed to induce flow.

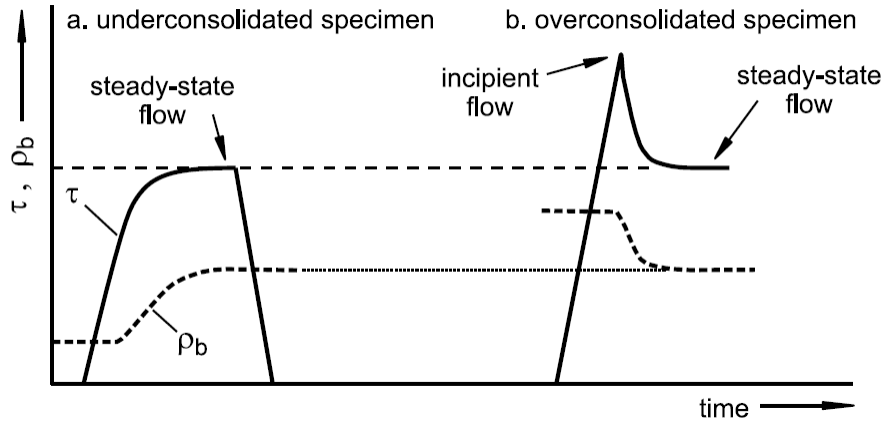

Figure 17. The shear stress and bulk density of an (a) underconsolidated powder bed and (b) overconsolidated powder bed[58].

As shown in Figure 17, the density of an underconsolidated bed increases when reaching steady-state flow. An underconsolidated powder has a looser packing fraction due to the structure provided by cohesion. When shear stress is applied, the particle structure collapses, increasing the packing fraction and the bulk density of the powder bed. As the packing fraction increases, the amount of shear stress to induce flow must also increase until the equilibrium level is reached. The shear zone as shown in Figure 16 is wide as the structure of the entire powder bed is collapsing under shear [58].

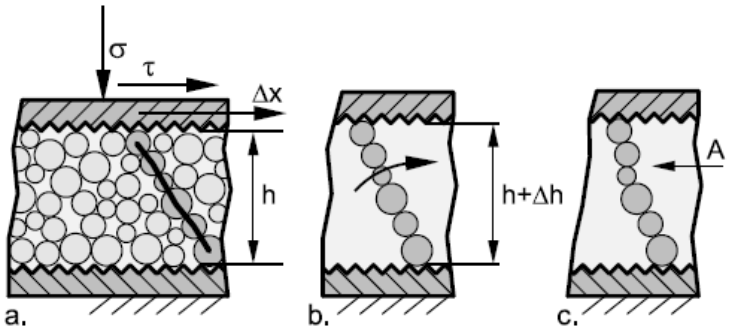

Figure 18. Configuration of a particle column with an overconsolidated powder bed under shear [58].

Conversely, for an overconsolidated sample, the particles are more tightly packed. As shown in Figure 18, when an over-consolidated sample is sheared, the particle columns are rotated. For this particle column to maintain its same length through rotation, the height of the entire bed must increase, or the powder must dilate. This is why Figure 17 shows a higher shear stress to induce flow, as the higher stress is necessary to dilate the powder bed. Consequently, the bulk density drops, and the shear stress then drops as well to reach the steady-state value [58].

The powder is first subjected to a preconsolidation load σ_{pre} and then a shear stress is applied. The shear stress is increased until steady state flow is reach. The critical shear at the preconsolidation load is called τ_{pre}. The axial load a shear stress is then removed from the powder. The same test is then measurement on the preconsolidated powder bed at a series of subsequent lower normal stresses, σ_{sh}. In between each σ_{sh}, the normal stress is raised to the preconsolidation stress and steady state flow is re-achieved to return the powder bed back to the same, precondition state. From the series of normal loads, σ_{pre} and σ_{sh}'s, and their corresponding critical shear stresses, τ_{pre} and τ_{sh}'s, a yield locus is constructed, shown in Figure 19 [9].

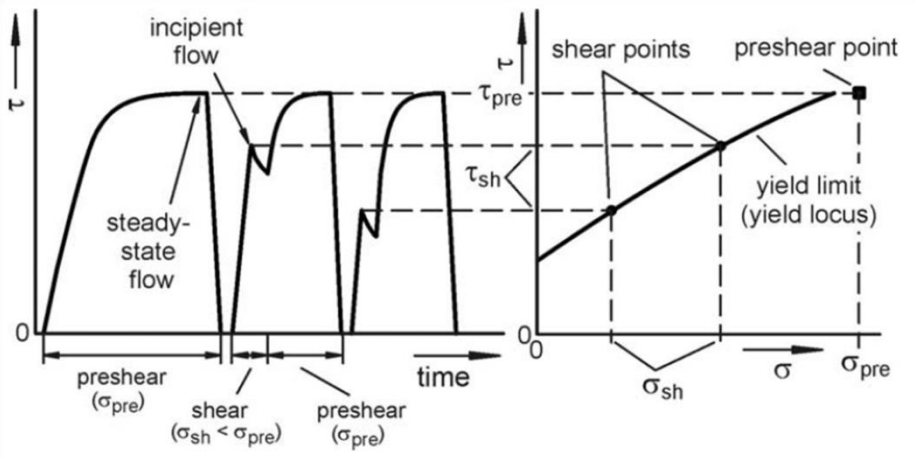

Figure 19. Construction of a yield locus of a powder bed from shear testing [9].

From the yield locus, a series of tangential Mohr's circles can be constructed. The Mohr circle tangential at the end point of the yield locus is used to find the major principal stress. The Mohr circle tangential to both the yield locus and the origin is used to find the unconfined yield stress [9]. This is shown in Figure 20.

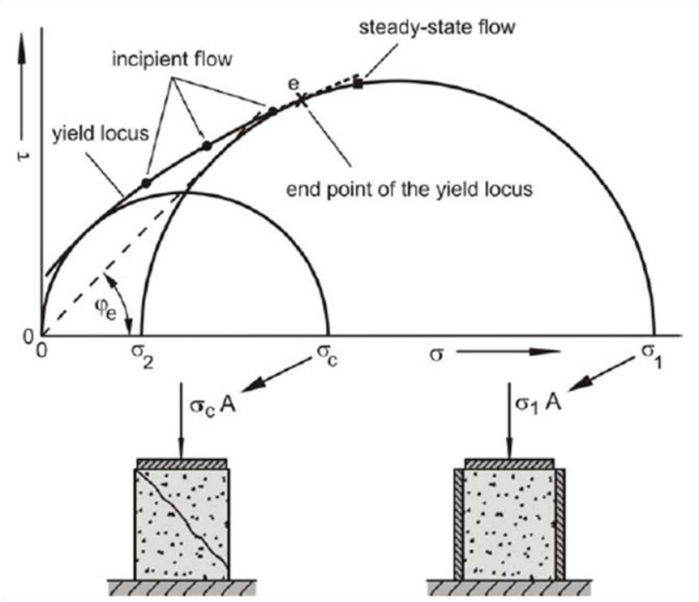

Figure 20. Correlation between the yield locus constructed by shear testing to the results of uniaxial testing of a powder [9].

Also shown in Figure 21 are several other flow properties of the powder. First are three different angles of friction of the powder. The simplest is the φ_{sf}, the angle of internal friction at steady-state flow. The effective angle of internal friction, φ_e, is taken by finding the angle of the dashed line, which runs linearly through the origin and is tangential to the greater Mohr circle. Both the angle φ_e and φ_{sf} is regarded as a measure of the internal angle of friction between the particles at steady-state flow. This measure is important in powder silo design. There is an angle of friction related to the incipient flow of the powder. This angle is known as the incipient angle of friction, and is found by finding the angle of the linearized yield locus. This is shown on Figure 21 as φ_{lin} and also called the linearized yield locus angle. Also shown is the value for cohesion and tensile stress of the powder, which are the y- and x- axis intercepts of the extrapolated yield locus respectively [58].

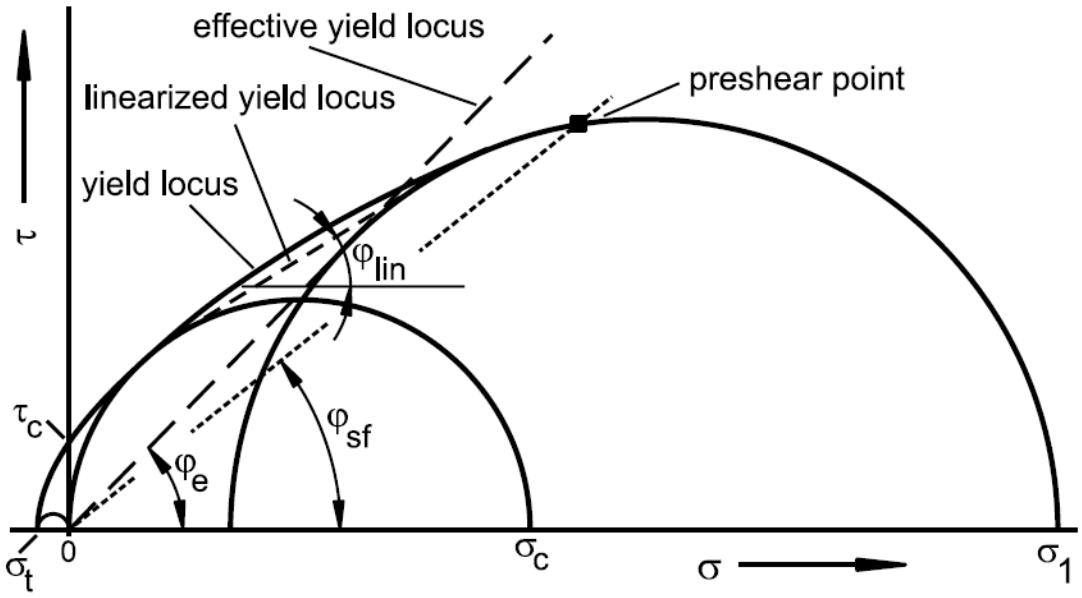

Figure 21. Flow properties of a powder bed given by the measurement of a powder yield locus by shear testing [58].

Shown in Figure 22 is a schematic of the Schulze annular shear cell. The shear cell is commonly used and well established in literature. By have an annular design, an infinite amount of strain can be induce on the powder bed. The consolidation force is exerted onto the lid to compact the powder axially. The lid is also locked into position by the crossbeam, to prevent any rotation. The base of the cell is rotated to shear the sample, with the applied stress and strain of the bed being measured [9].

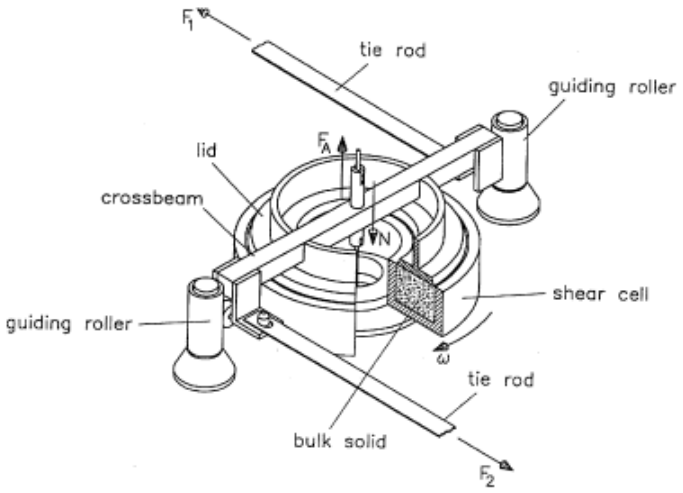

Figure 22. Schulze annular shear cell [9].

3.1.3.1. Effect of moisture

As the moisture is added to a dry powder bed, first water molecules adsorb onto the surface as bound water. As the moisture content is increased further, the surface become saturated and free water begins to bond on the surface. If enough free water becomes present on the surface of particles, capillaries may form at interparticle contacts. These capillaries can increase the adhesion between particles, resulting in increase cohesion and decrease of flowability in the bulk bed [59].

Emery [59] shows such a behavior in hydroxypropyl methylcellulose powder, where up to 10% moisture was added to the powder. The flow properties were then tested on a shear cell and showed a decrease in flowability up to 5% moisture. Above 5% moisture, the flowability of the bulk powder increased. This was attributed to the amount of free water on the particles becoming so great that a layer of moving water became present between particles, acting as a lubricant and decreasing friction between the particles [59].

In relatively dry powders where the moisture level is low, the effect of adsorbed moisture is not as significant. Landi *et al.* [60] measured the flow properties of glass beads at different relative humidity levels. The relative humidity was varied from 13-98%, and in that range, the glass beads adsorbed from 0.02-0.14 wt.% of moisture. At such low moisture contents, no significant change in flow properties was observed, although there was an increased variance in the data when measured at higher relative humidity levels [60]. A similar result was observed by Saw *et al.* [61], who measured various lactose powders in relative humidity levels ranging from 36% to 54%. Although the moisture uptake of the powders was not measured, the effect on the flow properties was insignificant [61].

3.1.4. Vibration behaviors of shallow powders beds

Vibration is very common in particulate process, with it used for applications such as powder conveyers, flow promotion. sieving and screening, comminution, compaction, mixing, and granulation [10]. Furthermore, unintentional vibrations commonly can be a byproduct of noise from other industrial processes [12]. For these reasons, the dynamic behavior of powders under mechanical vibration is of great importance to powder processing.

Thomas *et al*. [13] identified two main states of powders under vertical, mechanical vibration. There is an expanded state, where the bed undergoes turbulent flow and intense particle mixing. It can be characterized by powder bed dilation, with the increased volume facilitating the powder flow. In contrast, there is condensed state, where the bed can be treated as a single coherent mass, and there is a decrease in porosity

and compaction of the bed. These behaviors were observed in samples of glass beads, with sizes ranging from 74 to 841 μm. The frequency of the vibration was held constant at 25 Hz, with the amplitude varied between runs in the range of a few millimeters [13].

Research conducted by Gray and Rhodes [62] concentrated on studying the compaction behavior due to vibration. Powder beds were modeled under a sinusoidal vibration, and compaction of the powder was found to be related to the amount of energy transferred to the bed from the vibrator. Compacting behavior only occurred when the bed acted as a coherent mass. It was concluded that the cohesion within the powder must be high enough to maintain the bed as a coherent mass for compaction to occur [62]. If the powder cohesion was too low, the bed would exhibit an expanded state and bulk particle flow.

Hsiau and Pan [63] investigated the behavior of a powder bed under a wide range of vibration intensities to observe the different motion states of the powders and investigate transitions in behavior. For the study, relatively large glass beads with diameters of 3.00 mm were used. A vibration amplitude of 5 mm was used with the frequency of vibration adjusted to achieve different vibration accelerations. At low accelerations, the bed exhibited a heaping-like behavior, where convective motion within the bed would create a pile of particles with avalanches occur along the powder surface down the slope. As acceleration was increased, the granular bed began to jump, but maintained a coherent, condensed state. Higher acceleration values triggered a transition into an expanded state [63]. This leads to the conclusion that even cohesive powders can exhibit an expanded state if the vibration intensity is high enough to overcome the interparticle cohesion and create bed instability.

While empirical observations have created a base understanding of the dynamic behavior of powders under mechanical vibration, there is limited linkage between reasons for this bulk behavior to properties of the constituent particles [64]. In situ measurements of the intrinsic forces exerted on particles within a vibrated powder bed cannot be directly measured. The key may be the usage of modeling work to simulated vibrated powder beds [65-67] to advance the understanding of this behavior.

3.2. Experimental method

3.2.1. Uniaxial bulk compaction

Bulk powder compaction was conducted on an Instron 5566 Universal Testing Machine (Instron, Massachusetts, USA) using a cylindrical die. Attached to the instrument was a 20 mm diameter plunger and matching 20 mm diameter die. The die had a depth of 20 mm. A 1.40 mm aperture (14 mesh) sieve and funnel was used to load the powder sample into the die. The powder sample was preconditioned by passing it through the sieve to break up any large agglomerates that were present due to powder storage and handling as well as to distribute the powder homogeneously over the surface of the die [36]. Enough powder was used to fill approximately 70% of the die. The mass of the powder sample was measured before compaction.

The piston speed was set at 1 mm/minute to allow rate of compaction to occur in the static regime. For each powder, a sample was compacted to pressures of 5, 10, 20, 30, and 40 kPa. After compaction, the height of the plunger was taken as the height of the powder compact. The volume of the powder was then calculated, and the mass of the

powder sample was used to determine the contact of the density. For each measurement, three runs were made and average taken.

3.2.2. Shear cell measurements

Flowability measurements of the powder were conducted using a Schulze annular shear cell (Model RST-XS, Wolfenbüttel, Germany) following the standard operating procedure [68]. Eight different preconsolidation loads were chosen, ranging from the minimum to maximum load capable by the instrument in order to understand the full behavior of the powder. For each load, five evenly spaced, lower consolidation stresses were tested to measure incipient flow, shear points. This allows for a reliable yield locus to be constructed, necessary in an accurate calculation of bulk cohesion. The preconsolidation loads and subsequent shear point consolidations are shown in Table 5.

Table 5. Full test conditions for yield locus construction in shear testing, showing each preconsolidation stress (σ_{pre}) and shear point consolidation stress (σ_{sh}).

σ_{pre} (Pa)	**500**	**σ_{pre} (Pa)**	**750**	**σ_{pre} (Pa)**	**1000**	**σ_{pre} (Pa)**	**2500**
$\sigma_{sh,1}$	450	$\sigma_{sh,1}$	650	$\sigma_{sh,1}$	900	$\sigma_{sh,1}$	2200
$\sigma_{sh,2}$	400	$\sigma_{sh,2}$	550	$\sigma_{sh,2}$	800	$\sigma_{sh,2}$	1900
$\sigma_{sh,3}$	350	$\sigma_{sh,3}$	450	$\sigma_{sh,3}$	700	$\sigma_{sh,3}$	1600
$\sigma_{sh,4}$	300	$\sigma_{sh,4}$	350	$\sigma_{sh,4}$	600	$\sigma_{sh,4}$	1300
$\sigma_{sh,5}$	250	$\sigma_{sh,5}$	250	$\sigma_{sh,5}$	500	$\sigma_{sh,5}$	1000
σ_{pre} (Pa)	**5000**	**σ_{pre} (Pa)**	**10000**	**σ_{pre} (Pa)**	**15000**	**σ_{pre} (Pa)**	**20000**
$\sigma_{sh,1}$	4200	$\sigma_{sh,1}$	8200	$\sigma_{sh,1}$	12200	$\sigma_{sh,1}$	16200
$\sigma_{sh,2}$	3400	$\sigma_{sh,2}$	6400	$\sigma_{sh,2}$	9400	$\sigma_{sh,2}$	12400
$\sigma_{sh,3}$	2600	$\sigma_{sh,3}$	4600	$\sigma_{sh,3}$	6600	$\sigma_{sh,3}$	8600
$\sigma_{sh,4}$	1800	$\sigma_{sh,4}$	2800	$\sigma_{sh,4}$	3800	$\sigma_{sh,4}$	4800
$\sigma_{sh,5}$	1000	$\sigma_{sh,5}$	1000	$\sigma_{sh,5}$	1000	$\sigma_{sh,5}$	1000

The effect of the absolute humidity of the environment was tested on the flowability of the powders. This was achieved by storing and testing the powders under controlled environmental conditions. The environment was controlled by conducting the test in a sealed glove box with the absolute humidity kept constant with the use of saturated salt solutions. If kept in a closed system, the different vapor pressures of different saturated salt solutions create different absolute humidity levels of enclosed air [69].

The cohesion of the two powders was measured using a Schulze annular shear cell. The original run of measurements at varying major consolidation stresses was conducted in ambient laboratory conditions, with the relative humidity at roughly 20% to 40%, or absolute humidity of 4 to 8 g/L. The powders were rerun under controlled conditions. The shear cell was placed in a glove box and the absolute humidity was controlled using saturated salt solutions. The low relative humidity was achieved by using magnesium chloride, yielding a relative humidity of 30-31.5% and, and the high value by using sodium chloride, yielding a relative humidity of 70.8-72.2%. These values corresponded to absolute humidity values of 6 and 14 g/L, respectively, given the temperature and barometric pressure of the laboratory at the time of testing. The powders were stored for at least 24 hours under the stable humidity before testing within the same chamber.

3.2.3. Mechanical vibration

An electrodynamic shaker (Model K2007E01, The Modal Shop Inc., Ohio, USA) was used to apply the mechanical vibration to the powder bed. A schematic diagram of

the experimental setup is shown in Figure 23. A signal generator (Model TG315, Thurlby Thandar Instruments Ltd., Huntingdon, UK) created a digital, sinusoidal wave, which is converted to a mechanical vibration by the electrodynamic shaker. The powder was placed in an acrylic box with side dimensions of 60 mm, which was vibrated by the electrodynamic shaker in a vertical motion. The motion was monitored using a FASTCAM SA5 high speed camera (Photron, California, USA) to independently check the applied frequency and amplitude. For the test, the amplitude of the mechanical vibration was varied from 0.64 to 1.00 mm and the frequency of vibration varied from 35 to 50 Hz.

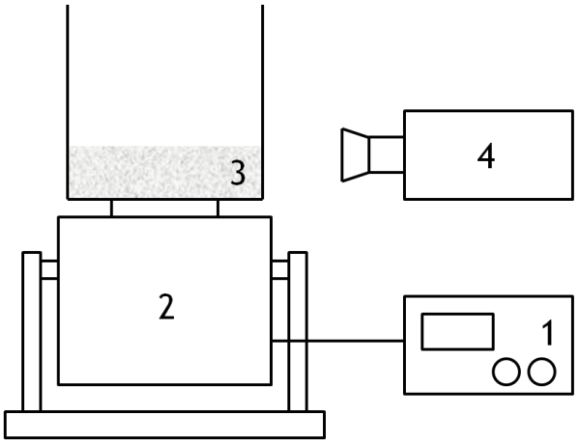

Figure 23. Experimental setup showing the (1) signal generator, (2) electrodynamic shaker, (3) powder bed in acrylic container, and (4) high speed camera.

3.3. Results and discussion

3.3.1. Loose-packed bulk density

The loose-packed bulk density of powder samples were measured using a Freeman FT4 powder tester (Freeman Technology, Tewkesbury, UK). The default

method to measure conditioned bulk density was used. The preconditioning step using impeller blade resulted in a reliable and robust measurement of the loose-packed density of dried powders. The results are shown for the four powder samples in Table 6. Since the particles densities, shown in Table 3, are relatively similar for each of the powder samples, the differences in loose-packed bulk density of the samples can be attributed to powder cohesion. The two titania powders, AT1 and DT51, have a considerably lower bulk density than the A16SG and A3500SG alumina powders. This would imply the titania powder samples are more cohesive than the alumina powders.

Table 6. Conditioned bulk density of powder samples measure of a Freeman FT4.

Powder	Loose-packed BD (g/cm^3)
A16SG	1.13
A3500SG	1.21
DT51	0.40
AT1	0.66

3.3.2. Powder compaction

The compaction behaviors of the powder samples were measured by uniaxial compaction and shown in Figure 24. Each data point represents an average of three measurements. Powder bulk densities were measured at 5, 10, 20, 30, and 40 kPa. It is important to note the data is an absolute bulk density instead of a percent bulk density, and the differences in the bulk densities of the powders are caused not only by the different compressibility of the powders, but also the different particle densities. There are not clearly defined stages of compaction in the compaction curves of the powders. Therefore, a transition yield point cannot be determined.

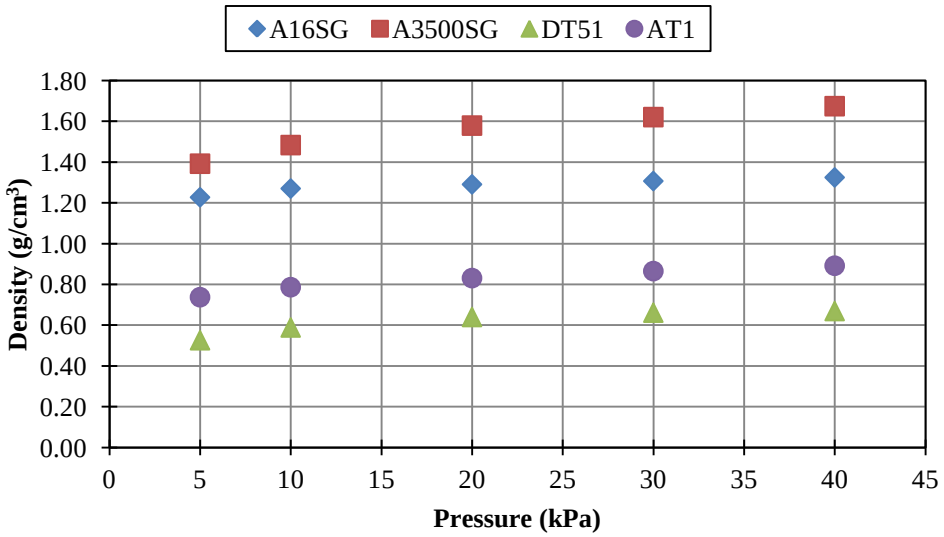

Figure 24. Uniaxial compaction data of powder samples.

The results of the powder compaction were graphed to analyze the data using the Kawakita analysis. To calculate relative volume decrease of each powder, the compressed volume was measured by uniaxial compaction at each applied pressure. The initial volume of each powder was taken as the loose-packed density of the powder, and the values for each sample is shown in Table 6. The ratio of the applied pressure to the relative volume decrease was graphed as a function of the applied pressure and shown in Figure 25. Figure 25 also shows the linear regression for each curve generated. Each curve exhibits a R^2 value greater than 0.95 or 95%. Therefore, the linear fits are considered significant [70].

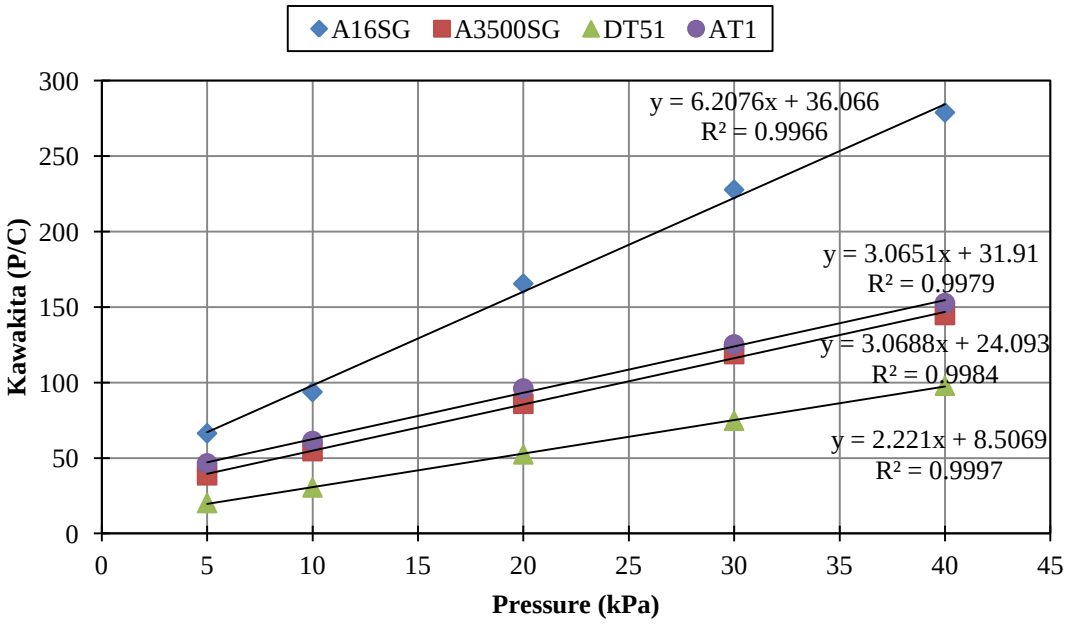

Figure 25. Kawakita analysis data of bulk powder compression data.

From the Kawakita equation, the *a* and 1/*b* parameters were calculated from the slopes and y-intercepts of the linear regressions. The values are shown in Table 7. The A16SG alumina powder has the smallest *a* parameter. This is indicative of a powder that has a high default packing and does not compact further greatly with compression. This behavior is common with very flowable powders. The other powders exhibit a higher *a* parameter, which suggests a more cohesive behavior. Concerning the 1/*b* parameter, the DT51 titania powder has the lowest value. This implies the powder compresses a high degree under low loads. In contrasts, the AT1 titania has the highest 1/*b* parameter value, which suggests a strong powder structure and relatively high amount of pressure necessary to compress the powder.

Table 7. Kawakita parameters of powder samples.

	a	1/*b*
A16SG	0.16	5.81
A3500SG	0.33	7.85
DT51	0.45	3.83
AT1	0.33	10.41

3.3.3. Shear cell testing

Shown in Figure 26, the flow function of the powders is presented as a function of major principal stress. Each data point represents the average of three measurements. The flowability of the powder increases with greater values of flow function. From the measurements, it is apparent that the two titania powder, AT1 and DT51, and the least flowable over the range of major principal stresses. Likewise, the A16SG alumina is the easiest flowing powder. The A3500SG powder had the greatest variation as major principal stress was altered, with the powder exhibiting extremely cohesive behavior at low pressures while being relatively free flowing at high pressures. While it is often expected that the flow function of powders increase with increasing major principal stress, the AT1 titania exhibits the opposite trend, with a very constant flowability that even decreases at higher major principal stresses.

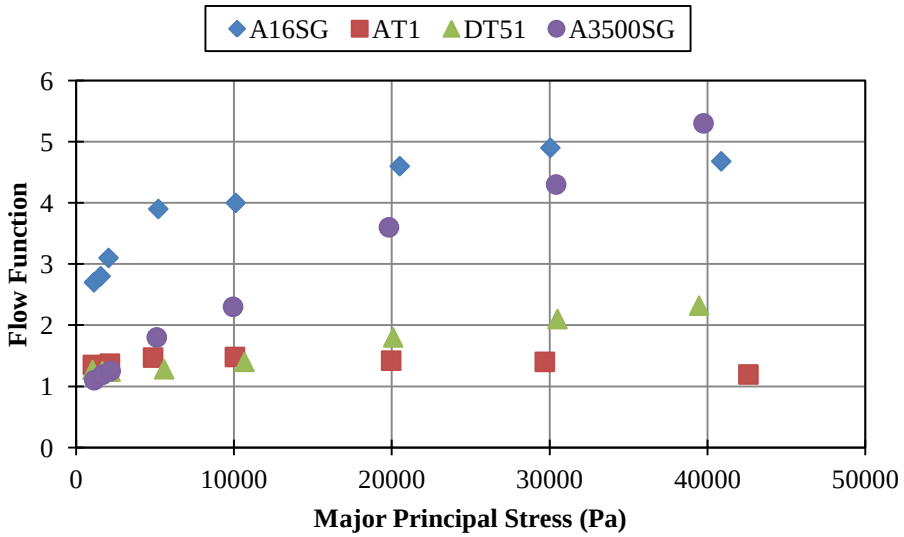

Figure 26. Flow function of powder samples measured on a Schulze annular shear cell.

The unconfined yield stress of the powder over the full range of major principal stresses is shown in Figure 27. As expected, the less flowable a powder behaves, the greater the stress that must be applied to induce flow. The AT1 titania, which exhibited a relatively constant flow function, shows the most linear relationship between unconfined yield stress and pressure. In Figure 28, the low values of major principal stresses are only shown to emphasize the behavior of the powder with relatively little compaction. The AT1, DT51, and A3500SG powders all have very similar yield stresses at the low pressures, with only A16SG, which is the most flowable, having a noticeably lower unconfined yield stress.

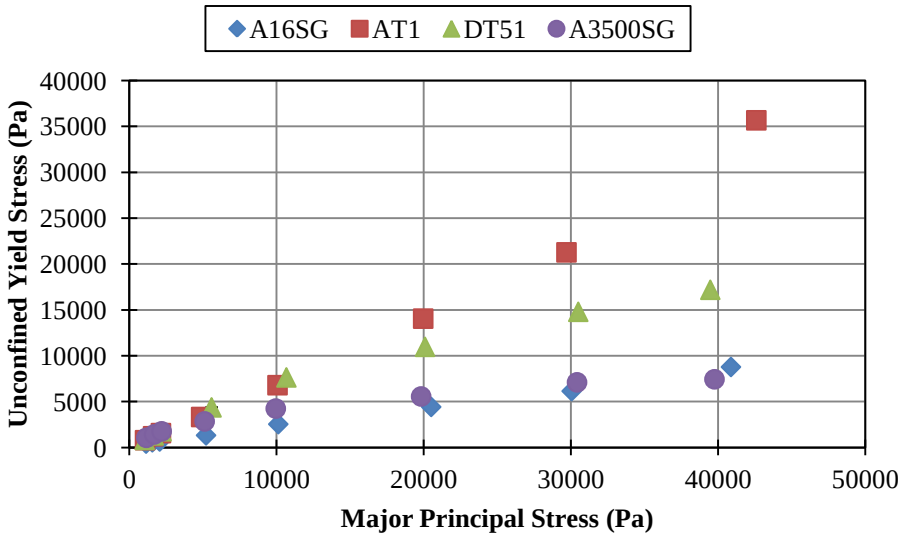

Figure 27. Unconfined yield stress of powder samples measured on a Schulze annular shear cell.

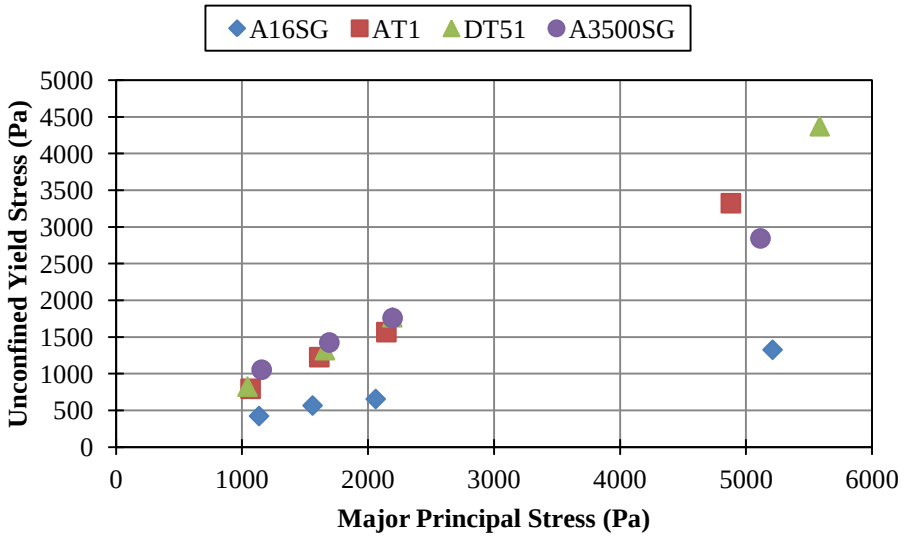

Figure 28. Unconfined yield stress of powder samples measured on a Schulze annular shear cell at low pressures.

In Figure 29, the extrapolated cohesion of the powders shows a very similar trend that is shown with the unconfined yield stress. The two powders having the greatest range of cohesion values, AT1 and DT51, also have the highest flow functions. A note should be made of A3500SG, which has a cohesion value that does not increase as dramatically relative to the other three powders. When viewing the flow function of the A3500SG powder, it is shown that the powder becomes very flowable at higher pressures. The fact the cohesion does not greatly increase explains why the flowability rises so dramatically.

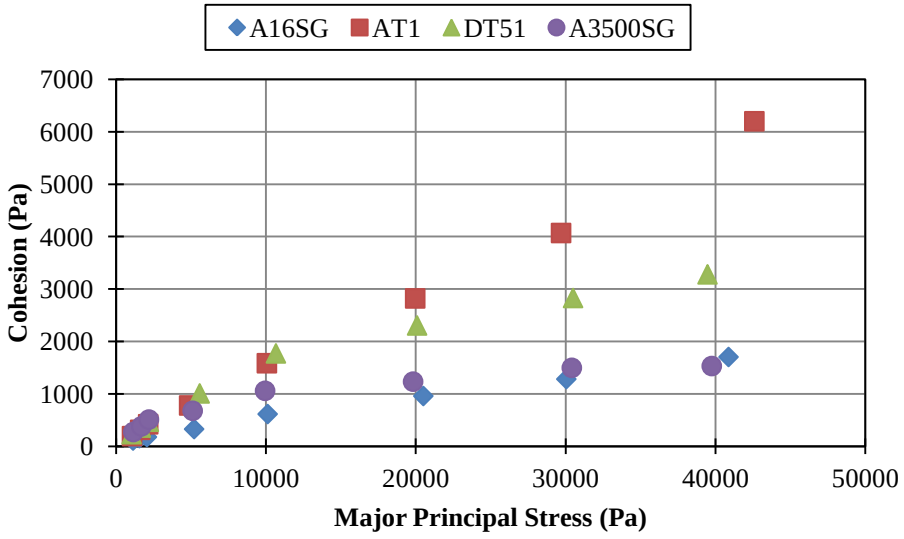

Figure 29. Cohesion of powder samples measured on a Schulze annular shear cell at low pressures.

The bulk cohesion of the powders measured by the shear cell testing shown in Figure 29 can be traced back to the physical properties of the constituent powder variants. The most cohesive powder, the AT1 titania, has the finest particle size of the four variants, with a d_{50} particle size of only 0.1 μm. This result is in agreement with the

theory of Etzler and Uddin [2] that cohesion increases with decreasing particle size. The DT51 titania powder, the second most cohesive powder, has the highest BET surface area at 80.88 m^2/g, as shown in Table 1, agreeing with the theoretical model set forth by Johnson *et al.* [5].

3.3.3.1. Effect of relative humidity on powder flowability

The effect of moisture on the powder behavior was studied by storing and testing the powders at different levels of absolute humidity. The cohesion of the AT1 and DT51 powders were measured on the Schulze shear cell within a controlled environment to test the effect of the absolute humidity on the flow behavior. The environment was controlled by conducting the test in a sealed glove box with the absolute humidity kept constant with the use of saturated salt solutions. Only the AT1 titania, the most cohesive powder, and the DT51 titania, the powder that adsorbs the greatest amount of water, were investigated in this study.

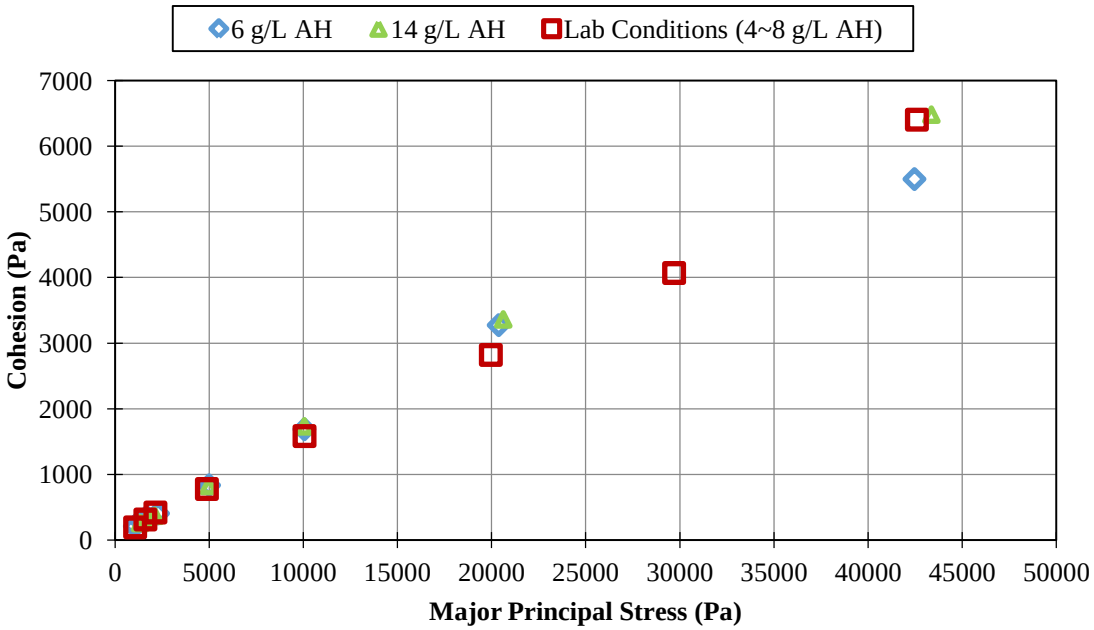

Figure 30. Cohesion of AT1 titania at different absolute humidity levels.

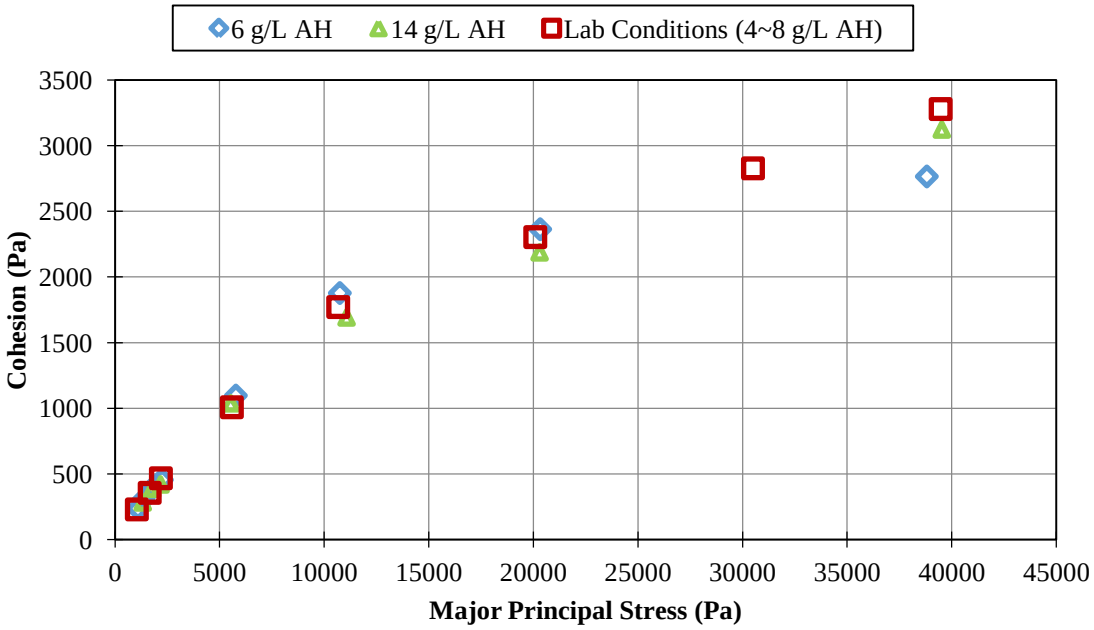

Figure 31. Cohesion of DT51 titania at different relative humidity levels.

The results, shown in Figures 30 and 31, show a comparison of the cohesion measurement for the two powders tested at different relative humidity level ranging from 30-31.5% and 70.8-72.2%. These relative humidity values corresponded to absolute humidity values of 6 and 14 g/L, respectively, and were also compared to tests conducted in ambient laboratory conditions. Between the three measurements at different relative humidity levels, there was no change in cohesion. Therefore, the results show no effect of the relative humidity of the environment on the cohesion of the powder.

Even though the previous results discussed in Section 2.3.4. showed that the two powders adsorbed a significant amount of water, the shear cell results shown in Figures 30 and 31 show the adsorbed moisture does not affect the flowability of the powder. Therefore, for the work conducted in this thesis, all powder testing was conducted in normal, ambient laboratory conditions, which was maintained with the tested range of absolute humidity levels, 4 to 14 g/L absolute humidity.

The implications of this result for powder processing is that procedures dealing with powder flow, such as powder conveying or compression, are not affected by changes in the relative humidity of the ambient conditions. Moisture is still adsorbed by the particles and can affect formulations later in the processing, but the physical behavior of the powder will not be affected.

The powders used in this test were both inorganic materials that adsorbed moisture physically and completely reversibly. The author speculates the effect can be different for powders that chemically or irreversibly adsorbed water. Such moisture on the powders can change the surface chemistry of the particles. As particle adhesion is

related to particle surface energy [5], chemisorbed water could change the cohesion of the bulk powder.

3.3.4. Dynamic behavior of powders under mechanical vibration

The different powder samples exhibited very different dynamic behaviors under mechanical vibration. This behavior was captured by imaging the powder bed during the vibration. Video clips were taken by placing a camera above the powder bed, looking down at the surface of the bed. From these overhead videos, still shot images were taken of the powder bed surface, shown in Figures 32, 33, and 34. From the perspective of the camera, the vertical vibration of the powder bed is in-and-out of the page. On the left and right side of each image are clear panes of acrylic acting as braces on the top of the sample box. Each figure shows a series of three images, with a 30 second time lapse between each image. The first image was taken after the powder bed had been vibrated for 15 minutes. The images were taken under a vibration condition of 1 mm amplitude and 50 Hz frequency. Roughly the same dynamic behavior of each sample as shown in the images was viewed for all vibration conditions tested.

The dynamic behavior of the A3500SG alumina powder is shown in Figure 32. In each of the three images, the surface of the powder is different due to the observed convection of powders under mechanical vibration. The powder sample exhibited an expanded-state, fluidized bed. This same behavior is also exhibited by the A16SG alumina powder sample.

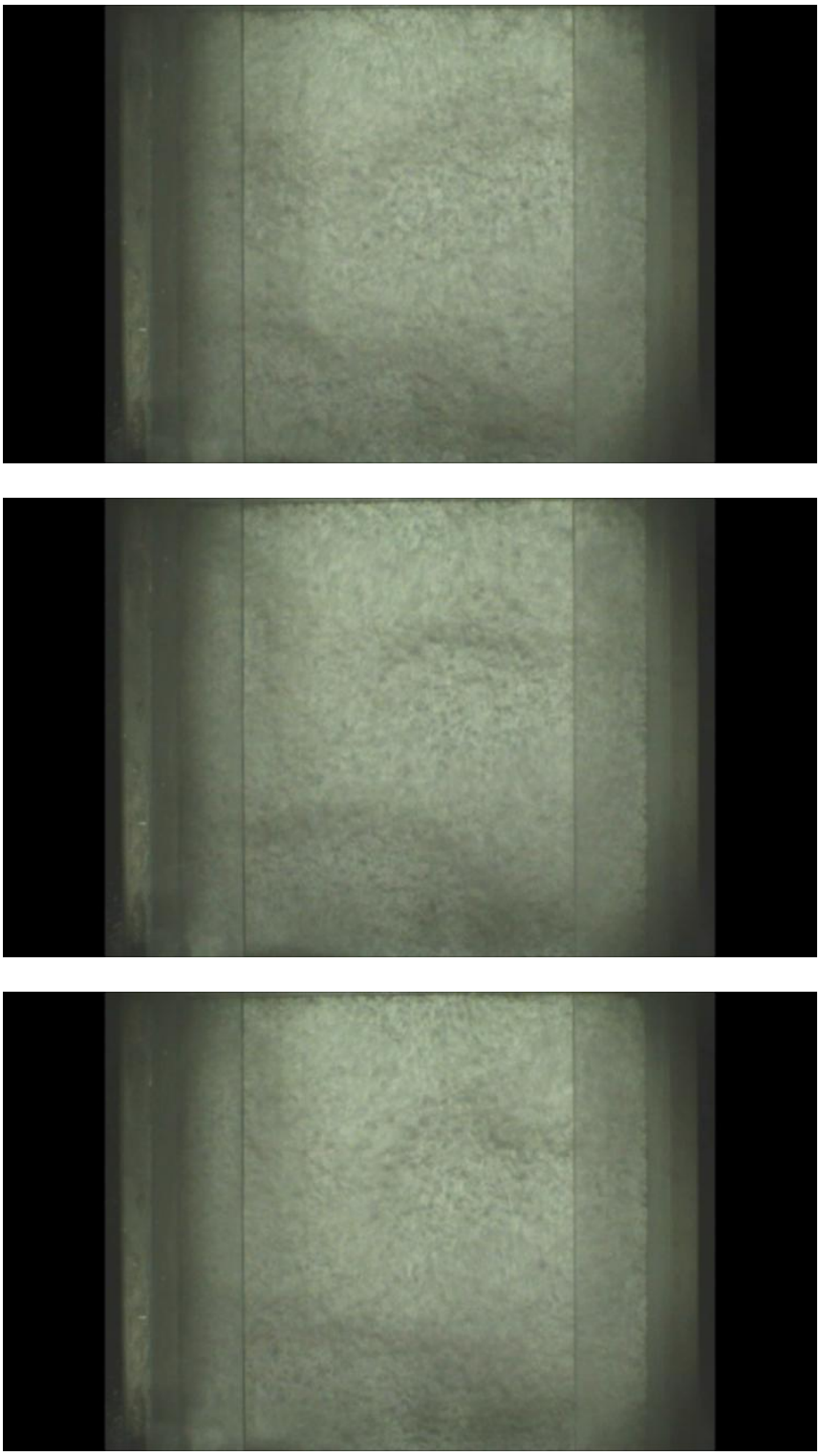

Figure 32. Overhead view of A3500SG powder bed after (top) 15 minutes, (middle) 15 minutes 30 seconds, and (bottom) 16 minutes of mechanical vibration.

Figure 33. Overhead view of DT51 powder bed after (top) 15 minutes, (middle) 15 minutes 30 seconds, and (bottom) 16 minutes of mechanical vibration.

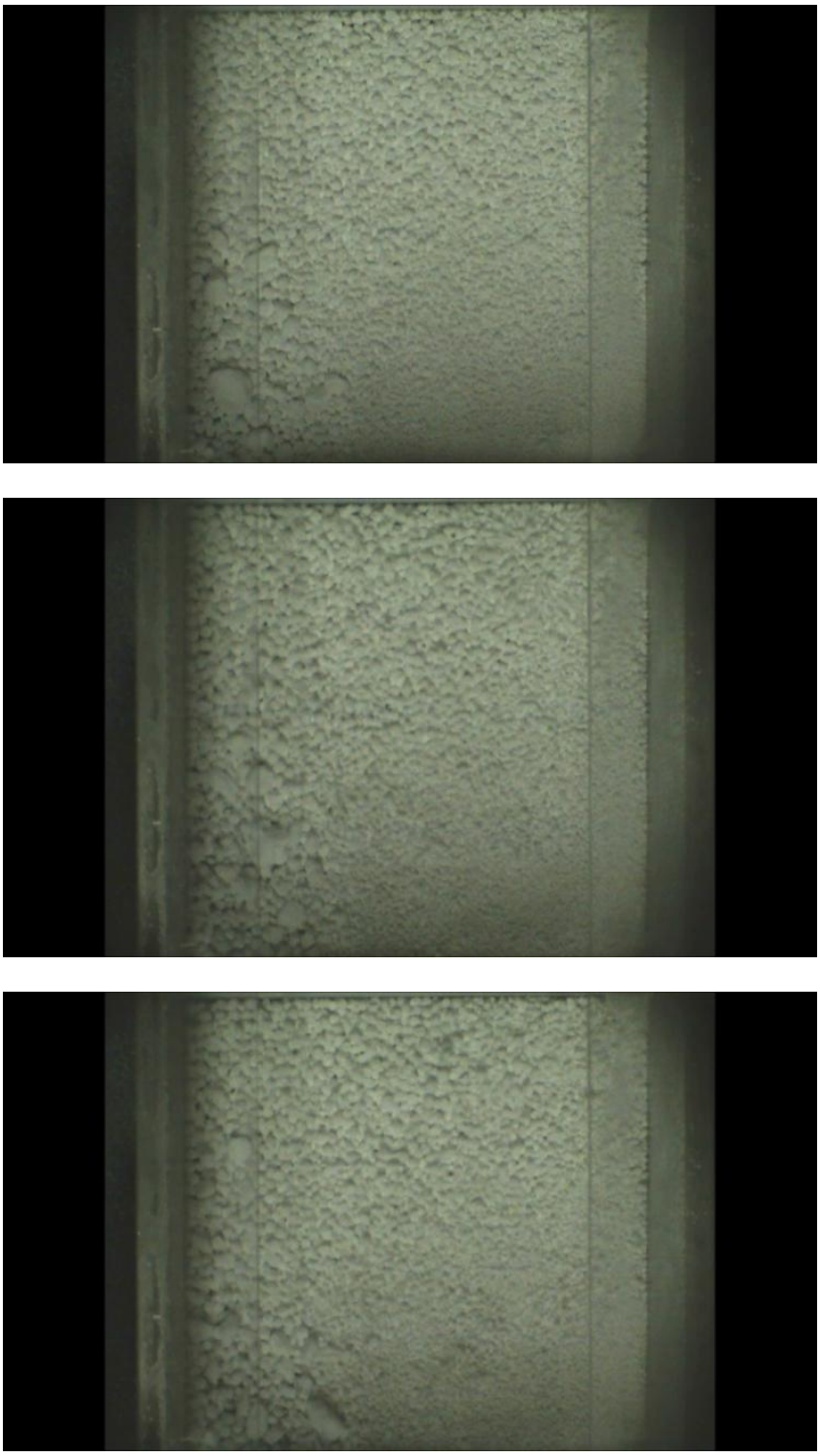

Figure 34. Overhead view of AT1 powder bed after (top) 15 minutes, (middle) 15 minutes 30 seconds, and (bottom) 16 minutes of mechanical vibration.

Shown in the Figure 33, the behavior of the DT51 titania powder is different than the observed behavior of the alumina powder samples. In each image, the surface of the powder bed is static and unchanged. The powder bed is in a coherent, condensed-state and has formed a dense, compacted cake on the base of container. There is no observed movement to the powder cake under mechanical vibration after the cake has formed.

Figure 34 shows the behavior of the AT1 titania powder sample under mechanical vibration. Clearly visible on the surface of the bed are discrete, individual granules. The granules on the surface move around over the series of the three images, showing a convection of the granular bed. This granulation behavior is known as auto-granulation and discussed in detail in Chapter 4.

To provide a clearer description of the powder behavior, illustrations of the observed behaviors is shown in Figure 35 as a side view of the container during vibration. Insight into the mechanisms of the powder behavior can be gained by reviewing the bulk properties of the powder.

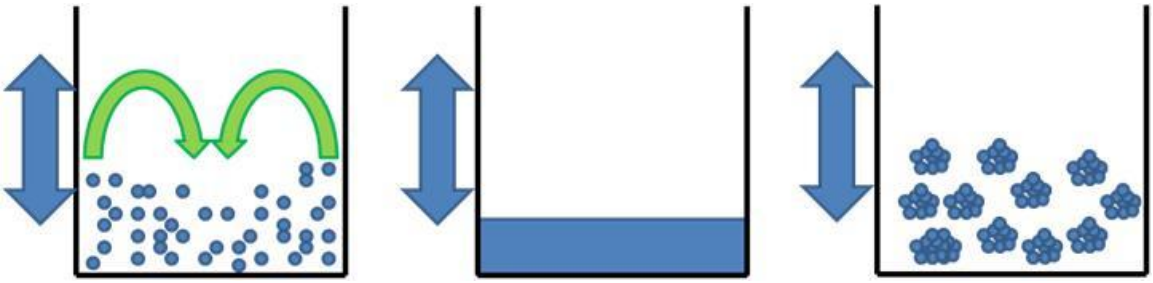

Figure 35. Illustrations of powder behaviors under mechanical vibration with (left) fluidization exhibited by A16SG and A3500SG, (center) compaction exhibited by DT51, and (right) auto-granulation exhibited by AT1. Arrows show the direction of vibration.

The A16SG and A3500SG powder samples exhibited bulk fluidization under mechanical vibration. This is similar to the expanded state powder bed characterized by powder bed dilation and convection described by Thomas *et al.* [13]. The two powders exhibiting this behavior, A16SG and A3500SG, have the lowest cohesion values at higher major principal stresses, as shown in Figure 29. This would allow the powder bed to flow, even under the applied stress of the vibration.

The DT51 titania sample compacted under vibration and had the highest *a* parameter and lowest 1/*b* parameter from the Kawakita analysis of powder compression, shown in Table 7. The high *a* parameter is a property of a powder that undergoes a high degree of compaction when compressed. A low 1/*b* parameters means the powder compacts under relatively little pressure, or is "easy" to compact. This is indicative of a powder that will compact a high degree under relatively low pressure, which would be a necessary property of a powder that compacts into a dense cake under vibration, such as the DT51 titania powder.

In contrast, the AT1 titania powder has the highest cohesion values and highest 1/*b* Kawakita parameter. This powder exhibited auto-granulation, where the mechanical vibration induced the nucleation and growth of particle clusters which maintained a structural integrity. The inherent strength of the formed granules allowed them from deforming under their own weight. These two properties, the high powder cohesion, to prevent fluidization of the powder bed, and the high 1/*b* Kawakita parameter, to prevent bulk compaction, are the critical properties controlling the dynamic behavior of the powder beds under mechanical vibration.

4. Meso-scale – Auto-granulation behavior

4.1. Background

4.1.1. Granulation theory

The behavior of size enlargement is common in many powder processes [10, 71]. For this reason, there is an interest to be able to understand how size enlargement of powders occurs under given conditions. A process conducted specifically to induce size enlargement in a powder is known as granulation. Granulation is an example of particle design and is used to produce desired attributes of a powder, such as reducing dusting, improving flow, increasing bulk density, reducing the pressure loss for fluid flow through a packed bed, and increasing the co-mixing of particles that would otherwise segregate [72].

4.1.1.1. Wet granulation

The most common methods for granulation include the addition of a wetting agent or binder solution to the powder to promote the clustering of particles [1]. This is commonly achieved by spraying a liquid binder onto particles as they are agitated in a device such as a tumbling drum, fluidized bed, or high shear mixer. The wetting of the dry powder is a key step to the granulation process. The particles of the powder must be coated by the liquid for the powder to begin to coalesce into granules and grow [72]. Ennis *et al.* [3] created a model of this behavior by viewing the causes of granulation in particles at a micro-level. The approach assumed that within the granulation process,

there were particle-to-particle collisions. When a collision occurred, there were two potential outcomes: coalescence, where the two particles stick together to form a larger particle; or nothing, where the two particles rebound off one another. This is illustrated by Figure 36 [3].

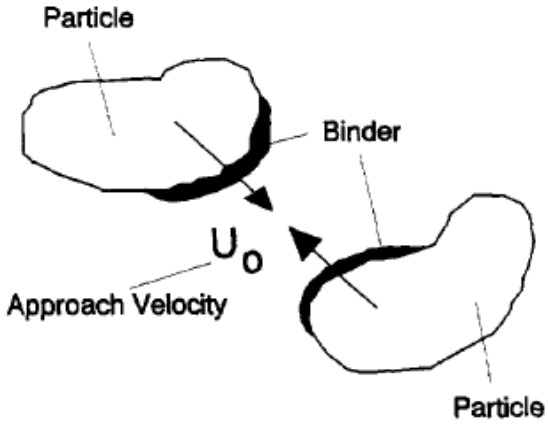

Figure 36. Illustration of two particles coated with binder layers colliding with approach velocity of U_0 [3].

In the studied system, the particles are coated with a viscous binder and the mechanism in which the particles granulated is said to be controlled by a dimensionless Stoke's number, which is a function of relevant factors. This Stoke's number for coalescence of a particle is a ratio of the kinetic energy of the colliding particles over the dissipating energy of the liquid binder bridge between the two particles, given by

$$St_{coal} = \frac{initial\ kinetic\ energy}{dissipated\ energy\ in\ the\ bridge} = \frac{2m_p U_0^{\,2}}{2F_{vis}h} \qquad \text{Equation 8}$$

$$St_{coal} = = \frac{8\rho_p U_0 a}{9\mu} \qquad \text{Equation 9}$$

where m_p is the mass of the particle, U_0 is the particle velocity, F_{vis} is the viscous force of the binder, and h is the half the thickness of the liquid bridge between the colliding

particles. Equation 8 can be simplified to Equation 9 by substituting parameters of the binder, where ρ_p is the particle density, a is the particle radius, and μ is the viscosity of the binder. If a critical Stoke's number, St^*_{coal}, is assumed where below this value the outcome of the collision is coalescence and above this value is no coalescence, the condition for successful coalescence has been defined [3].

In terms of particles of two different sizes, this theory can explain the snowball-effect of granulation, where a large granule consumes smaller particles. This is due to St_{coal} and particle size, a, being directly proportional. If a small particle collides with a large granule, the particle size, a, of the particle will be small, resulting in a small St_{coal} and the coalescence of the particle onto the granule. Conversely, as a large agglomerate or a granule collides with another granule, the a and St_{coal} will both be large, resulting in no coalescence.

Tardos *et al.* [4] built on the work by Ennis [3], using the same Stoke's number approach to define the condition for the deformation, or breakage, of a granule. For a given granule subjected to a shearing force, the Stoke's number for deformation, St_{def}, is given by the ratio of the kinetic energy of the shearing mass over the resisting internal energy of the granule. There would also exist a critical Stoke's number, St^*_{def}, in which conditions with a greater St_{def} result in breakage of the granule and a lower St_{def} result in the granule remaining undeformed. The St_{def} of a sheared granule is given by

$$St_{def} = \frac{externally\ applied\ kinetic\ energy}{energy\ required\ for\ deformation} = \frac{m_p U_0^2}{2V_p \tau(\gamma)} \qquad \text{Equation 10}$$

where V_p is the volume of the particle and $\tau(\gamma)$ is the strength of the granule as a function of the shear rate[4].

As both the St_{coal} and St_{def} are functions of particle size, the particle size of each can be solved for as a function of the Stoke's number. If the critical Stoke's number of each condition, St^*_{coal} and St^*_{def}, are known, the critical particle size at each condition can also be known, allowing the model to predict the resultant granule size of a sheared powder bed given certain relevant factors. This is shown schematically in Figure 37 and implies that the powders would grow to an equilibrium granule size for a given processing shear rate at a regime where the driving force for growth is cancelled by the driving force of deformation. As there is a range between the equilibrium particle sizes, a_{coal}^* and a_{def}^*, for the two mechanisms, there would be a distribution of sizes in the equilibrium population of particles after the granulation process. Also, as the particle sizes are a function of collision velocity of the particles, U_0, which is controlled by the granulation process parameters, the process can be tuned to create granules of a given equilibrium particle size distribution [4].

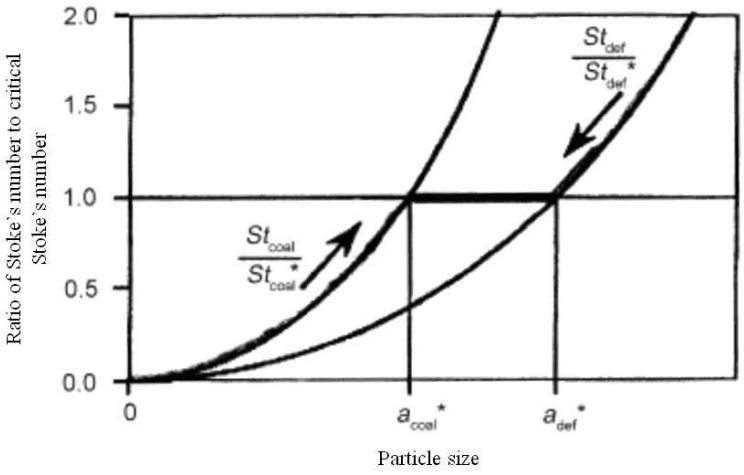

Figure 37. Graph of both St_{coal} and St_{def} as a ratio as a function of the particle size [4].

4.1.1.2. Dry granulation

Dry granulation is the term given to a granulation process that does not include the use of a binder or wetting agent. Without the presence of a binder layer, there is only inter-particle adhesion to dissipate the collision energy between two like-sized particulate units. Unless the adhesive properties of the particles are relatively large, the collision between two particles would most likely result in rebound [71]. While the work by Ennis *et al.* [3] and Tardos *et al.* [4] was on granulation with binder present in the system, the same premise can be applied the binderless, auto-granulation except by replacing the viscous force of the binder layer with the adhesive force between particle.

Horio has researched into binderless granulation using the method of pressure swing granulation (PSG). In PSG, the powder is placed in a fluidized bed column and the air flow within the column is cyclically changed between a compacting, downward flow and fluidizing, upward flow through the bed [73]. The process, shown in Figure 38, compacts the powder bed into a cake, then switches the airflow to break the cake into large clusters which collide with other clusters and the column wall to form granules. This alternating compacting downward flow and upward fluidizing flow created granules with an inherit strength [73].

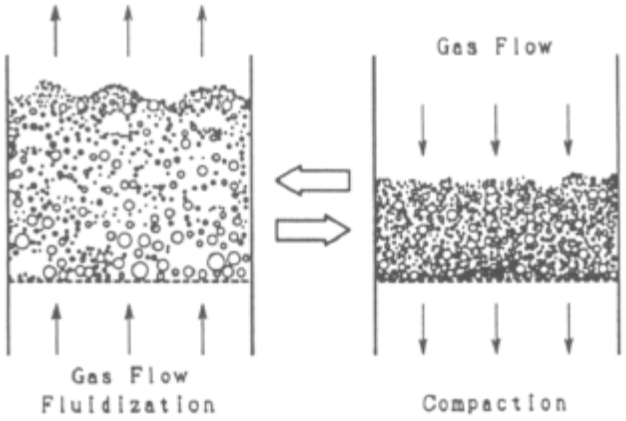

Figure 38. Schematic of pressure swing granulation (PSG) showing both the fluidizing and compacting gas flows of the cyclic process [73].

This process has been used to produce dry granules from TiO_2 and ZnO [73], Al_2O_3 [6], and lactose powders [74]. The size of the granules produces ranged from 100 to 1000 μm, which was dependent on not only the material properties, but also the processing parameters, such as the compaction and fluidizing air pressure amplitude and frequency of the air flow cycle [73]. Horio [6] conducted analysis of the microstructure of the granules by splitting formed granules with a needle. Figure 39 shows the split surface of the granules. The images show the granules produced by this method exhibit a core-rim structure, where the surface of the granule had a denser particle packing than the core. Horio [6] suggested that the motion of the granules around the chamber during the fluidization step leads to surface deformation of the granules, creating the denser outer shell. This denser outer shell also explains the inherent strength of the granules, as the increased packing fraction at the surface creates an increased mechanical strength [6].

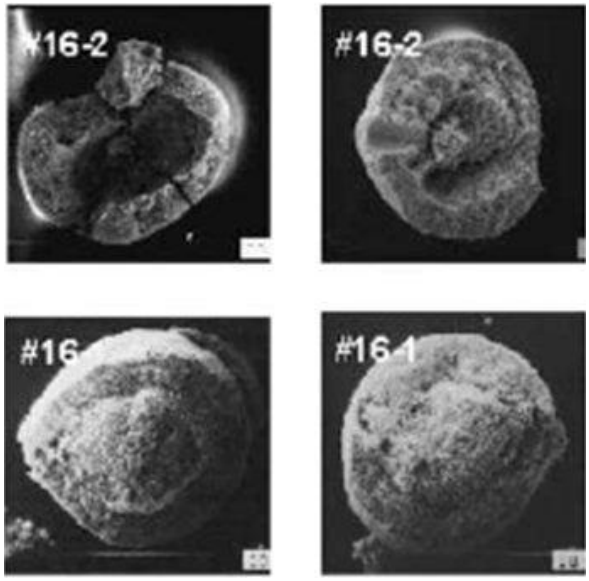

Figure 39. Split surfaces of granules created by PSG showing core-rim structure [6].

4.1.1.3. Effect of mechanical vibration on agglomeration

Barletta and Poletto [75] investigated the agglomeration of cohesive powders by mechanical vibration within a fluidized bed. In their work, silica and potato starch powder was mechanically vibrated while being aerated within a fluidization column. The size of the agglomerates formed was measured by the Ergun equation using the pressure drop of the gas through the bed. This measurement was compared to a theoretical calculation of the agglomerate size by a force balance [75].

Using Newton's Second Law, the force being exerted on an agglomerate is

$$F_{detach} = \frac{\pi d_a^3}{6} \rho_a a \qquad \text{Equation 11}$$

where d_a is the agglomerate diameter, a is the acceleration of the agglomerate, and ρ_a is the agglomerate density. This external force acting on the agglomerate is preventing the it from attaching to other agglomerates and growing. Therefore, this is the detachment force of the agglomerate [75].

The acceleration imparted onto the agglomerate is the sum of the acceleration due to gravity and the acceleration due to the vibration. Given that the vibration is sinusoidal, the acceleration is

$$a = A(2\pi f)^2 + g \qquad \text{Equation 12}$$

where A is the amplitude and f is the frequency of the vibration, and g is the acceleration due to gravity [76].

The attachment force holding two agglomerates together would be the tensile strength of that agglomerate divided by the contact density of that agglomerate. This contact density can be expressed as a ratio of the number of contacts between an agglomerate and its neighbors on another layer or plane to the square area inhabited by the agglomerate. This is shown by

$$F_{attach} = \frac{\sigma_t}{k/d_a^2} \qquad \text{Equation 13}$$

where σ_t is the tensile strength of theagglomerate and k is the number of contacts [75].

By setting the attachment and detachment force equal to each other, the critical situation for agglomeration can be found. This is shown below by combining Equation 11 and Equation 12.

$$\frac{\pi d_a^3}{6}\rho_a a = \frac{\sigma_t d_a^2}{k} \qquad \text{Equation 14}$$

As the σ_t, ρ_a, and k are parameters of the powders and a is a parameter of the vibration, for a given powder and given vibrational motion, there is a characteristic, equilibrium agglomerate size, d_a. By solving for d_a, Equation 14 becomes

$$d_a = \frac{6\sigma_t}{k\pi a\rho_a} \qquad \text{Equation 15}$$

For the number of effective contacts between an agglomerate and its neighbors on another layer, *k*, the value is set to three for the maximum packing of mono-sized spheres [77], representing hexagonal close packing of spheres. The values for σ_t and ρ_a are dependent on the consolidation stress being exerted on the powder bed. To find the consolidation stress, Newton's Second Law is again utilized. The powder bed of a given mass, *m*, is accelerated by gravity and the vibration given by Equation 12. This force is then divided by the area of the base of the powder container, as shown in Equation 16 to find the consolidation stress, σ_1.

$$\frac{Force}{Area} = \frac{m \times a}{Area} = \sigma_1 \qquad \text{Equation 16}$$

Using the traditional Mohr-Coulomb approach, for a given consolidation stress, σ_1, there is a characteristic yield locus, giving a certain value for the cohesion, τ_c, and incipient internal angle of friction, φ_i [9]. From these values, the approach allows the tensile stress of the bed, σ_t, to be calculated by

$$\sigma_t = -\frac{2\tau_c \cos\varphi_i}{1 + \sin\varphi_i} \qquad \text{Equation 17}$$

Likewise, the bulk density of a powder, ρ_a, is dependent on the consolidation stress applied, and for the calculated σ_1, the bulk density can be measured by a method such as uniaxial compaction. These values can then be used to solve Equation 15 for the size of agglomerates for a given vibration acceleration.

While the mentioned model to predict granule size in vibro-fluidized beds used a force balance approach [75], work has been conducted to investigate energy balance approaches [78] as well. Both models balanced the two competing mechanism of growth by particle adhesion and deformation from mechanical vibration. The results of both models showed a decreasing trend of granule size with increase vibration intensity [75,

78]. As both models were constructed for powders within an aerated bed, neither addresses the compaction of a powder. In the absence of fluidizing air flow, the agglomerates formed within the bed would experience a level of compaction due to the mechanical vibration. The compaction will increase the packing fraction and therefore the strength of the particle structure within the agglomerates, potentially allowing the agglomerates to grow to a larger size.

4.1.1.4. Auto-granulation

Auto-granulation is the growth of particle clusters of fine, cohesive powders due to agitation of the bed, such as mechanical vibration. The powder clusters become loosely bound due to the highly cohesive nature of the inter-particle contacts. This clustering occurs without the addition of any binder to the system and the granules reach an equilibrium size due to the balance between disruptive and adhesive forces experienced by the clusters during process operations. Due to the lack of research in the area, the process of how the powder forms clusters during auto-granulation is not completely understood [79].

The mechanism of growth during auto-granulation was proposed by Ku *et al.* [79] to be a snow-balling process, where fine particles are consumed by larger granules by sticking onto their surface. Due to the mismatch in size and consequently the mismatch in mass, the kinetic energy of the collision due to the fine particles would be insignificant to the adhesive energy of the much larger granule. As a greater number of fine particles stick to the surface of the granule, the granule grows larger, as shown in Figure 40.

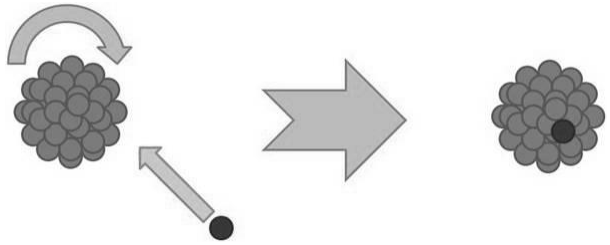

Figure 40. Schematic of a fine particle attaching to a larger granule.

The mechanism controlling the maximum granule size is the deformation related to the agitation process applied to the powder. In agitation by mechanical vibration, the impacts experiences by the granule with granules or with the container can result in deformation and breakage. As the granules grow by the snow-ball process, there is a size at which the granules become unstable from the forces acting upon it, breaking back down to a smaller size. An illustration of this deformation is shown in Figure 41. Therefore, the process is controlled by the two competing mechanisms of granule growth by snow-balling and granule deformation from impacts.

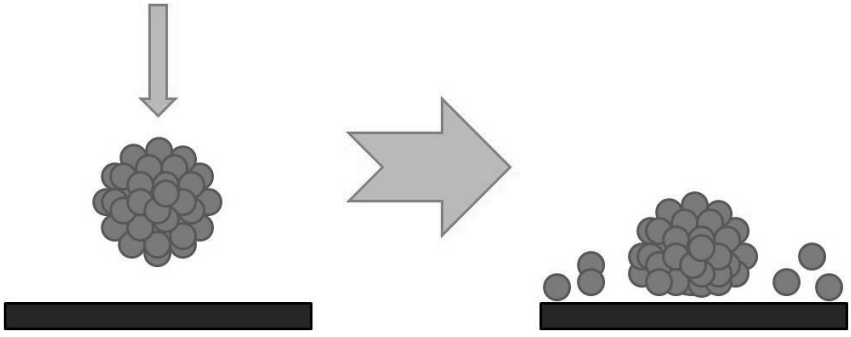

Figure 41. Schematic of granules deformation from an impact.

4.1.2. Breakage behavior of granules

It is important to study not only the clustering and growth of the granules, but also the deformation and breakage of the granules, which control the auto-granulation

behavior. Thornton [80] outlined the terminology used to describe the breakage phenomena of particle agglomerates. The term "fracture" is used to describe the breakage pattern which the agglomerate splits into two or more daughter fragments. This crack-like behavior is in contrast to the type of breakage termed "disintegration." In "disintegration," the end product of the breakage is one daughter cluster surviving, with the rest of the original reduced in the area of the impact reduced to the scale of the primary particles. If the entirety of the agglomerate if disintegrated to individual particles with no daughter cluster remaining, the breakage is referred to as "total disintegration" [80].

Thorton [80] showed through simulations that the type of breakage that occurs depends on the force of impact. If a strong force transmission occurs through the agglomerate, a heterogeneous velocity field results. The velocity discontinuity created within the agglomerate then causes fracture behavior of the agglomerate. If there is a weak force transmission, the breakage force will be localized to the impact area, causing disintegration [80].

Golchert *et al.* [81] investigated the effect of granule microstructure on the compressive strength of the granule. This study suggested the breakage behavior is heavily dependent on the structure of the granule, with both the mechanism and extent of breakage experienced by the granule changing between samples. The propagation of cracks was shown to be dependent on the network of contacts between the particles within a granule [81]. Therefore, the ability to characterize the internal microstructure of a granule is of extreme importance to understand the granule strength.

Subero and Ghadiri [82] showed experimentally the effect of the agglomerate microstructure on the breakage behavior. In their work, agglomerates of glass beads were engineered with controlled amounts of porosity and impacted at a range of velocities. The results showed that in samples with a low number of macro-pores and impacted at low velocities, disintegration occurred and was localized to the impact area only. As the number of pores or the impact velocity was increased, fragmentation dominated and a larger volume of the original agglomerate was deformed in impact [82]. The results show not only the importance of microstructure on the breakage, but the importance of the deformation rate on the breakage as well.

Moreno and Ghadiri [83] was able to link the breakage of an agglomerate back to the properties of the constituent primary particles. The theoretical approach used was the same as Rumpf's model, which states the strength of agglomerates as the force required to break all particle-particle contacts on the failure plane [84]. Through computational modeling, agglomerates were constructed with the difference being that in each case, the primary particles making up the agglomerate had a different surface energy. The surface energy of the particle relates to the strength of the particle-particle contact formed within the agglomerate. It was shown that the energy required to break a particle, W, can be related to the number of broken contacts, N, and the surface energy of the particles, Γ, by

$$W = N\Gamma A \qquad \text{Equation 18}$$

where it is assumed the contact area, A, of the particles within the agglomerate are all the same [83]. Equation 18 shows the breakage energy is directly proportional to the number of broken particle contacts. Therefore, granules with a higher packing fraction will have more interparticle contacts, thus being "stronger."

There are not many methods suitable for testing the breakage of granules. Most commonly, granule compression [84] is the method used. In this method, a single granule is placed between two flat platens, which exert an axial load upon the granule until failure. This method, although simple and well documented, is limited to testing in the static regime, using relative low deformation rates [85]. While useful in some processes, when dealing with dynamic processes, such as mechanical vibration of granules, the properties measured and behavior observed in the static regime cannot be translate to higher rates [82].

The method to directly measure breakage behavior at high deformation rates is by impacting the granule at relatively high velocities on a target and observing the deformation. An experimental setup for such an experiment is shown in Figure 42 [85, 86]. The granule would be dropped from the top of the apparatus where it can be accelerated using compressed air. The trigger unit placed directly above the target measures the velocity of the granule at impact [86]. The limit to this method is that the stresses placed upon the granule cannot be directly measured. Models are available to estimate the impact stress based on the impact velocity, but most make assumptions about the shape and mechanical properties of the granule.

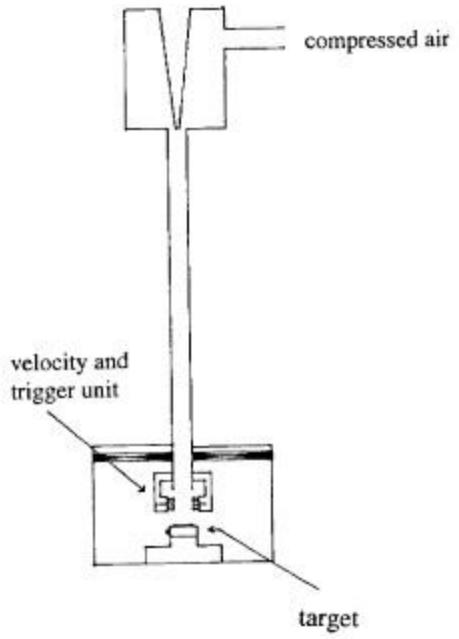

Figure 42. Schematic of impact test rig for measuring impact strength of granules where the granule would be dropped at the top, accelerated with compressed air, and impacted on the target with the trigger unit used to measure the impact velocity [86].

Generally, there are two modes of fracture in semibrittle granules under impact: chipping and fragmentation. The plastic deformation of the material is dependent on both the material property, namely hardness and fracture toughness, and mode of loading. The mode of loading includes the strain rate and loading area. Chipping is defined by broken portions of the granule being significantly smaller than the original granule. The result of the breakage is a small chip or chips and a larger mother particle. Chipping occurs from the propagation of lateral cracks. Fragmentation is defined by the granule splitting into multiple large fragments. The propagation of radial and median cracks leads to fragmentation. In general, chipping occurs at lower impact velocities and the breakage behavior transitions into fragmentation at higher velocities [87].

4.2. Experimental method

4.2.1. Auto-granulation by mechanical vibration

For this study, auto-granulation was induced using mechanical vibration. The setup using an electrodynamic shaker is discussed in Section 3.2.3. The range of vibration frequencies and amplitudes used are shown in Table 8. The amplitude and frequency of each test condition was converted to a vibration energy associated with one period, *E*, using simple harmonic motion (Equation 19).

$$E = \frac{1}{2}kA^2 = 2m(\pi f A)^2 \qquad \text{Equation 19}$$

where *k* is the wave number, *A* is the amplitude, *m* is the mass of the sample, and *f* is the frequency. The acceleration, *a*, and power, *P*, are given by Equations 20 and 21, respectively.

$$a = A(2\pi f)^2 \qquad \text{Equation 20}$$

$$P = Ef = 2\mathrm{m}f^3(\pi\mathrm{A})^2 \qquad \text{Equation 21}$$

For test conditions 1-4, the amplitude of the vibration was kept constant at 1.00 mm and the frequency was varied from 35 to 50 Hz. For test condition 5, the frequency was held at 50 Hz but the amplitude was changed to 0.80 mm to create a vibration with an energy equal to test condition 2. Likewise, in test condition 6 the frequency was held constant but the amplitude was changed to 0.64 mm to create a vibrational acceleration equal to test condition 2. This allows for an evaluation of the effects of frequency and amplitude, and explore if the applied energy or acceleration can unify the data. A

vibration time of 20 minutes was used for all test conditions, since the granules were found to grow to their equilibrium size by this point [79].

Table 8. Test conditions for mechanical vibration of the powder.

Test condition	Frequency (Hz)	Amplitude (mm)	Energy (mJ)	Acceleration (m/s^2)	Power (W)
1	35	1.00	5.6	48.36	0.20
2	40	1.00	7.3	63.17	0.29
3	45	1.00	9.2	79.94	0.41
4	50	1.00	11.4	98.70	0.57
5	50	0.80	7.3	78.96	0.36
6	50	0.64	4.6	63.17	0.23

4.2.2. Granule sizing

After mechanical vibration of the powder, the granules formed were gently poured from the acrylic box for collection. The size of the granules was then measured by gently scattering the granules over a flat surface and taking a high-resolution, overhead image of the entire population using a Canon SL1 DSLR (Canon Inc., New Jersey, USA). The images had a pixel size of 0.058 mm. The images of the granules were analyzed using ImageJ (http://imagej.nih.gov), with the pixel area of each granule being measured and converted to a diameter of a sphere of equivalent projected area. This process is shown in Figure 43. Using this optical method, the size of the granule population was measured as a number distribution. A model of the granule size as a function of the mechanical vibration was constructed, investigating the effects of

vibrational energy, acceleration, and power separately. The statistical significance of data was analyzed using Minitab 17.1.0.0 by Minitab, Inc. (Pennsylvania, USA).

Figure 43. Image analysis process for granule sizing, showing (a) the optical image of the granule, (b) the background of the image removed, and (c) the granule pixilated for measurement of pixel area.

4.2.3. Granule density measurement

Granule envelope density was measured using a Micromeritics GeoPyc 1360 (Micromeritics Instrument Corporation, Georgia, USA). The GeoPyc instrument is a unique displacement technique that uses a quasi-fluid composed of small, rigid spheres having a high flowability called DryFlo (Micromeritics Instrument Corporation, Georgia, USA). By placing a sample within a bed of DryFlo and gently agitating and consolidating the sample, the volumetric displacement of the sample can be measured and used to calculate the sample density. This density is an envelope density of the sample, as the DryFlo particles cannot infiltrate into the pores, open or closed, of the sample.

4.2.4. Mechanical testing of granules

To fully understand the behavior of auto-granulation, both of the processes, granule growth and deformation, must be studied. The deformation of the granules under mechanical vibration occurs by impacts and collisions, which occur at relatively high rates. To view the deformation behavior of the granules within the same dynamic regime, impact testing was conducted. The setup of the test is shown in Figure 44. The granule is dropped through a glass tube onto an acrylic target. The glass tube is used to help line the granule onto the target. By using different lengths of glass tubes, different drop heights can be achieved. The higher the drop height, the greater the velocity of the granule will be when it impacts the target. The impact is captured by a FASTCAM SA5 high speed camera (Photron, California, USA), and the images are used to calculate the impact velocity and observe the impact behavior.

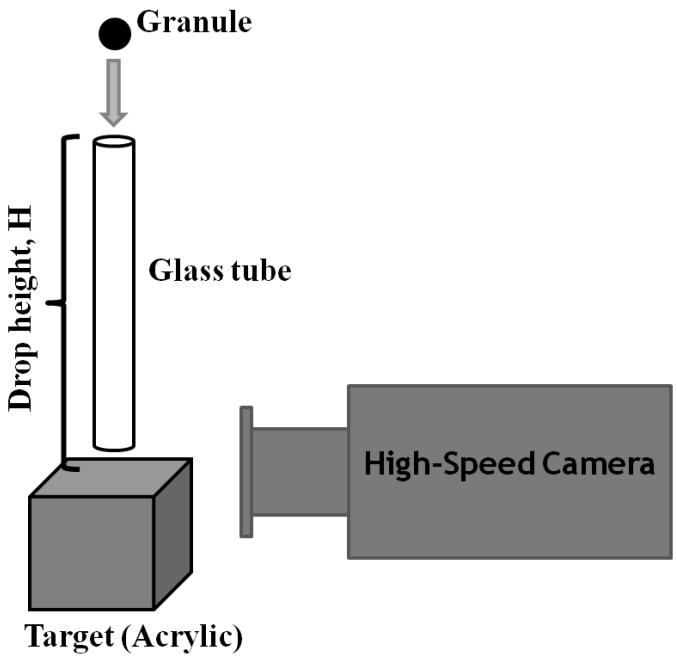

Figure 44. Schematic of granule impact test rig to observe breakage behavior.

4.2.5. Microstructural analysis

Imaging of fragile structures provides a challenging problem in finding a way to preserve the internal microstructure during sample preparation for microscopy. Embedding the sample in an epoxy resin to lock-in the structure is a solution to the sample preparation problem [88]. The epoxy resin has a low viscosity before curing, allowing for complete infiltration of the resin into the pores within the granule when under vacuum. To prevent the granules from dispersing when immersed in the liquid resin, the granules were heat treated to cause necking between particles to increase their mechanical strength [89]. After curing, the epoxy allows the granule to be polished in order to expose cross-sections without damaging or disturbing the internal microstructure. Imaging of the granules was conducted on a scanning electron microscope (SEM) to provide the necessary magnification and resolution to view the individual primary particles within the granule.

The goal of the heat treatment was to increase the mechanical strength of the granules to survive the epoxy infiltration procedure, but not to alter the microstructure of the granules in the process. The granules were heat treated in an alumina boat with a box furnace. The temperature was increased at 10°C/minute to various target temperatures: 700°C, 800°C, and 900°C. The sample was held at the target temperature for a dwell time of 60 minutes. The furnace was then cooled back to room temperature at a rate of 25°C/minute.

The effects of the various heat treatments were compared using two methods; granule immersion in water and SEM imaging of granule fragments. Granules were immersed in water to observe if they had sufficient strength to resist dispersion in a

dispersing fluid. For SEM imaging, granules were broken into fragments after heat treatment and fixed to an SEM sample stud using colloidal silver paste. The fragments were imaged to view if there were any observable changes to the primary particles, such as grain growth, due to the heat treatment.

The epoxy used for sample preparation was the Spurr Low Viscosity Kit (Ted Pella, Inc., California, USA) epoxy resin, which mixes in a liquid state and hardens with exposure to heat. The low viscosity epoxy resin allows for infiltration into the interparticle pores within the granule without dispersion or breakage. The epoxy was mixed using the following recipe: 4.10 g of ERL 4221, 1.90 g of diglycidylether of polypropyleneglycol (DER 736), 5.90 g of nonenyl succinic anhydride (NSA), and 0.10 g of dimethylaminoethanol (DMAE). The mixed epoxy resin was then placed in a Buehler Cast N' Vac 1000 castable vacuum system (Buehler, Illinois, USA) with the heat treated granule under a vacuum of 660 mmHg. After allowing 60 minutes to ensure any bubbles formed within the epoxy due to mixing had dissipated, the epoxy was poured slowly on top of the granule sample under vacuum. The sample was then kept under vacuum a further 60 minutes after combining the epoxy and granule. Upon removing the sample from vacuum, the sample was placed in an oven at 60°C for 12 hours to allow the epoxy to cure.

After epoxy infiltration, the samples were polished to expose the hemispherical plane of the granule. Polishing was conducted using a 0.05 μm diamond suspension to polish through the epoxy and particles to create a flat, 2-dimensional cross-section of the granule. The sample was then coated with a 5 nm layer of gold to minimize charging of the sample in the SEM. Imaging in the SEM was conducted using the in-lens detector,

which allows for a compositional contrast to distinguish between particles and epoxy. A gun voltage of 5 kV was used to minimize charging of the sample but maintain compositional contrast.

4.3. Results and discussion

4.3.1. Auto-granulation behavior

4.3.1.1. Effect of vibration time

Auto-granulation behavior becomes quickly evident in the fine powder bed, as shown in Figure 45. Within one minute, clusters form and grow within the fine powder bed to an easily observable size. For reference, the length of the container wall in Figure 45 is 60 mm. As expected with a snow-balling growth behavior, the granules continued to grow over time by consuming the finer particles within the powder bed at 5 minutes of vibration. The granules continue to grow until reaching an equilibrium maximum size limited by the vibration conditions.

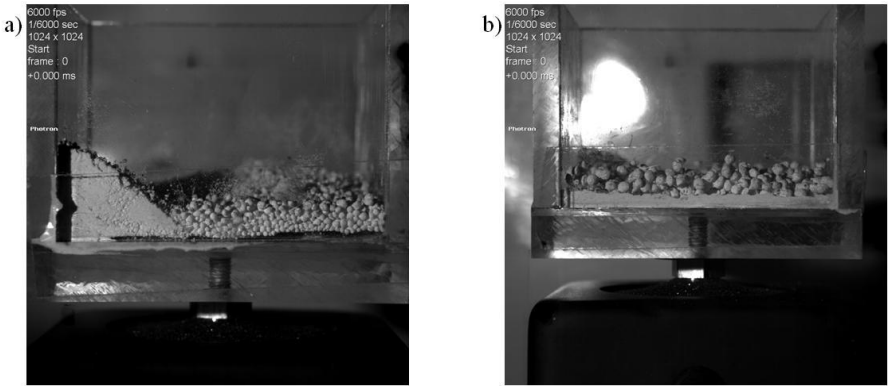

Figure 45. High-speed imaging of powder under 50 Hz and 1.00 mm amplitude mechanical vibration after (a) 1 minute and (b) 5 minutes.

High speed images of the granules are shown in Figure 46 after varying amounts of time under mechanical vibration at 50 Hz and 1 mm amplitude. In Figure 46, the changes in size and shape with vibration time can be observed. The granules are smallest in Figure 46a, after only 60 seconds of vibration. At 5 minutes of vibration time in Figure 46b, the granules are larger in size, but still maintain a relatively spherical shape and smooth surface. In Figure 46c, after 20 minutes of vibration, the surfaces of the granules become faceted. With the increase in vibration time, there would be a greater number of collisions experienced by the granules with other granules and the container wall. These collisions can cause local deformation of the granule surface, leading to the formation of these observed facets.

a) 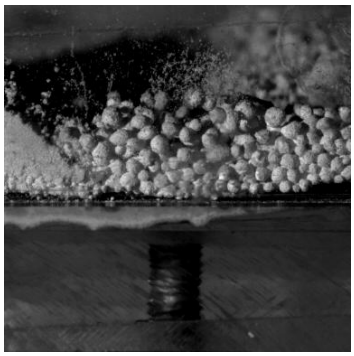 b)  c) 

Figure 46. Images of granules formed under 50 Hz and 1.00 mm amplitude vibration after (a) 1 minute, (b) 5 minutes, and (c) 20 minutes. The diameter of the screw at the bottom of the image is 4 mm.

At the 50 Hz and 1.00 mm amplitude condition, granules were created and collected with vibration times of 5, 8, 11, 14, 17, and 20 minutes. These granules were then sized, with the d_{10}, d_{50}, and d_{90} of the population at each time shown in Figure 47.

The data point at 20 minutes shows the average of three different runs, with the error bars giving the range of the measurements. The data show the granules size increases to an equilibrium value of about 1.5 mm after 14 minutes of vibration.

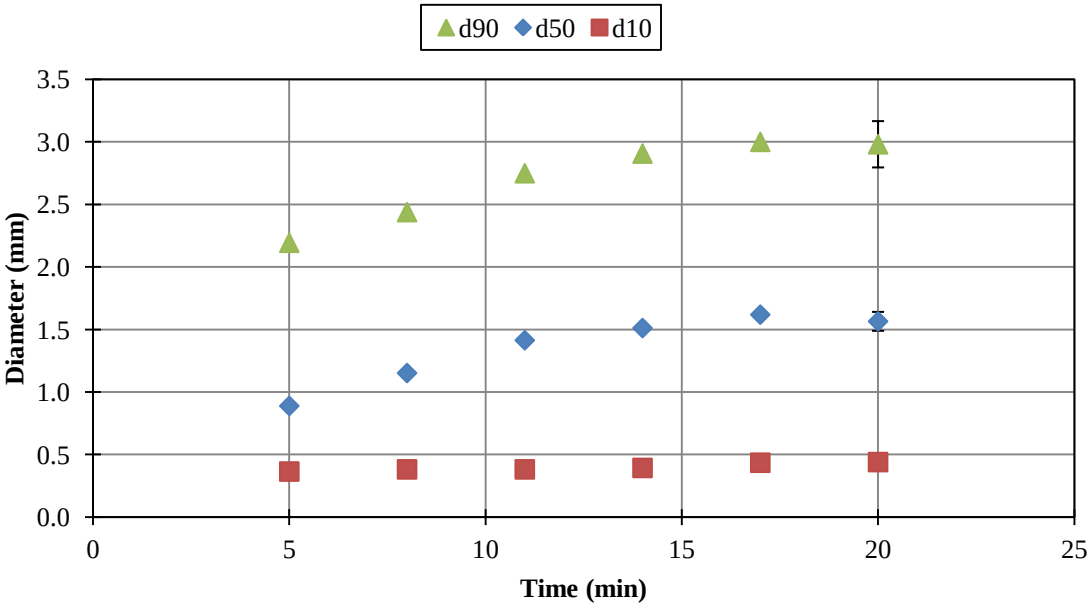

Figure 47. The granule diameter at 50 Hz and 1.00 mm as a function of vibration time.

This phenomenon of the granules reaching an equilibrium size agrees with the previously discussed theoretical model presented by Ennis *et al*. [3], showing the granulation process reaching an equilibrium when the growth due to coalescence and deformation due to the processing shear rate reach a balance. As a result, for each vibration condition shown in Table 8, the time for vibration was kept constant at 20 minutes to ensure the granules have grown to their equilibrium size.

4.3.1.2. Effect of vibration intensity

4.3.1.2.1. Equilibrium granule size

For each test condition, the entire population of granules produced by auto-granulation was optically imaged and sized. The sizes of the granules produced for all test conditions are shown as a function of vibration energy, acceleration and power in Figures 48, 49, and 50, respectively. The size was measured as the diameter of a sphere with equivalent projected area and represented as the d_{10}, d_{50}, and d_{90} of the number distribution of the population. Three repeats of each test condition were made, with each data point denoting the average and the bars showing the range of the three measurements.

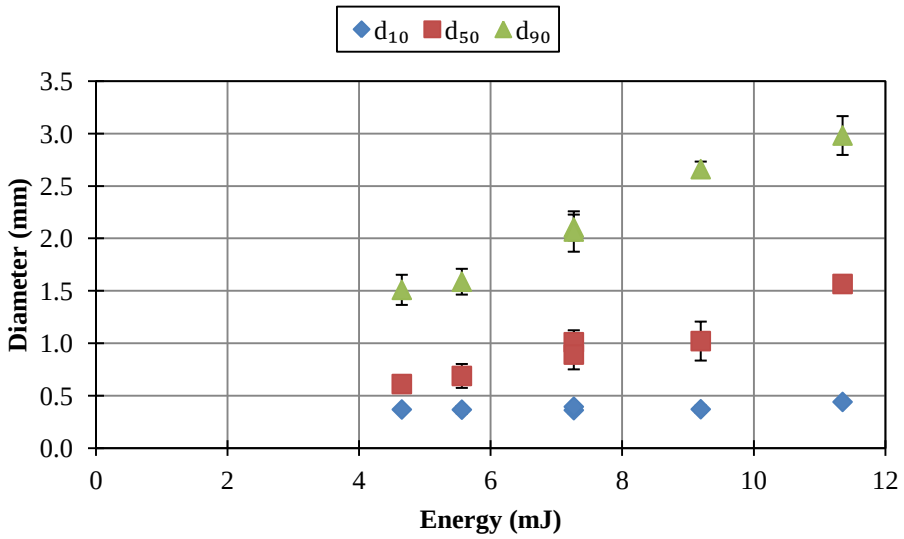

Figure 48. Diameter of produced granules as a function of the vibrational energy.

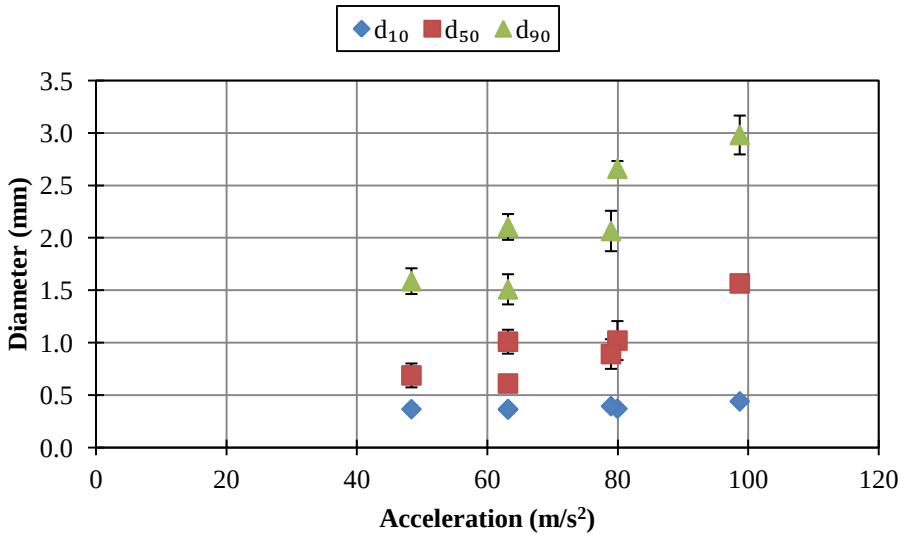

Figure 49. Diameter of produced granules as a function of the vibrational acceleration.

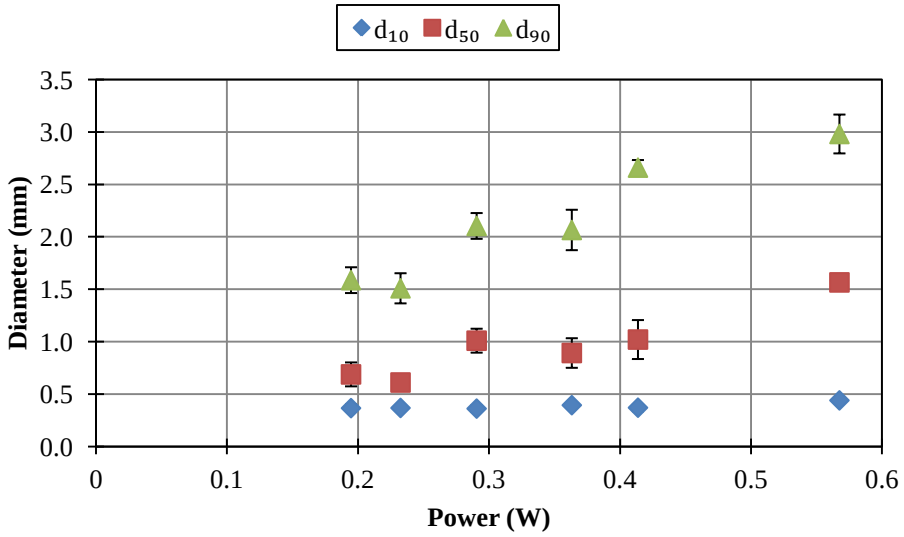

Figure 50. Diameter of produced granules as a function of the vibrational power.

The results show the d_{10} of the distribution remains relatively constant, but both the d_{50} and d_{90} increase with increasing vibration energy. This is in direct contrast to the behavior observed by Barletta *et al.* [7] and Zhou *et al.* [8], who modeled the behavior of

a fluidized powder bed under vibration. In these works, which are discussed in detail in Section 4.1.1.3., the effect of mechanical vibration on the agglomerate size of a fluidized powder bed was discussed. Both sets of results found a decreasing agglomerate size with increasing vibration intensity. The works, which was conducted on an aerated bed in a fluidized bed column, dealt with a powder bed in a vastly different condition. Without the fluidizing air flow, compaction of the powder is allowed to take place, as shown in Section 3.1.4.

The critical values to note are the two data sets at vibration energies of 7.3 mJ in Figure 48 and the two data sets at vibrational accelerations of 63.17 m/s^2 in Figure 49. These are run at separate vibration parameters, but the energy calculation and acceleration calculation for the conditions are the same. The granule radii for the equal conditions are shown in Table 9. For vibrational energy, the equal data sets nearly overlap, with the difference in values being 0.01, 0.05, and 0.02 mm for the d_{10}, d_{50}, and d_{90} values, respectively. These differences are within the range of the measurement, as shown by the error bars in Figure 48. In contrast, the results for vibration acceleration differ significantly. This confirms the controlling vibration parameter in relation to granule size is the vibrational energy input into the powder bed.

Table 9. Granule radius for vibration conditions with equal energy and equal acceleration.

Frequency (Hz)	Amplitude (mm)	Energy (mJ)	Acceleration (m/s^2)	Radius – d_{10} (mm)	Radius – d_{50} (mm)	Radius – d_{90} (mm)
40	1.00	7.3	63.17	0.18	0.50	1.05
50	0.80	7.3	78.96	0.19	0.45	1.03
50	0.64	4.6	63.17	0.18	0.31	0.75

There is a general increasing trend of granule size with increasing vibration intensity, regardless of whether the intensity is considered in terms of energy, acceleration, or power. The largest dependence on vibration intensity is observed in the d_{90} of the size distribution, with the d_{10} and d_{50} showing a less sharply increasing trend. Thus, the d_{90} data were chosen to fit to linear models of each vibrational parameter, with the terms shown in Table 10. The y-intercept of each model is positive and larger than the primary particle size of the titania powder, representing that the powder is in a granulated state even without any applied vibration. As the unaltered, as-received dry powder is in an agglomerated state before testing, the statement is rational.

Table 10. Terms and statistical significance of linear fit of vibrational intensity parameters to d_{90} granule size.

Parameter	Slope	y-intercept (mm)	R^2 (%)
Energy (mJ)	0.236	0.37	98
Acceleration (m/s^2)	0.029	0.04	78
Power (W)	4.071	0.75	91

The R^2 value of each linear fit of vibrational intensity parameter to the d_{90} of the granule size is shown in Table 10. As the criteria for statistical significance is an R^2 value that is greater than 95% [70], only the linear fit of the energy parameter is statistically significant. The linear fit is shown in Equation 22, where d_{90} is the 90^{th} percentile of the granule diameter distribution and E is the vibrational energy. The regression analysis of the linear model yielded a p-value of 0.044 for the y-intercept term, and a p-value of 0.010 for the energy coefficient. As both p-values are less than 0.050, a

rejection of the null hypothesis is made [70] and both terms are presumed to be significant to the linear model.

$$d_{90} = 0.37 + 0.236E \qquad \text{Equation 22}$$

The conception of this linear model in Equation 22 capturing the auto-granulation behavior is an important result. By being able to predict the equilibrium d_{90} granule size as a function of the vibrational energy, one can tune a process to create granules of a desired size by controlling the energy of the applied mechanical vibration. Emphasis must be made that this model is an empirical fit only to the range of vibrational energies studied. Also, there is no theoretical reason as to why the data should follow an increasing linear model, as it is not expected that an infinitely large granule can be created by simply increasing the vibrational energy to infinity.

4.3.1.2.2. Granule density

For granule density measurements, a sample size of 30 granules from each test condition was used for measurement. The results, shown in Figure 51, have error bars representing the standard deviation of the data. The values show an increasing trend with vibrational energy, correlating well with the granule sizing data. An increasing density implies an increasing consolidation stress imparted on the powder. As shown in Figure 29, the cohesion of the titania powder increases with increasing consolidation stress. Therefore, the powder within the granules created under higher vibration energies can be assumed to have a higher cohesion than the powder within the granules processed at lower energies.

This trend explains the size increase shown in Figure 48 with increasing vibration energy, as the higher strength of the granules allows them to remain stable to a larger equilibrium size. This compaction and density increase of the granules is not taken into account in previous works [75, 78] that found the inverse trend of size with intensity of vibration.

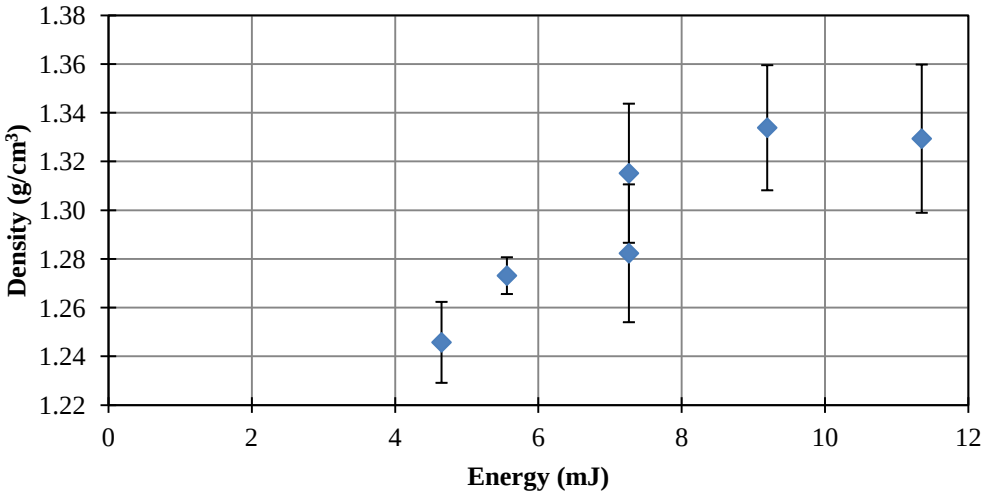

Figure 51. Effect of vibrational energy on radius of granules produced by auto-granulation.

4.3.2. High speed imaging of granules

4.3.2.1. Granule tracking

Under mechanical vibration, high speed imaging of the powder bed from a side view was conducted, as shown in Figure 45. The images were collected at a rate of 300 frames per second (fps). At a vibration frequency of 50 Hz, this frame rate collects 6 images per period of vibration. The granules were tracked to find the velocity of the granules under vibration by measuring the distance traveled by the centroid of each

granule between frames. As the images were two-dimensional side views of the powder bed, the granule tracking only measured a two-dimensional velocity in the plane of the image. Rotation of the granule was also not taken into account.

Granules were tracked during vibration conditions of 1.00 mm amplitude and three different frequencies: 50, 45, and 40 Hz. Five granules from each condition were tracked for 50 to 100 frames, or a timeframe of 0.167 to 0.333 seconds. The varying length of tracking was due to the granules only being tracked for the duration they remain in the view of the camera.

The magnitude of the granule velocity as a function of time is shown in Figure 52. Each graph shows a different vibration condition. No cyclic pattern was observed in the velocities, as may be expected due to the vibration being applied to the powder bed being cyclic. If the velocity was tracked as a vector, the direction of the granule motion may exhibit the cyclic pattern. The maximum velocity was observed to increase with increasing vibration frequency. The maximum observed velocity of the granules was 0.583, 0.294, and 0.257 m/s for vibrational frequencies of 50, 45, and 40 Hz respectively.

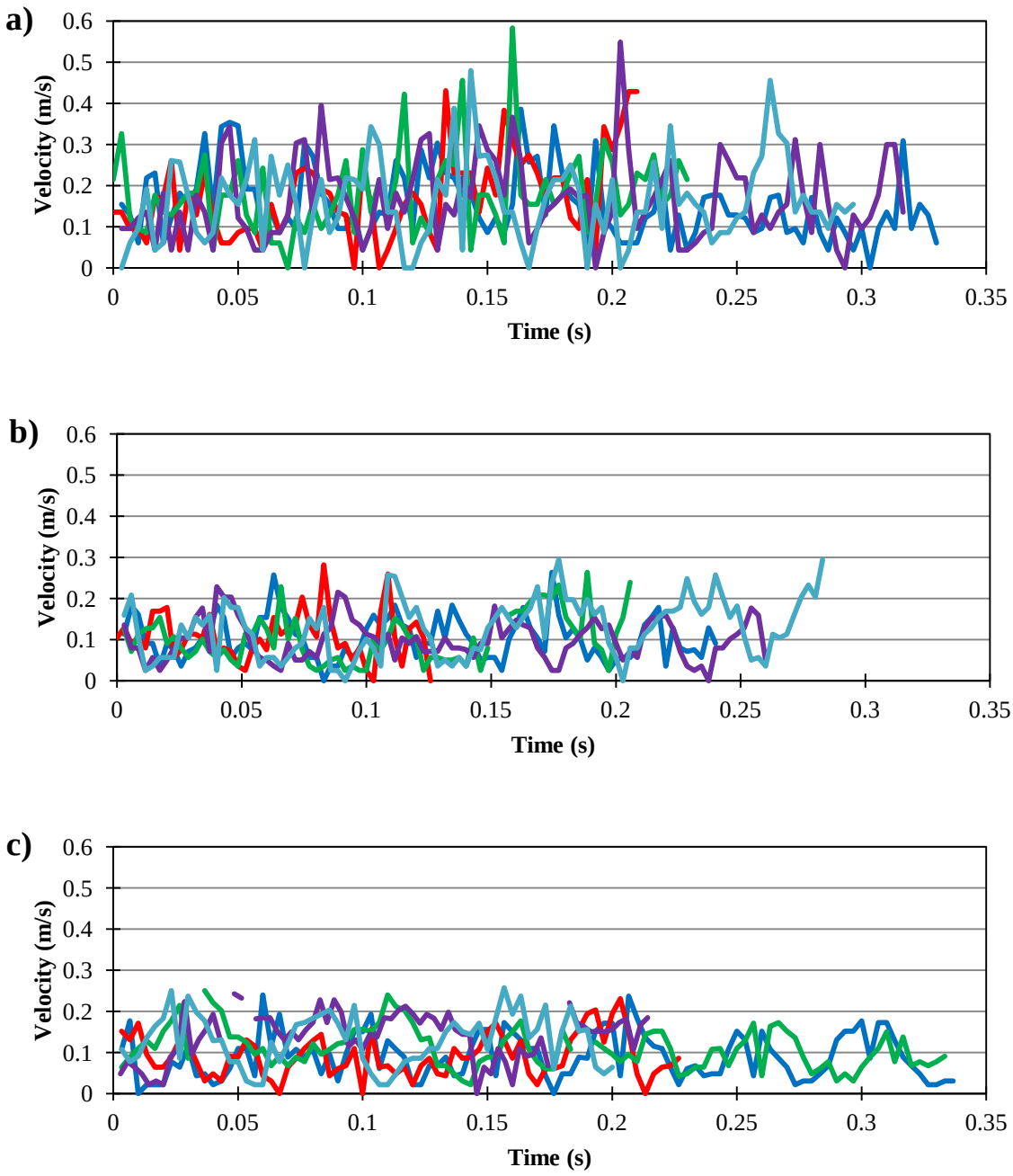

Figure 52. Absolute velocity of granules under vibrational conditions of 1.00 mm amplitude and frequency of (a) 50 Hz, (b) 45 Hz, and (c) 40 Hz.

4.3.2.2. Impact testing

Mechanical testing of the granules was conducting by granule impact testing to correctly mimic the dynamic deformation that would be imparted on the granules under mechanical vibration. The granules were dropped at varying heights to achieve different impact velocities, and high speed imaging was used to capture the granule deformation. These are shown in Figures 53 to 56 as a series of four consecutive frames for granules produced under a vibration condition of 50 Hz and 1.00 mm amplitude.

At the low impact velocity, no damage is observed upon impact, as shown in Figure 53 with an impact velocity of 0.917 m/s. Increasing impact velocity to 1.115 m/s leads to dusting, where fine particles are broken off the surface. This is shown in Figure 54. Figure 55 shows an impact at 2.241 m/s where a large fragment chips off the surface of the granule, which is due to the propagation of lateral cracks within the granule. At a high impact velocity, the granule undergoes complete breakage, with the granule fracturing into many different pieces. This behavior is shown in Figure 56, at an impact velocity of 2.693 m/s. This fragmentation is due to the propagation of radial and median cracks within the granule.

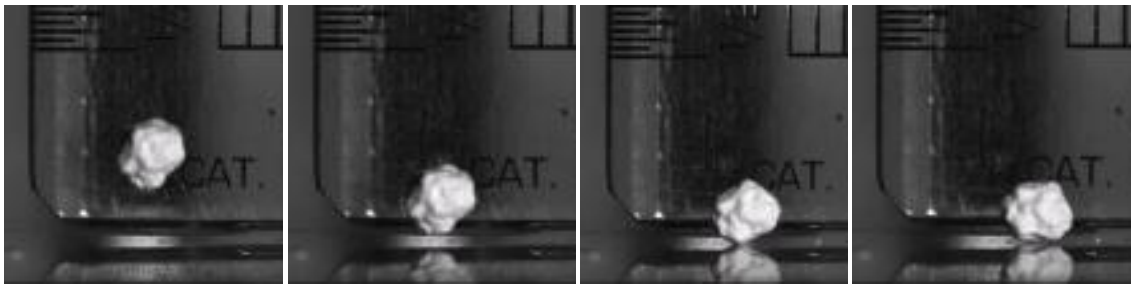

Figure 53. High speed imaging of a granule impact at a velocity of 0.917 m/s.

Figure 54. High speed imaging of a granule impact at a velocity of 1.115 m/s.

Figure 55. High speed imaging of a granule impact at a velocity of 2.241 m/s.

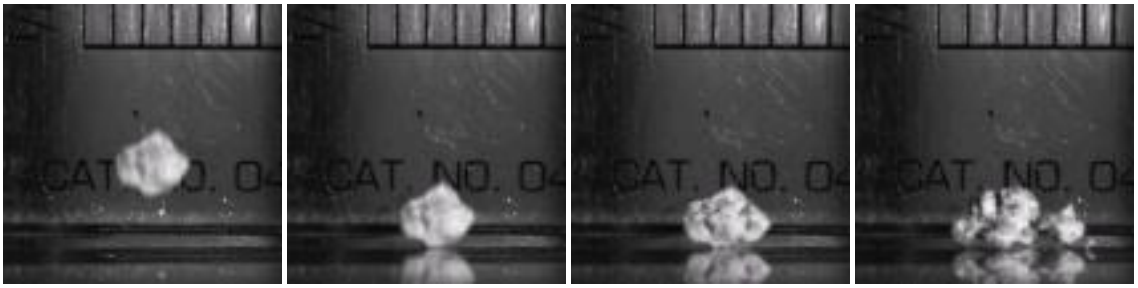

Figure 56. High speed imaging of a granule impact at a velocity of 2.693 m/s.

The maximum observed velocity of the granules was measured in Figure 52 to be 0.583 m/s under a vibration of 50 Hz and 1.00 mm amplitude. If two granules were both travelling at one another at that maximum velocity, the maximum net impact velocity that would be experienced by the granules would be twice the measured value, or 1.166 m/s. Therefore, the granule deformation to be expected under the mechanical vibration

conditions would be minimal localized deformation to a slight dusting, as illustrated by Figures 53 and 54. The relatively extreme chipping and fragmentation behaviors in Figures 55 and 56 occur at much higher impact velocities than what would be expected due to the granule tracking measurement. Thus, during the auto-granulation process, the granules under vibration are limited in size by the localized deformation they receive from impacts. As the granules become too large, the particles on the surface beginning to dust off to reduce the size to a stable regime, but the granules do not break and fragment under vibration.

4.3.3. Granule microstructure

4.3.3.1. Heat treatment

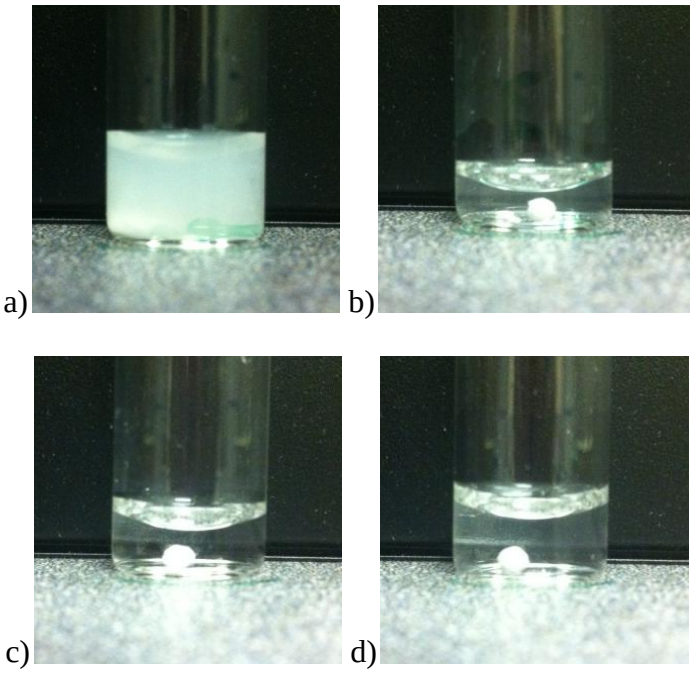

Figure 57. Granules (a) with no heat treatment, (b) heated to 700°C, (c) heated to 800°C, and (d) heated to 900°C immersed in water.

The results of immersing the heat treated granules in water are shown in Figure 57. With no heat treatment, the granule easily dispersed when submerged in water. With a heat treatment to a target temperature of 700°C, the granule fragmented into several pieces upon immersion. The granules heat treated to 800°C and 900°C were unaffected by the water. Therefore, granules heat treated up to 700°C would not survive being immersed in the liquid epoxy resin but those treated to 800°C or higher have the ability to survive the infiltration process.

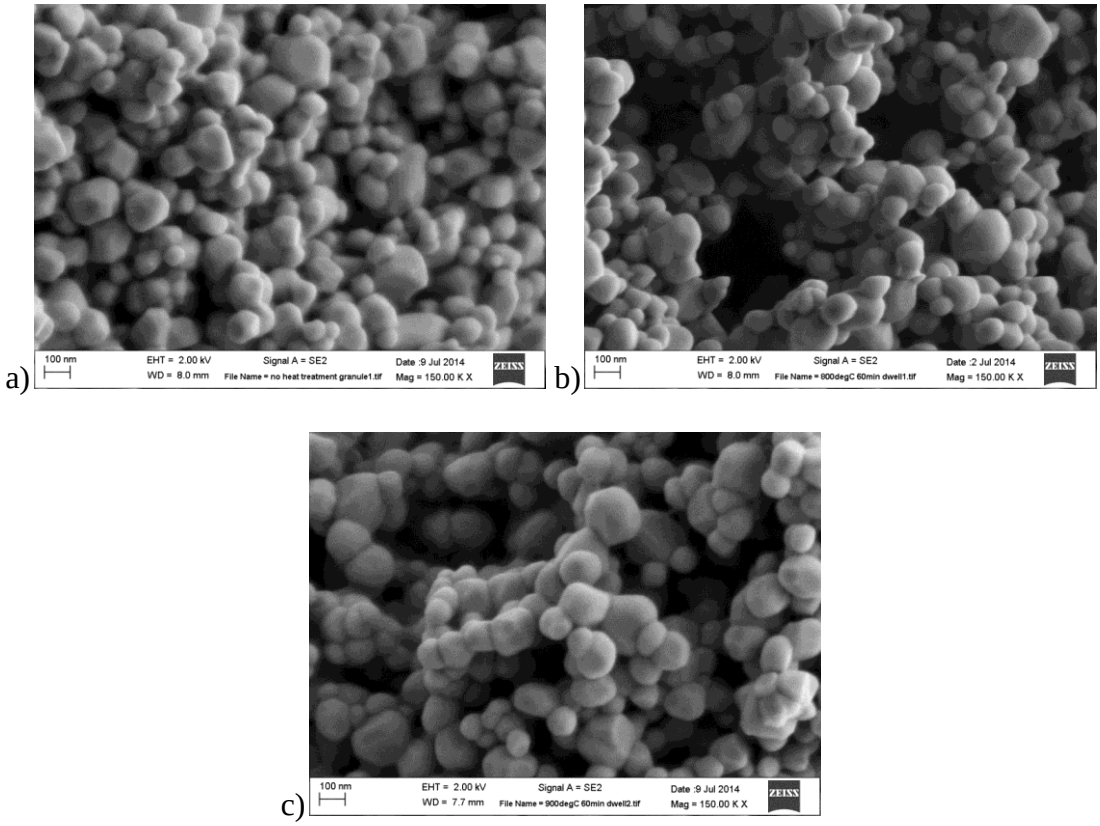

Figure 58. SEM imaging of primary particles of granule fragments after (a) no heat treatment, (b) heated to 800°C, and (c) heated to 900°C.

Granules that underwent heat treatments at 800°C and 900°C were broken into fragments to view if the heat treatment had any visible effect on the size or shape of the constituent particles. Images of the particles within the granules after heat treatment at the two temperatures were compared to the particle within an untreated granule, as shown in Figure 58. No visible sign of particle growth or shape change was evident in the images. Due to this SEM imaging and the results of the immersion of granules in water, it was determined that the heat treatment at 800°C and 900°C had no effect on the microstructure within the granule, other than creating interparticle necks at particle contacts to increase the granule strength. The subsequent heat treatment of granules for epoxy infiltration in this study used a target temperature of 900°C.

4.3.3.2. SEM imaging

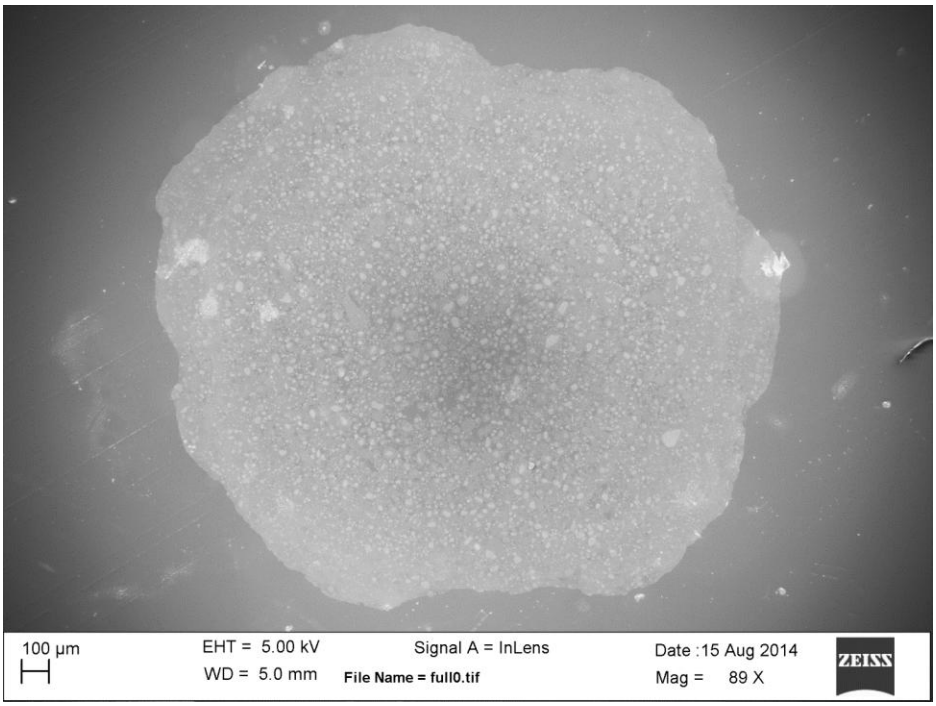

Figure 59. Infiltrated and polished cross-section of granule formed under 40 Hz and 1.00 mm amplitude vibration.

An SEM image of the granule cross-section is shown in Figure 59. Due to the compositional contrast provided by the in-lens detector, particles within the granule appear brighter, while the epoxy resin occupying the pores within the granule appears darker. From the image, it is clear that the granule does not have a homogeneous microstructure. The multiple lighter and darker regions seen in the cross-section imply the granule was not produced by a uniform "snow-balling" of fine particles, but a multi-scale structure of smaller clusters of particles comprising the larger granule. However the higher magnification image of Figure 60 indicates that a mixture of fines and small clusters exists within the granule structure.

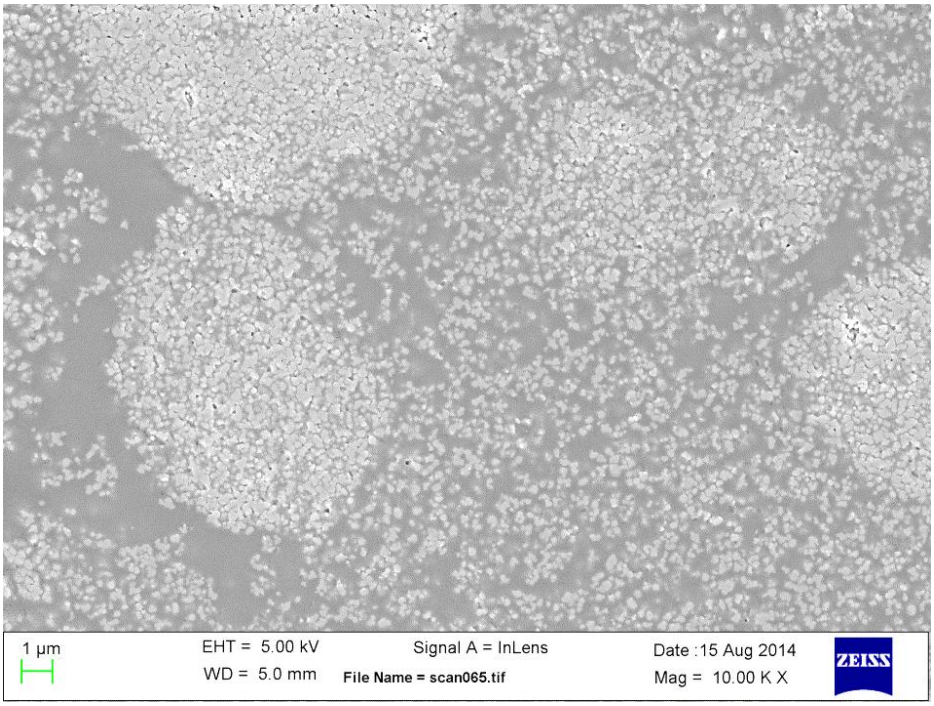

Figure 60. Image of granule cross-section at 10,000× magnification showing individual primary particles of the 40 Hz and 1 mm amplitude granule sample.

Looking at the higher magnification image of the surface of the cross-section shown in Figure 60, it is apparent that the epoxy resin has completely infiltrated the pores of the particle structure. With polishing, the structure of the granule had been maintained with no significant damage to the granule structure due to pull-out. The area of the image is roughly 27 μm by 27 μm. To view how the microstructure of the granule changes across its width, a series of images was taken over the horizontal diameter of the cross-section using the same magnification. Images were then spliced together to create a mosaic view of the granule microstructure. Figure 61 shows the first three images of the surface of the granule. The particles were configured with a high packing fraction, creating a dense outer shell on the granule. Conversely, the center three images of the granule (Figure 62) show a much looser pack configuration.

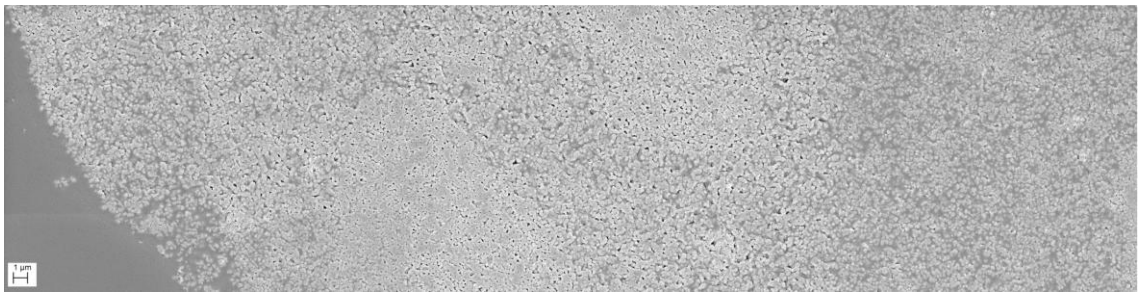

Figure 61. Mosaic of three images at 10,000x magnification of the outer rim of the 40 Hz and 1 mm amplitude granule sample.

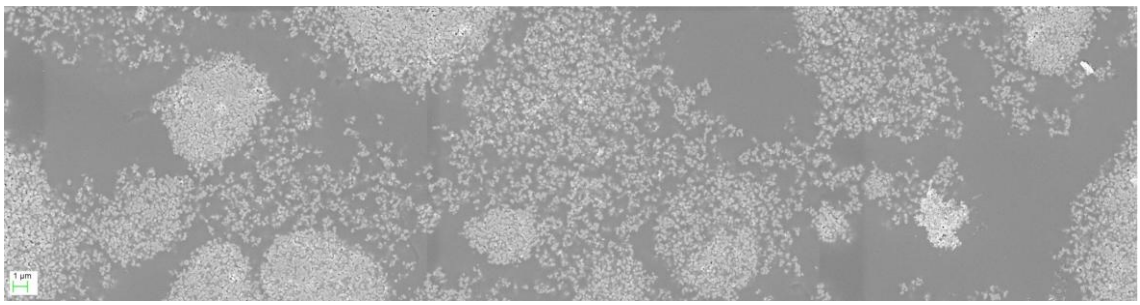

Figure 62. Mosaic of three images at 10,000x magnification of the inner core of the 40 Hz and 1 mm amplitude granule sample.

To obtain a quantitative measure of the change in packing fraction, the series of SEM images was used as a line scan across the granule measuring the packing fraction with spatial resolution of 27 μm by 27 μm, or the area of the SEM image at 10,000× magnification. This was conducted using ImageJ to convert each grayscale SEM image from the entire series into a binary, black-and-white image. This allowed for the actual packing fraction of each image to be calculated by dividing the number of white pixels by the total number of pixels in the image. A comparison could then be made to other images of the scan, providing a measure of the packing fraction as a function of the location across the horizontal diameter of the granule cross-section.

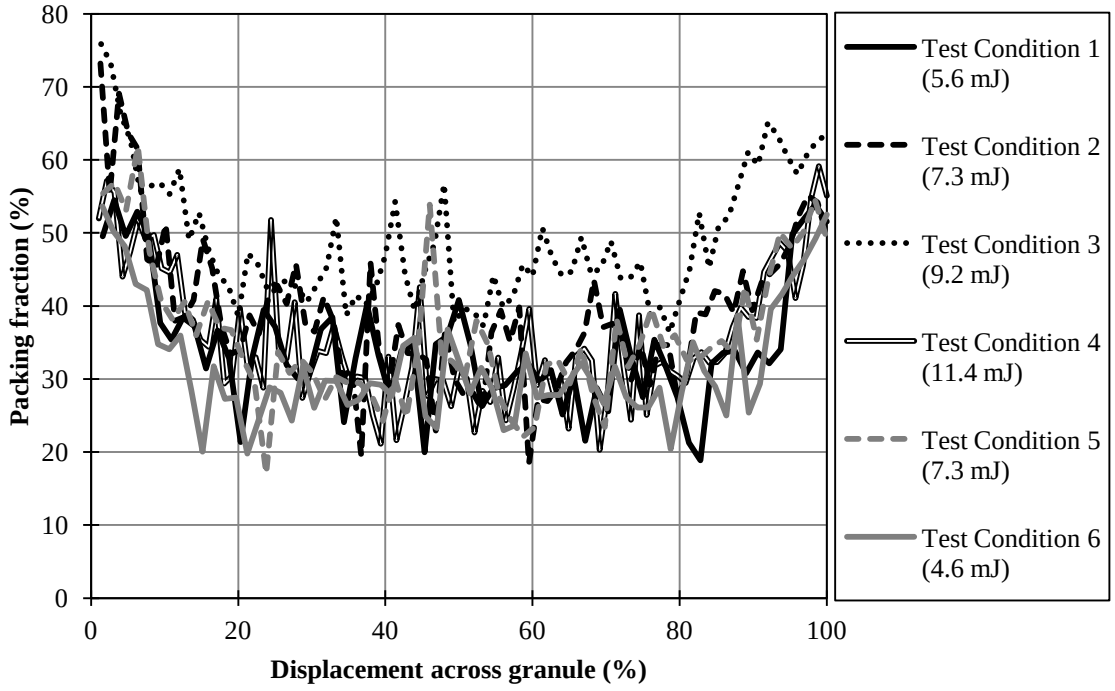

Figure 63. Packing fraction of the granule cross-section across its horizontal diameter for each vibration test condition.

The results of the scans are shown in Figure 63 for granules from all test conditions. The displacement across the granule is shown as a percentage, with 0% and 100% being the left and right edges of the granule, respectively, and 50% being the center. From the data, the packing fraction of the granules is highest between the first and last 10% to 15% of the granule displacement. The central area of the granule produced a lower packing fraction. This leads to the conclusion that granules from all the test conditions exhibit the same core-rim microstructure, where the outer rim of the granule is at a higher density than the inner core. This conclusion is also confirmed by the SEM images in Figures 61 and 62. No noticeable variation of packing fraction with vibrational condition is observed.

This microstructure offers insight into the process of the auto-granulation. As the central 60-70% of the granule core shown in Figure 63 has a relatively low packing fraction, the nucleation and growth of the granule, when small, is a snow-balling process of smaller particles adhering to the surface of the granule with no or minimal compaction taking place. As the rise in packing fraction at the outer rim is concentrated to the outer 10-15%, compaction only takes place when the granule reaches a larger size. Therefore, the localized deformation by compaction while the granule is bounced by the mechanical vibration requires the granules to reach a certain size. Only when the granule becomes large enough is the mass of the granule, and thus energy while travelling around the vibration container, large enough to cause the compaction.

This compaction is important to the structural integrity of the granules, as discussed in Section 4.3.1.2. The observed core-rim microstructure is the same as in granules produced by PSG [6], which was stated to cause the inherent strength of the

granules produced by the method. PSG and auto-granulation produce very similar granule, both in microstructure and mechanical behavior. The imaging conducted by Horio [6] in his characterization of the PSG microstructure was strictly qualitative, with no measure of the variation in packing fraction within the granule. The method conducted in this thesis is an improvement on that work, allow for a quantitative measure of the packing fraction of the core and rim. Furthermore, such an imaging method would be useful for investigating the microstructure of other granules produced by other granulation methods, to provide insight into the process of granule growth and deformation.

5. Summary

The work in this dissertation was presented in three separate chapters dealing with different size scales of powder characterization. Chapter 2 dealt with the micro-scale topic of the individual, constituent particles making up the powder, while Chapter 3 viewed the powder in the macro-scale, as a continuum, bulk material. Chapter 4 investigated the meso-scale, looking at processes leading to growth and deformation of particulate structures. This chapter will discuss the work in all three as a summary and will present overarching links between the multi-scale properties.

Table 11. Summary of various micro-scale and macro-scale properties of the powder samples.

	Alumina		Titania	
	A16SG	A3500SG	AT1	DT51
Micro-scale				
Particle Size, d_{50} (μm)	0.5	2.3	0.1	1.0
Surf. Area (m^2/g)	8.80	3.49	10.53	80.88
Particle density (g/cm^3)	3.942	3.939	3.760	3.668
Macro-scale				
Loose Bulk Density (g/cm^3)	1.13	1.21	0.66	0.40
Loose Packing Fraction	0.29	0.31	0.18	0.11
Kawakita parameter, a	0.16	0.33	0.33	0.45
Kawakita parameter, $1/b$	5.81	7.85	10.41	3.83
Flow Function, avg.	3.80	2.61	1.38	1.58
Cohesion at $\sigma_1 = 5$ kPa (kPa)	0.33	0.68	0.78	1.01
Cohesion at $\sigma_1 = 20$ kPa (kPa)	0.96	1.23	2.82	2.30
Behavior under vibration	Fluidization	Fluidization	Auto-gran.	Compaction

5.1. Correlation of powder properties

A list of selected powder properties is shown in Table 11. The d_{50} particle size that is listed is the manufacturer supplied data corroborated by SEM imaging in this

study. For each material, alumina and titania, there is a fine and coarse powder variant. It is important to note that the particle size of the DT51 titania powder refers to a hard-aggregate size, as discussed in Chapter 2. This artifact is illustrated in the particle surface areas, measured by BET. For the A16SG, A3500SG, and AT1 powders, the trend follows the surface area increasing with finer particle size. The DT51 powder, being a hard-aggregate particle, has a primary particle size which is much finer, yielding a much higher surface area value than the other three samples. The particle densities measured by He pycnometry show each powder is very dense.

The loose bulk density of the powder was measured using a Freeman FT4 Powder Tester, as described in Chapter 3. The value, along with the particle density, was used to calculate the powder packing fraction, as shown by Equation 1. There is a correlation between the packing fraction of the powder and cohesion measured on the Schulze annular shear cell. At a relatively low major principal stress of 5 kPa, the loose packing fraction decreases with increasing cohesion. As the cohesion of the powder increases, there is a stronger structure within the powder, which allows the looser packing [23-25]. The lower major principal stress of 2.5 kPa for the cohesion measurement is appropriate as the powder is in a low stress condition to measure the loose bulk density.

The flow functions of the powders shown in Table 11 is an average value for measurements taken with a major principal stress of 1 to 40 kPa. All four powder exhibit flow functions in the cohesive regime, but the two titania powders, AT1 and DT51, are very cohesive. The physical characteristics of the powders explain this low flowability behavior. The AT1 titania sample has the finest particle size, and Chapter 3 discusses the trend of decreased powder flowability with decreasing particle size [2]. As powder

cohesion has been found to linked to the surface energy responsible for interparticle adhesion [5], the DT51 powder, with a significantly higher surface area than the other powder variants, is expected to have a poor flowability as well.

The effect of relative humidity on the flow behavior of the powder samples was also found to insignificant. Tests were conducted on the AT1 and DT51 titania powders. The DT51 powder adsorbed a much larger mass percent of water than the AT1 powder, which is due to the increased surface area of the former powder. This data is presented in Figure 10. The ceramic powders were found to only physically adsorb moisture with the environment, with the entire process being reversible from the adsorption isotherms. There was no visible effect of this moisture on the powder flow properties, presented in Figures 30 and 31, which leads to the conclusion that the environmental effect of relative humidity is insignificant to bulk behavior of ceramic powders.

The behavior of the powders under mechanical vibration is listed in Table 11 and discussed in more detail in Chapter 3. The two alumina powder variants, A16SG and A3500SG, both exhibit bulk fluidization under mechanical vibration. When compared to the powder cohesion values listed at a major principal stress of 20 kPa, it shows the two powders have the lowest cohesion which would allow the powder bed to flow, even under the applied stress of the vibration. While the exact stress being applied to the powder bed due to the vibration was not measured in this study, it is expected to be relatively high. Therefore, the absolute values listed for cohesion at 20 kPa may not be correct, but the order of powder cohesiveness of the samples is the same from 10 to 40 kPa, implying the same conclusion.

The two titania powders, AT1 and DT51, both exhibit very high cohesion values under a major principal stress of 20 kPa, but behave very differently under mechanical vibration. The DT51 powder compacted under vibration, while the AT1 powder underwent auto-granulation. The Kawakita analysis parameters explain the difference in the powder variants. The DT51 powder had the highest *a* parameter and lowest 1/*b* parameter, which is indicative of a powder that will compact a high degree under relatively low pressure, an expected property for compacted powder. The AT1 powder had the highest 1/*b* parameter, a property of powders exhibiting a strong particle structure. This powder property, along with the high cohesion of the powder, would lend itself to the process of auto-granulation.

5.2. Characterization of auto-granulation

The work conducted in Chapter 4 investigated the characteristic behavior known as auto-granulation exhibited by the AT1 titania powder. Auto-granulation is the snow-balling growth of particle clusters within a dry, fine powder bed due to the powder cohesion. These granules grow to an equilibrium maximum size over time dependent on the vibration conditions imparted on the powder bed. Both the granule size and density were found to increase with increasing vibrational energy. The increased granule density implies greater powder cohesion within the granule, which can explain the larger equilibrium granule size. This shows that the vibrational energy is not purely a disruptive force limiting the granule size, but consolidates the granules, increasing their internal cohesion and allows them to grow to a larger equilibrium size. The trend shows, along with the data presented in Table 11, that compaction is a key process in auto-granulation.

When comparing the behavior of all four powders, insight into the cause of auto-granulation behavior can be made. For snow-balling growth of the powder to occur, a high powder cohesion is necessary to facilitate the clustering a particles. A lack of such cohesion results in a fluidization behavior, exhibited by the A16SG and A3500SG alumina powder samples. Powders with a high cohesion value but that are also easily compressible, such as the DT51 titania powder, will form a dense powder cake. The lack of strength in the particle structure of the DT51 powder, which causes the ease of consolidation, prevents the powder from forming stable granules. A balance between the powder cohesion and compressibility is necessary for auto-granulation to occur, such as with the AT1 powder. The powder must have the cohesion required for granule growth, but a high-strength particulate network to provide the structural integrity of the granules. The two properties, the powder cohesion and Kawakita bulk compression strength, were found to be the critical mechanisms controlling the bulk behavior under mechanical vibration.

Furthermore, a novel method to image the microstructure of the porous granules was developed as part of this thesis. This method involved heat treatment and epoxy infiltration of the granules before polishing to provide a slice of the granule. The images showed a heterogeneous microstructure, with smaller clusters of particles clearly visible near the core within the larger granules. Analysis of the particle packing fraction showed the granules exhibited a core-rim microstructure, with the center core of the granule having a lower density than the outer rim, for all vibrational intensities investigated. This structure provided the strength for the inherent integrity of the granules formed by auto-granulation. This method has yet to be used in investigating the structure of particulate

granules and can be a useful tool for understanding the growth process of granules grown by other methods.

5.3. Additional remarks

The identification of the critical powder properties controlling the behavior of powders under mechanical vibration, powder cohesion and Kawakita compressibility, is an important result of this work. This thesis laid the groundwork with the identification of these critical properties for the building of a regime map of powder behavior as to allow for the prediction of powder performance. This study only involved investigation of four powder variants, so the logical next step for further research would involve testing a wider range of various powders. From the results of this thesis, the regime map of powder behavior would look like the schematic shown in Figure 64. The relative positions of the powders variants tested in this thesis are shown, but the boundaries showing transitions between behaviors are entirely speculative. Powders with low cohesion are expected to fluidize under mechanical vibration. As cohesion is increased, the powders with a high 1/*b* Kawakita parameter would exhibit auto-granulation. In contrast, powders with a low 1/*b* Kawakita parameter would exhibit compaction.

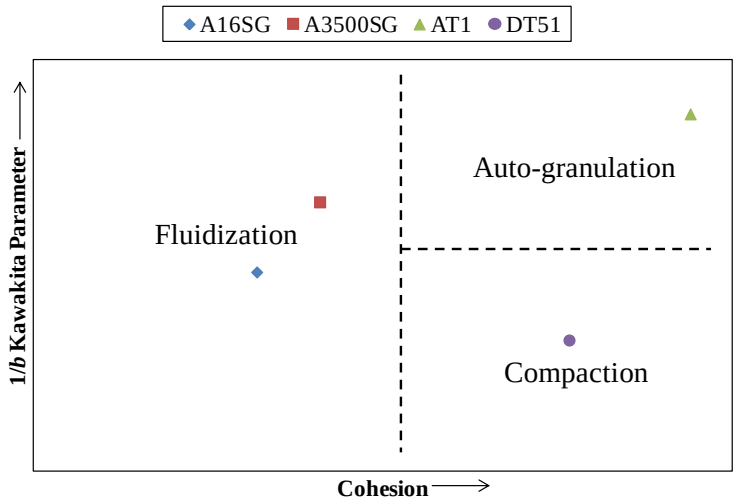

Figure 64. Speculative regime map of dynamic powder behaviors under vibration as a function to powder cohesion and Kawakita compressibility.

This work has broad implication in the area of powder processing. This includes various industries such as pharmaceutical, food, detergent, and geology, as well as the area of ceramics. In many processes involving powders, mechanical vibration is often involved in the transportation and conveying of the powder. This step is often assumed to have no affect on the state of the powder, which may be incorrect. The results of this thesis shows that powders can have vastly different, and a process where mechanical vibration is used to induce flowability in one powder variant can cause compaction in another variant, leading to costly and time-consuming problems in situations such as hopper flow. In addition, the granules created by auto-granulation under mechanical vibration were found to have a significant structural integrity, which can create problems further in processing if agglomerates are unwanted in the final product.

In the opinion of the author, the auto-granulation behavior studied in this thesis has the potential to be a useful processing tool. Size enlargement is often used in

production as a method to increase the flowability of the material. Traditional size enlargement often involves wet granulation, where binder and liquid is added to the powder to facilitate the granule growth. In many circumstance, the addition of these additives is detrimental to the desired properties of the product, such as the modification of the surface properties in catalytics (the most common usage of the Cristal Global titania powders), or the use of the additives is entirely prohibited, such as when dealing with products which require all ingredients to be fit for human consumption, as in the food and pharmaceutical industry. Exploiting the auto-granulation behavior of powder variants allows for size enlargement of powders without the need for additives.

6. Conclusions

The work conducted in this thesis demonstrated the wide range of powder behavior that can be exhibited under mechanical vibration. The goal of this thesis, to evaluate the differences in the bulk behaviors of powders under mechanical vibration, was achieved. By creating links between the properties of the powder samples to the bulk dynamic behavior, the powder cohesion and Kawakita compressibility were identified as the mechanisms controlling powder performance under mechanical vibration. Furthermore, the behavior of auto-granulation was extensively characterized, with a linear model developed of the equilibrium granule size as a function of the vibrational energy.

Several important results from the work performed in thesis are discussed in this section:

1) Classification of dynamic behavior: The behavior of four ceramic powder variants under mechanical vibration were studied and characterized: the Almatis A16SG and A3500SG alumina powders underwent fluidization, the Cristal Global DT51 titania powder underwent compaction, and the Cristal Global AT1 titania powder underwent auto-granulation.
2) Cause of fluidizing behavior under vibration: The A16SG and A3500SG powders had relatively high flow function values at a major principal stress of 20 kPa of 4.6 and 3.6, respectively, when tested in the Schulze annular shear cell, leading to a dynamic fluidizing behavior under mechanical vibration. The cohesion values of these powders were both below 1.25 kPa at the same major principal stress. In

contrast, the titania powders, which exhibited different behaviors, had cohesion values above 2.30 kPa.

3) Cause of compaction behavior under vibration: The DT51 titania powder had a high cohesion but a Kawakita 1/*b* parameter of only 3.83. This parameter, or ease of compression of the powder, causes compaction behavior under vibration.
4) Cause of auto-granulation behavior under vibration: The AT1 powder, which had a similar high cohesion to the DT51 titania powder, had a Kawakita 1/*b* parameter of 10.41. The high powder cohesion allows for clustering of particles, but the high 1/*b* parameter allows for the resistance of bulk compaction.
5) Process of auto-granulation: Granules grow due to a snow-balling effect of particle layering caused by high cohesion between particles. As the granule size and mass increases, the subsequent increased impact energy experienced by the granule causes local deformation in compaction and particle dusting.
6) Effect of mechanical vibration: The AT1 titania powder required a minimum of 14 minutes of vibration to reach an equilibrium granule size. The equilibrium diameter of the granules ranged from 1.5 to 3.0 mm, increasing with vibrational energy for the range of 4.6 to 11.4 mJ. The granule density also increased with vibrational energy from 1.25 to 1.33 g/cm^3.
7) Model of granule size and vibrational energy: An empirical model of the d_{90} granule size as a function of the energy of the applied vibration for the range of vibration amplitude and frequencies tested. The granules size was found to follow a linear trend with the equation $d_{90} = 0.37 + 0.236E$.

8) Epoxy infiltration: Successful vacuum-assisted infiltration of a porous granule was conducted. The application of this method was novel to the imaging of granules allowed SEM imaging of a hemispherical plane of a porous and friable granule without damage to the delicate microstructure.
9) Granule microstructure: Granules formed by auto-granulation exhibited a core-rim microstructure, where the outer rim exhibited a higher packing fraction of particles than the inner core. The variation in packing fraction between the core and rim was as much as 40% and the dense rim comprised the outer 10% to 15% of the granule diameter. This core-rim microstructure is responsible for the structural integrity of the formed granules.
10) Effect of particle absorption value on DLS: An incorrect particle absorption value can have a profound effect on the particle size distribution given by dynamic light scattering. Using a method comparing the measured and calculated scattering patterns, the absorption value of all four powders samples was found to be 0.001. Using a different value greatly changed the distribution, except for the DT51 powder, which is speculated to be due to the aggregated structure of the particles.
11) Humidity and flowability: The titania powders samples adsorbed moisture from the humidity in the ambient environment in an entirely reversible process, yet this moisture had no effect on the flowability of the powders. The DT51 powder adsorbed up to 2.32% of its mass in moisture at 12 g/L absolute humidity, but no significant change was observed in the powder cohesion.

7. Suggestions for future work

The characterization of powder properties outlined in this thesis has the potential to be used as a predictive tool for classifying the dynamic powder behavior during processes involving mechanical vibration. This would allow for choosing constituent powders with a desired performance for an industrial process by performing characterization rather than actual processing tests. It can also highlight the powder properties to avoid, due to those powder variants being prone to a behavior that can be detrimental to the processing. Furthermore, the auto-granulation behavior has the potential to be a processing method for producing dry granules, which is a desired product in powder processing.

Extending these concepts will require completing certain tasks. In general, these tasks can be listed as followed:

1) The creation of a regime map of powder behavior under mechanical vibration can be used as a predictive tool for classifying the performance of powders for a specific process. This thesis, in identifying the powder cohesion and Kawakita compressibility as critical properties controlling the dynamic behavior under vibration, has already laid the ground work. A map can be constructed by graphing the behavior of the powder as a function of the two critical properties. The additional powders must vary in the aforementioned properties to create a matrix to find the transitions between the behaviors of fluidization, compaction, and auto-granulation under vibration. The desired properties of future powders are illustrated in the speculative regime map in Figure 64 to determine the location of the transition boundaries between behaviors under vibration. Powder

variants with intermediate cohesion values between the relative low cohesive aluminas and high titanias would be desired. Additionally, highly cohesive powders with 1/*b* Kawakita parameters falling between the two titania powders should be tested.

2) The selection of additional powders for testing, as mentioned in the previous task, requires careful consideration. In the opinion of the author, the follow powders may exhibit interesting properties and would be suggested for future testing. The alumina powders tested in this study were A16SG and A3500SG. The "SG" in the powder names stands for "Super Ground," but Almatis offers "UG" or "Un-Ground" variants of the same powders. These powders do not undergo a milling procedure in their process, which would result in a coarser and broader size distribution of the particles. For titania, Degussa (New Jersey, USA) offers an Aeroxide P25 titania powder which exhibits an extremely low loose bulk density. The dynamic behavior can be of interest in the scope of further studies. Furthermore, the materials to be studied do not have to be linked to alumina and titania. Degussa produces a fused silica powder called AeroSil 200, which also exhibits a low loose bulk density. Silica is a powder of great concern when agitated due to potential health concerns dealing with dusting. Carbon black is a commonly used powder that is generally considered difficult to process due to its cohesive behavior.
3) The stress being imparted onto the powder under mechanical vibration must be identified. By knowing the major principal stress on the powder due to the vibration, the actual cohesion value of the powder bed can be determined, as

cohesion is a function of the applied major principal stress. This is no trivial task, as there if no empirical way of measuring the stress in situ under the vibration process. Therefore, modeling must be used. Distinct element method (DEM) models have been used successfully to simulate particulate systems, and can be effective in modeling the bulk powder under mechanical vibration.

4) By studying the effect mechanical vibration on binary systems of powder, the effect on powder mixedness can be investigated. Vibration has been claimed to both increase mixedness, as with vibratory mixers, and increase segregation, as with the Brazil nut effect. A study on the role of the constituent powder properties on the mixing or segregation of a binary powder system under vibration should be studied. An interesting variable to examine would be the mixture of a fluidizing and compacting powder under vibration to see if the convective behavior of the fluidizing powder prevents powder compaction. Also, a powder normally exhibiting auto-granulation can behave differently when mixed with a variant that does not. A potential method for quantifying mixedness is by measuring the variance in the distribution of phases.
5) The application of using auto-granulation as an industrial process for size enlargement has been discussed in this work. To examine the possibility of scale-up of the process, certain aspects of the mechanical vibration process must be studied further. The container used in this study was acrylic, which would interact with the powder through static charge. Investigation of different container materials should be, such as steel or aluminum, to observe the effect of a conducting container. The study involved a fixed bed dimension as well. The

effect of the container walls can be viewed by increasing the surface area of the powder bed, specifically by using a larger container but keeping the bed height constant at 1 cm. Furthermore, increasing the mass of powder used in the same size container would allow for investigation into the effect of powder bed height.

6) The performance of the powder after auto-granulation should be characterized. Often, granulation is used as an intermediate step to improve the flow behavior of a powder for later processing. For example, in tableting processes, cohesive powders are often granulated to allow them to flow into compacting dies easier and more predictably. Therefore, the change in performance of the powder before and after auto-granulation should be measured. In order to mirror the tableting process, the compaction behavior of the constituent powder and powder after auto-granulation can be both measured and compared.

8. References

[1] J. S. Reed, *Principles of ceramics processing*: Wiley New York, 1995.

[2] F. M. Etzler and M. N. Uddin, "Powder Technology and Pharmaceutical Development: Particle Size and Particle Adhesion," *Kona,* vol. 30, p. 2013, 2013.

[3] B. J. Ennis, G. Tardos, and R. Pfeffer, "A microlevel-based characterization of granulation phenomena," *Powder Technology,* vol. 65, pp. 257-272, 1991.

[4] G. I. Tardos, M. I. Khan, and P. R. Mort, "Critical parameters and limiting conditions in binder granulation of fine powders," *Powder Technology,* vol. 94, pp. 245-258, 1997.

[5] K. L. Johnson, K. Kendall, and A. D. Roberts, "Surface Energy and the Contact of Elastic Solids," *Proceedings of the Royal Society of London. Series A, Mathematical and Physical Sciences,* vol. 324, pp. 301-313, 1971.

[6] M. Horio, "Binderless granulation—its potential, achievements and future issues," *Powder technology,* vol. 130, pp. 1-7, 2003.

[7] V. A. Hackley and C. F. Ferraris, *The use of nomenclature in dispersion science and technology* vol. 960: US Department of Commerce, Technology Administration, National Institute of Standards and Technology, 2001.

[8] K. Johanson, "Effect of particle shape on unconfined yield strength," *Powder Technology,* vol. 194, pp. 246-251, 2009.

[9] D. Schulze, "Flow properties of powders and bulk solids," *Braunschweig/Wolfenbu ttel, Germany: University of Applied Sciences,* 2006.

[10] M. E. Fayed and L. Otten, *Handbook of powder science and technology*: Van Nostrand Reinhold Co., 1984.

[11] D. Geldart, "Types of gas fluidization," *Powder Technology,* vol. 7, pp. 285-292, 5// 1973.

[12] J. Hidaka, "Vibrational and Acoustic Characteristics " in *Powder Technology Handbook*, H. Masuda, K. Higashitani, and H. Yoshida, Eds., Third Edition ed: Taylor & Francis, 2006, pp. 383-397.

[13] B. Thomas, M. O. Mason, Y. A. Liu, and A. M. Squires, "Identifying states in shallow vibrated beds," *Powder Technology,* vol. 57, pp. 267-280, 4// 1989.

[14] ISO, "Metallic powders -- Determination of apparent density -- Part 1: Funnel method," ed, 3923-1:2008.

[15] Malvern, "Determination of the particle absorption for laser diffraction size calculations: MRK1308-01," Malvern.

[16] Y. Kousaka and Y. Endo, "Particle Density," in *Powder Technology Handbook*, H. Masuda, K. Higashitani, and H. Yoshida, Eds., Third Edition ed: Taylor & Francis, 2006, pp. 49-52.

[17] S. Watano, "Moisture Content," in *Powder Technology Handbook*, H. Masuda, K. Higashitani, and H. Yoshida, Eds., Third Edition ed: Taylor & Francis, 2006, pp. 265-268.

[18] K. Zhu, R. B. H. Tan, W. Kiong Ng, S. Shen, Q. Zhou, and P. W. S. Heng, "Analysis of the influence of relative humidity on the moisture sorption of particles and the aerosolization process in a dry powder inhaler," *Journal of Aerosol Science,* vol. 39, pp. 510-524, 6// 2008.

[19] W. D. Callister, *Materials Science And Engineering: An Introduction*: John Wiley & Sons, 2007.
[20] N. Venugopal, "Aggregate breakdown of nanoparticulate titania," PhD, Ceramic and Materials Engineering, Rutgers, The State University of New Jersey, 2008.
[21] Vaisala, "Humidity Conversion Formulas," 2013.
[22] L. Svarovsky, *Powder testing guide: methods of measuring the physical properties of bulk powders*: British Materials Handling Board by Elsevier Applied Science, 1987.
[23] E. C. Abdullah and D. Geldart, "The use of bulk density measurements as flowability indicators," *Powder Technology,* vol. 102, pp. 151-165, 3/3/ 1999.
[24] N. Harnby, A. Hawkins, and D. Vandame, "The use of bulk density determination as a means of typifying the flow characteristics of loosely compacted powders under conditions of variable relative humidity," *Chemical engineering science,* vol. 42, pp. 879-888, 1987.
[25] D. Geldart and A. Wong, "Fluidization of powders showing degrees of cohesiveness—I. Bed expansion," *Chemical Engineering Science,* vol. 39, pp. 1481-1488, 1984.
[26] M. S. Mohammadi and N. Harnby, "Bulk density modelling as a means of typifying the microstructure and flow characteristics of cohesive powders," *Powder Technology,* vol. 92, pp. 1-8, 6// 1997.
[27] A. Faqih, B. Chaudhuri, A. W. Alexander, C. Davies, F. J. Muzzio, and M. Silvina Tomassone, "An experimental/computational approach for examining unconfined cohesive powder flow," *International Journal of Pharmaceutics,* vol. 324, pp. 116-127, 11/6/ 2006.
[28] R. Freeman, "Measuring the flow properties of consolidated, conditioned and aerated powders — A comparative study using a powder rheometer and a rotational shear cell," *Powder Technology,* vol. 174, pp. 25-33, 5/16/ 2007.
[29] A. Vasilenko, S. Koynov, B. J. Glasser, and F. J. Muzzio, "Role of consolidation state in the measurement of bulk density and cohesion," *Powder Technology,* vol. 239, pp. 366-373, 5// 2013.
[30] ASTM, "Standard Test Methods for Determining Loose and Tapped Bulk Densities of Powders using a Graduated Cylinder," ed. West Conshohocken, PA: ASTM International, D7481-09.
[31] H. Hausner, "FRICTION CONDITIONS IN A MASS OF METAL POWDER," Polytechnic Inst. of Brooklyn. Univ. of California, Los Angeles1967.
[32] R. Grey and J. Beddow, "On the Hausner ratio and its relationship to some properties of metal powders," *Powder Technology,* vol. 2, pp. 323-326, 1969.
[33] R. L. Carr, "Evaluating flow properties of solids," *Chem. Eng,* vol. 72, pp. 163-168, 1965.
[34] D. Geldart, N. Harnby, and A. Wong, "Fluidization of cohesive powders," *Powder Technology,* vol. 37, pp. 25-37, 1984.
[35] J. K. Beddow, *Particle Characterization in Technology: Morphological analysis*: CRC Press, 1984.
[36] U. Zafar, "Assessing Flowability of Cohesive Powders by Ball Indentation," PhD, University of Leeds, 2013.

[37] N. Venugopal and R. Haber, "Yield Strength of Nanoparticulate Titania Via Compaction," *MATERIALS SCIENCE AND TECHNOLOGY-ASSOCIATION FOR IRON AND STEEL TECHNOLOGY-*, vol. 4, p. 393, 2006.
[38] D. Niesz, R. Bennett, and M. Snyder, "STRENGTH CHARACTERIZATION OF POWDER AGGREGATES," DTIC Document1970.
[39] N. A. Golomb, "Compaction behavior of spray dried alumina," Master, Ceramic Science and Engineering, Rutgers, The State University of of New Jersey, 1997.
[40] S. W. Smith, "Influence of granule characteristics on the compaction behavior of granulated ceramic powders," Master, Ceramic and Material Engineering, Rutgers, The State University of New Jersey, 2000.
[41] J. Nordström, I. Klevan, and G. Alderborn, "A particle rearrangement index based on the Kawakita powder compression equation," *Journal of Pharmaceutical Sciences*, vol. 98, pp. 1053-1063, 2009.
[42] P. J. Denny, "Compaction equations: a comparison of the Heckel and Kawakita equations," *Powder Technology*, vol. 127, pp. 162-172, 10/16/ 2002.
[43] R. W. Heckel, "Density-pressure relationship in powder compaction," *Transaction of the Metallurgical Society of AIME*, vol. 221, pp. 671-5, 1961.
[44] K. Kawakita and K.-H. Lüdde, "Some considerations on powder compression equations," *Powder Technology*, vol. 4, pp. 61-68, 1// 1971.
[45] J. Nordström, K. Welch, G. Frenning, and G. Alderborn, "On the physical interpretation of the Kawakita and Adams parameters derived from confined compression of granular solids," *Powder Technology*, vol. 182, pp. 424-435, 3/10/ 2008.
[46] I. Klevan, "Compression Analysis of Pharmaceutical Powders : Assessment of Mechanical Properties and Tablet Manufacturability Prediction," PhD, University of Tromsø, 2011.
[47] M. J. Adams and R. McKeown, "Micromechanical analyses of the pressure-volume relationship for powders under confined uniaxial compression," *Powder Technology*, vol. 88, pp. 155-163, 8// 1996.
[48] R. Ramberger and A. Burger, "On the application of the Heckel and Kawakita equations to powder compaction," *Powder Technology*, vol. 43, pp. 1-9, 7/1/ 1985.
[49] ASTM, "Standard Test Method for Measuring the Angle of Repose of Free-Flowing Mold Powders," ed. West Conshohocken, PA: ASTM International, C1444-00.
[50] ASTM, "Standard Test Methods for Flow Rate of Metal Powders Using the Hall Flowmeter Funnel," ed. West Conshohocken, PA: ASTM International, B213-13.
[51] J. Cooke and R. Freeman, "The flowability of powders and the effect of flow additives," in *World Congress on Particle Tech*, 2006, pp. 1-12.
[52] J. Tomas, "Fundamentals of cohesive powder consolidation and flow," *Granular Matter*, vol. 6, pp. 75-86, 2004.
[53] M. Leturia, M. Benali, S. Lagarde, I. Ronga, and K. Saleh, "Characterization of flow properties of cohesive powders: A comparative study of traditional and new testing methods," *Powder Technology*, vol. 253, pp. 406-423, 2// 2014.
[54] J. Schwedes, "Review on testers for measuring flow properties of bulk solids," *Granular Matter*, vol. 5, pp. 1-43, 2003.

[55] J. Tomas, "Product design of cohesive powders–mechanical properties, compression and flow behavior," *Chemical engineering & technology,* vol. 27, pp. 605-618, 2004.
[56] A. W. Jenike, *Storage and Flow of Solids*: University of Utah, 1964.
[57] J. Bridgwater, "Particle Breakage due to Bulk Shear," *Handbook of Powder Technology,* vol. 12, pp. 87-116, 2007.
[58] D. Schulze, *Powders and bulk solids: behavior, characterization, storage and flow*: Springer, 2008.
[59] E. Emery, "Flow properties of selected pharmaceutical powders," Master, Chemical Engineering, University of Saskatchewan, 2008.
[60] G. Landi, D. Barletta, and M. Poletto, "Modelling and experiments on the effect of air humidity on the flow properties of glass powders," *Powder Technology,* vol. 207, pp. 437-443, 2/15/ 2011.
[61] H. Y. Saw, C. E. Davies, J. R. Jones, G. Brisson, and A. H. J. Paterson, "Cohesion of lactose powders at low consolidation stresses," *Advanced Powder Technology,* vol. 24, pp. 796-800, 7// 2013.
[62] W. A. Gray and G. T. Rhodes, "Energy transfer during vibratory compaction of powders," *Powder Technology,* vol. 6, pp. 271-281, 11// 1972.
[63] S. S. Hsiau and S. J. Pan, "Motion state transitions in a vibrated granular bed," *Powder Technology,* vol. 96, pp. 219-226, 5/15/ 1998.
[64] B. Thomas, M. O. Mason, and A. M. Squires, "Some behaviors of shallow vibrated beds across a wide range in particle size and their implications for powder classification," *Powder Technology,* vol. 111, pp. 34-49, 8/21/ 2000.
[65] L.-S. Lu and S.-S. Hsiau, "Mixing in vibrated granular beds with the effect of electrostatic force," *Powder Technology,* vol. 160, pp. 170-179, 12/13/ 2005.
[66] S. E. Naeini and J. K. Spelt, "Development of single-cell bulk circulation in granular media in a vibrating bed," *Powder Technology,* vol. 211, pp. 176-186, 7/25/ 2011.
[67] R. D. Venkatesh, M. Grmela, and J. Chaouki, "Simulations of vibrated fine powders," *Powder Technology,* vol. 100, pp. 211-222, 12/1/ 1998.
[68] ASTM, "Standard Shear Test Method for Bulk Solids Using the Schulze Ring Shear Tester," ed. West Conshohocken, PA: ASTM International, D6773-08.
[69] L. Greenspan, "Humidity fixed points of binary saturated aqueous solutions," *Journal of Research of the National Bureau of Standards - A. Physics and Chemistry,* vol. 81A, pp. 89-96, 1977.
[70] R. A. Fisher, *Statistical Methods for Research Workers*: Oliver & Boyd, 1936.
[71] J. Litster, B. Ennis, and L. Lian, *The Science and Engineering of Granulation Processes*: Springer, 2004.
[72] S. M. Iveson, J. D. Litster, K. Hapgood, and B. J. Ennis, "Nucleation, growth and breakage phenomena in agitated wet granulation processes: a review," *Powder Technology,* vol. 117, pp. 3-39, 6/4/ 2001.
[73] K. Nishii, Y. Itoh, N. Kawakami, and M. Horio, "Pressure swing granulation, a novel binderless granulation by cyclic fluidization and gas flow compaction," *Powder technology,* vol. 74, pp. 1-6, 1993.

[74] K. Takano, K. Nishii, A. Mukoyama, Y. Iwadate, H. Kamiya, and M. Horio, "Binderless granulation of pharmaceutical lactose powders," *Powder Technology,* vol. 122, pp. 212-221, 1/22/ 2002.
[75] D. Barletta and M. Poletto, "Aggregation phenomena in fluidization of cohesive powders assisted by mechanical vibrations," *Powder Technology,* vol. 225, pp. 93-100, 2012.
[76] C. Soria-Hoyo, J. M. Valverde, and A. Castellanos, "Effect of vibration on flow properties of fine glass beads," *AIChE Journal,* vol. 54, pp. 886-896, 2008.
[77] D. J. Cumberland and R. J. Crawford, *The packing of particles*: Elsevier, 1987.
[78] L. Zhou, H. Wang, T. Zhou, K. Li, H. Kage, and Y. Mawatari, "Model of estimating nano-particle agglomerate sizes in a vibro-fluidized bed," *Advanced Powder Technology,* vol. 24, pp. 311-316, 1// 2013.
[79] N. Ku, C. Hare, M. Ghadiri, M. Murtagh, P. Oram, and R. A. Haber, "Auto-granulation of fine cohesive powder by mechanical vibration," in *WCPT7*, Beijing, 2014.
[80] C. Thornton and L. Liu, "How do agglomerates break?," *Powder Technology,* vol. 143, pp. 110-116, 2004.
[81] D. Golchert, R. Moreno, M. Ghadiri, and J. Litster, "Effect of granule morphology on breakage behaviour during compression," *Powder Technology,* vol. 143–144, pp. 84-96, 6/25/ 2004.
[82] J. Subero and M. Ghadiri, "Breakage patterns of agglomerates," *Powder Technology,* vol. 120, pp. 232-243, 2001.
[83] R. Moreno-Atanasio and M. Ghadiri, "Mechanistic analysis and computer simulation of impact breakage of agglomerates: Effect of surface energy," *Chemical engineering science,* vol. 61, pp. 2476-2481, 2006.
[84] H. Rumpf, "The strength of granules and agglomerates," in *Agglomeration*, W. A. Knepper, Ed., ed: Interscience Publications, 1962, pp. 379-418.
[85] P. H. Shipway and I. M. Hutchings, "Attrition of brittle spheres by fracture under compression and impact loading," *Powder Technology,* vol. 76, pp. 23-30, 7// 1993.
[86] Z. Zhang and M. Ghadiri, "Impact attrition of particulate solids. Part 2: Experimental work," *Chemical Engineering Science,* vol. 57, pp. 3671-3686, 9// 2002.
[87] M. Ghadiri, "Particle Impact Breakage," in *Powder Technology Handbook*, H. Masuda, K. Higashitani, and H. Yoshida, Eds., Third Edition ed: Taylor & Francis, 2006, pp. 205-212.
[88] N. A. Hardie, G. MacDonald, and E. W. Rubel, "A new method for imaging and 3D reconstruction of mammalian cochlea by fluorescent confocal microscopy," *Brain Research,* vol. 1000, pp. 200-210, 3/12/ 2004.
[89] M. Barsoum and W. Barsoum, *Fundamentals of Ceramics*: Taylor & Francis, 2002.